Gonçalo Santos Moura Trindade

BSc in Biochemistry

Pre-Clinical Evaluation of Targeted Therapies Using 3D Cell Models of Breast Cancer

Dissertation to Obtain the Master of Science Degree in
Biochemistry for Health

Supervisor: Giacomo Domenici, PhD, Researcher, IBET, ITQB-NOVA
Co-Supervisor: Catarina Brito, PhD, Principal Investigator, IBET, ITQB-NOVA

April 2021

Gonçalo Santos Moura Trindade

BSc in Biochemistry

Pre-Clinical Evaluation of Targeted Therapies Using 3D Cell Models of Breast Cancer

Dissertation to Obtain the Master of Science Degree in
Biochemistry for Health

Supervisor: Giacomo Domenici, PhD, Researcher, IBET, ITQB-NOVA
Co-Supervisor: Catarina Brito, PhD, Principal Investigator, IBET, ITQB-NOVA

Jury:

Chairperson: Pedro Manuel Henriques Marques Matias, PhD
Supervisor: Giacomo Domenici, PhD
Opponent: Sara Alexandra Vinhas Ricardo, PhD
Member of the Committee: Ana Maria de Jesus Bispo Varela Coelho, PhD

Instituto de Tecnologia Química e Biológica António Xavier,
Universidade NOVA de Lisboa

April 2021

Pre-Clinical Evaluation of Targeted Therapies
Using Breast Cancer 3D Cell Models

This thesis is dedicated to my family and friends,
but most of all, to my parents and my girlfriend,
those who have made who I am today,
and with whom I want to build a future.

May this be the beginning.

Acknowledgements

Throughout a year and a half, many were the people who directly or indirectly were involved with guidance, assistance and support for this thesis to be completed. To all, *Thank You!* I could not have undertaken this project without your contribution, unwavering support and belief in me.

First and foremost, I would like to start by sincerely thanking my supervisor, Dr. Giacomo Domenici, for his patience and commitment, for his insightful comments and hard questions. Undoubtedly, who I owe most of the skills and knowledge acquired during my master thesis and whose expertise has allowed me grow as a research scientist.

To Dr. Catarina Brito, my co-supervisor, I am deeply grateful for receiving me in the Advanced Cell Models Lab, for her determining role in my formation, for the leadership and inspiration. Thank you for the guidance during this thesis, for establishing pushful goals and for the opportunity entrusted.

To Dr. Paula Alves, I thank for the inspiration given with a single lecture and for the chance given and the optimal working conditions offered to do my master thesis at Animal Cell Technology Unit at ITQB and iBET. To all the elements from iBET, and TCA in particular, I would also like to extend my sincere appreciation.

To Dr. Saudade André and the Anatomic Pathology Unit from Instituto Português de Oncologia de Lisboa Francisco Gentil, as well as Dr. Jordi Joan Cairó Badillo and Dr. Joan Miret Minard from Universitat Autònoma de Barcelona, I am sincerely grateful for their partnership and collaboration within this project.

To the 3D Group, I would like to express my deepest gratitude., Francisca, Sofia, Nuno, Bia, Catarina, Rodrigo and Jhenifer, you all contributed for what was my most defiant academic experience, either with a wisely advice, a clever tip or a sincere laugh. For Luísa, particular gratitude for the guidance and help with primaries. To Teresa, The Immuno Queen, and Rita, The LDH Queen, I must specially thank you. From your endless patience, good mood and being confidents to my sanity, to your constant supply of cells, protocols proofreading and just being major supporters, you have helped me more than I can ever thank you enough!

To the best Squad of friends anyone could ask. Os meus amigos mais chegados e que me acompanharam melhor que ninguém nesta louca jornada. Com quem partilhei cada momento da faculdade, cada dor e cada sorriso. Que perceberam a loucura de Experimental, o significado do preto e de um quadrado de terra, e que no Fidalgo é que é, mas desde que haja comidjinha está tudo bem! You're the best Meggs, Trish, Mira e Van!

Ao Samu, pelo humor, pela randomness e pelo *bromance!* Pela companhia nesta jornada de aturar duas raparigas de Viseu, pela companhia mais em não ir ao ginásio do que a ir e pelas tardias discussões filosóficas sobre o sentido da vida. Acima de tudo por mais do que uma amizade, uma *La Família* para o resto da vida!

À Van, a quem palavras algumas serão suficientes. Obrigado por estes 6 anos em que foste mais do que uma melhor amiga, uma irmã. Por teres lá estado em todos, mesmo todos, os momentos! Por seres a minha pessoa *especial*, por me teres chamado à razão sempre que precisava e por teres puxado por mim quando ninguém mais conseguiria. Obrigado pela companhia, pela aventura do mestrado, por tudo isto e por muito mais. Esta tese não existiria sem ti!

À minha família, a quem devo tudo o que sou hoje. Aos meus avós pelo orgulho e amor que me fazem sentir a cada dia. Em particular aos meus pais, simultaneamente os meus maiores críticos e o meu "porto seguro", com quem posso sempre contar para me chamar à realidade e me pôr na linha. Obrigado por todo o encorajamento, sem o qual não conseguiria ter chegado a este ponto. Obrigado por todas as marmitas e descontos nos dias e semanas mais difíceis, pelo apoio incondicional, compreensão, carinho e paciência infinita, por aquele abraço forte quando mais precisava. Este trabalho é igualmente fruto da vossa dedicação. *Adoro-vos!*

À Carol, a quem agradeço por todos os momentos ao meu lado, mesmo quando a 300 km de distância. Fazes de mim uma pessoa melhor e és a minha inspiração, fonte de coragem e vontade. Quem me faz sonhar, e quem me prende ao chão. Desculpa por todos os momentos em que te fiquei a dever um pouco mais de carinho ou atenção. Significas mais do que posso expressar por palavras. *Obrigado Amoor!* Por todo o carinho e paciência, por me manteres o foco quando precisava e me distraíres quando também necessitei, por todos os planos de um futuro a dois. Esta tese não tinha chegado ao papel sem o teu apoio e incentivo. Devo-te tudo. Amo-te. *A nós.*

“There is nothing permanent except change.”

- Heraclitus -

Abstract

Breast cancer (BC) is the most frequent malignancy and the deadliest cancer death in women. It is a heterogeneous disease characterized by high variability in tumor morphology, molecular characteristics, and clinical response. Development of targeted therapies has revolutionized cancer treatment; however, these therapies are associated with increased resistance. Development of novel therapies often fails due to lack of representation of the tumor microenvironment (TME), revealing the need for recapitulative models.

In this thesis, the aim was the pre-clinical evaluation of the therapeutic potential of anti-BC targeted therapies resorting to 3D *in vitro* and *ex vivo* BC models previously established in the host Lab. Spheroids were generated from $HER2^+$ and $HER2^-$ BC cell lines (HCC1954 and HCC18906, respectively), encapsulated and cultured under agitation. These 3D *in vitro* models were challenged with antibody-drug conjugates (ADCs) derived from the anti-HER2 antibody trastuzumab. In $HER2^+$ spheroids, ADCs caused reduction of cell metabolic activity and viability, inducing apoptosis, which was neither observed for trastuzumab nor $HER2^-$ spheroids. These results corroborated the high specificity and efficacy of the ADCs, previously determined in 2D cell models.

In parallel, a patient-derived explants BC model was stimulated with estrogen and challenged with endocrine therapies. The results showed maintenance of estrogen receptor alpha (ER) expression and signaling. Upon estrogen stimulus, upregulation of ER target genes (*PGR*, *TFF1* and *AREG)* and downregulation of ER transcription and protein levels demonstrated active ER signaling. When challenged with endocrine drugs tamoxifen and fulvestrant, the same ER-target genes were downregulated, as described for ER antagonists, and fulvestrant showed increased effect compared to tamoxifen, reflecting the mechanism of action of these drugs.

In summary, this work established that these BC models represent useful research tools capable of evaluating the potential of novel targeted therapies in pre-clinical drug development and contribute to study resistance to current therapies.

Keywords: breast cancer; tumor microenvironment; 3D cell models; patient-derived explants; targeted therapies; drug assays.

Resumo

O cancro da mama (CM) é a doença mais frequente e o cancro com maior mortalidade na mulher. É uma doença heterogénea, caracterizada por elevada variabilidade tumoral, morfológica e molecular, e resposta clínica. O desenvolvimento de terapias dirigidas revolucionou o tratamento do CM; no entanto, estas terapias estão associadas a resistência. O desenvolvimento de novas terapias frequentemente falha devido à falta de representação do microambiente tumoral (TME), revelando a necessidade de modelos recapitulativos.

Nesta tese, o objetivo foi a avaliação pré-clínica do potencial terapêutico de terapias dirigidas anti-CM, recorrendo a modelos 3D *in vitro* e *ex vivo* de CM, previamente desenvolvidos pelo Laboratório de acolhimento. Esferoides gerados a partir de linhas celulares $HER2^+$ e $HER2^-$ (respetivamente HCC1954 e HCC1806), foram encapsulados e cultivados sob agitação. Estes modelos 3D *in vitro* foram expostos a conjugados anticorpo-fármaco (ADCs) derivados do anticorpo anti-HER2, trastuzumab. Em esferoides $HER2^+$, os ADCs induziram redução da atividade metabólica e viabilidade celular, induzindo apoptose, que não foi observada para o trastuzumab ou esferoides $HER2^-$. Estes resultados corroboraram a elevada especificidade e eficácia dos ADCs testados, previamente determinada em modelos celulares 2D.

Em paralelo, um modelo de explantes derivados de pacientes foi estimulado com estrogénio e exposto a fármacos endócrinos. Observou-se a manutenção da expressão e sinalização do recetor de estrogénio alfa (RE). Após o estímulo com estrogénio, observou-se regulação positiva de genes-alvo de RE (*PGR, TFF1 e AREG)* e regulação negativa da transcrição e níveis de proteína do RE demonstrou sinalização ativa do RE. A exposição a tamoxifeno e fulvestrant induziu uma regulação negativa dos mesmos genes regulados por ER, como descrito anteriormente para antagonistas de RE. Ademais, o fulvestrant mostrou um efeito superior ao tamoxifeno, refletindo o mecanismo de ação destas terapias.

Resumindo, este trabalho estabeleceu que estes modelos de CM representam ferramentas de investigação úteis na avaliação de novas terapias dirigidas durante a fase pré-clínica do desenvolvimento de fármacos e com o potencial de contribuir para o estudo de resistência a terapia.

Palavras-Chave: cancro da mama; microambiente tumoral; modelos celulares 3D; explantes derivados de pacientes; terapias dirigidas; ensaios de fármacos.

Table of Contents

List of Figures

List of Tables

Abbreviations

Ab	Antibody
ADCC	Antibody Dependent Cellular Cytotoxicity
AKT	Protein kinase B; PKB
ATCC	American Type Culture Collection
AREG	Amphiregulin
BC	Breast Cancer
bFGF	Basic Fibroblast Growth Factor
BPE	Bovine Pituitary Extract
BRCA1	Breast Cancer Type 1 Susceptibility Protein
BRCA2	Breast Cancer Type 1 Susceptibility Protein
CAF	Cancer-Associated Fibroblast
CCND1	Cyclin D1
CDC	Complement Dependent Cytotoxicity
CDR	Complementarity-Determining Regions
CO_2	Carbon Dioxide
Ct	Cycle threshold
DAPI	4′,6-diamidino-2-phenylindole
DAR	Drug-Antibody Ratio
ddH_2O	Double-distilled Water
DM1	Mertansine
DMEM	Dulbecco's Modified Eagle Medium
$DPBS^{(-/-)}$	Dulbecco's Phosphate Buffered Saline [-] Calcium, [-] Magnesium
DXd	Deruxtecan
E_2	17β-Estradiol; Oestradiol
EC	Endothelial Cell
EC50	Half Maximal Effective Concentration
ECD	Extracellular Domain
EGF	Epithelial Growth Factor
EGFR	Epidermal Growth Factor Receptor
EMA	European Medicines Agency
ER	Estrogen Receptor Alpha
ERE	Estrogen Response Element
ERK	Extracellular Signal-regulated Kinases
Fab	Antigen Binding Fragment
FBS	Fetal Bovine Serum
Fc	Fragment Crystallizable
FDA	Fluorescein Diacetate
FSG	Fish Skin Gelatin
FSH	Follicle Stimulating Hormone
GnRH	Gonadotropin-releasing hormone
HCC	Hepatocellular carcinoma
hDF	Human Dermal Fibroblast
HDI	Human Development Index
HEPES	4-(2-hydroxyethyl)-1-piperazineethanesulfonic Acid
HER2	Human Epidermal Growth Factor Receptor 2
HGF	Hepatocyte Growth Factor
HMEC	Human Mammary Epithelial Cells
HR	Hormone Receptor
HRP	Horseradish Peroxidase

IC	Invasive Carcinoma
Ig	Immunoglobulin
IgG	γ-Immunoglobulin
ILC	Invasive Lobular Carcinoma
IMC	Invasive Mucinous Carcinoma
IMDM	Iscove's Modified Dulbecco's Medium
INT	Iodonitrotetrazolium
kV	Kilovolt
L	Liter
LDH	Lactate Dehydrogenase
LDL	Lithium Dodecyl Sulfate
LH	Luteinizing Hormone
mAb	Monoclonal Antibody
MAPK	Mitogen-Activated Protein Kinase
MBC	Male Breast Cancer
MES	2-(N-morpholino)ethanesulfonic Acid
Min	Minute
mL	Milliliter
mm	Millimeter
mM	Millimolar
MMAE	Monomethyl Auristatin E
mOsm	Milliosmole
MTD	Maximum Tolerated Dose
MTT	3-(4,5-dimethylthiazol-2-yl)-2,5-diphenyl tetrazolium bromide
N	Number of Independent Experiments
NAD	Nicotinamide Adenine Dinucleotide
NAD^+	NAD oxidized form
NADH	NAD reduced form (H for hydrogen)
NCI	National Cancer Institute
NK	Natural Killer
NST	No Special Type
PAR%	Population Attributable Risk Percentage
PCR	Polymerase Chain Reaction
pCR	Pathologic Complete Response
PDE	Patient-Derived Explant
PDGF	Platelet Derived Growth Factor
PDMS	Polydimethylsiloxane
PDO	Patient-Derived Organoid
PDX	Patient-Derived Xenograft
PFA,	Paraformaldehyde
PI3K	Phosphatidylinositol 3-Kinase
PKC	Protein Kinase C
PR	Progesterone Receptor
PTEN	Phosphatase and TENsin homolog
PTFE	Polytetrafluoroethylene
RAS	Rat Sarcoma
RNA	Ribonucleic Acid
rpm	Rotations *per* minute
RPMI	Roswell Park Memorial Institute
RTK	Receptor Tyrosine Kinase
RT	Room Temperature
RT-qPCR	Reverse Transcription Quantitative Polymerase Chain Reaction
SD	Standard Deviation
SDF1	Stromal Cell Derived Factor 1

SDS	Sodium Dodecyl Sulfate
SMCC	Succinimidyl-4-(N-maleimidomethyl)cyclohexane-1-carboxylate
STAT3	Signal Transducer and Activator of Transcription 3
TBS	Tris Buffered Saline
TBST	Tris Buffered Saline Tween
Tcys_114	Trastuzumab_cys114
Tcys_114-MMAE 2	Trastuzumab_cys114-vcMMAE (DAR 2)
TFF1	Trefoil Factor 1
TGF-β	Transforming Growth Factor Beta
TME	Tumor Microenvironment
TNBC	Triple Negative Breast Cancer
TNM	Tumor size, presence of Nodal metastasis, and presence of distant Metastasis
T-ADC	Trastuzumab-Derived ADC
T-DM1	Trastuzumab-DM1 (DAR 3)
T-MMAE 2	Trastuzumab-vcMMAE (DAR 4)
T-MMAE 4	Trastuzumab-vcMMAE (DAR 8)
VEGF	Vascular Endothelial Growth Factor
v/v	Volume *per* volume
w/v	Weight *per* volume
2D	Two-Dimensional
3D	Three-Dimensional

Chapter 1. Introduction

1.1. Breast Cancer

Cancer has always afflicted humans, although for centuries its impact was overshadowed by early death from infectious diseases, hunger and wars, as well as lack of diagnosis, thus masking the global cancer burden.[1] Breast cancer (BC) is the most frequent malignancy in women, a heterogeneous disease characterized by a high variability in tumor morphology, molecular characteristics, and clinical response.[1] Over the past 10 to 15 years, treatment regimens have evolved to take this heterogeneity into account, with emphasis on therapies directed to specific molecular targets on the tumor cells and treatment de-escalation to reduce amount and intensity of medication while maintaining good outcomes.[2] Nevertheless, there is a need for novel local and systemic therapeutical approaches against BC, as resistance to treatment is increasingly common among patients. Novel therapeutic approaches have been leveraged by the fact that knowledge on BC biology evolves and increases continuously, and new molecular targets are identified.[2–4]

1.1.1. Epidemiology

1.1.1.1. Incidence, Mortality & Survival Rate

BC is the most frequently diagnosed cancer in women and the second most common cancer overall with 2.1 million new cases worldwide in 2018, according to the Global Cancer Observatory (GLOBOCAN).[1,5] The disease is also the leading cause of cancer death in women globally (627 000 deaths in 2018)[5] although a steady decline in BC mortality has been observed in numerous countries with high Human Development Index (HDI). This reduction is mostly attributable to early detection and efficient systemic therapies, and stabilization of incidence rates since 2000, as a result from the publication of two landmark studies [6,7] that reported on the harmful effects and increased BC risk from menopausal hormone replacement therapy.[1] Simultaneously, in countries in transition towards higher HDI levels, BC mortality trends have tended to parallel the increasing incidence trends that have consistently been observed, as it is example countries in Asia and Latin America, prompting World Cancer Report 2020 [1] to still predict, globally, a rise in incidence rates. Even though, in 2018, the overall survival rate of women diagnosed with BC in the USA was 89% at 5 years after diagnosis, 83% at 10 years, and 78% at 15 years.[8] Unfortunately, and because most cancer registries only record the incidence and mortality but not data on relapse, it is unknown how many of these women are living with metastatic disease and how many are cancer-free survivors.[2]

1.1.1.2. Genetic Alterations

Approximately 10% of BC are inherited and associated with a personal or family history of breast or ovarian cancer. These inherited genetic alterations are largely associated with mutation of two high-penetrance tumor suppressor genes, *breast cancer type 1 susceptibility protein - BRCA1* (17q21) and *breast cancer type 2 susceptibility protein - BRCA2* (13q13), that code for proteins involved in DNA damage repair through homologous repair. Even though, germline mutations of other BC susceptibility genes involved in DNA damage repair and maintenance of genomic integrity have been linked to inherited increased BC risk.[2] These mutations may be associated with Li Fraumeni , Cowden and Peutz–Jegher syndromes and include genes such as *ATM, CHEK2, CDH1, CCND1, NF1, PALB2, PTEN, STK11* and *TP53.* These encode cell-cycle

modulators that in BC are either repressed (for example, the tumor suppressor gene p53) or activated (for example, the gene encoding cyclin D1, a protein associated with cell cycle promotion, *CCND1*), respectively inhibiting apoptosis or activating cell proliferation. [2,9–13].

1.1.1.3. Risk Factors

Elevated incidence rates are attributed to a high prevalence of known risk factors. Reproductive factors in general alter sensitivity of the mammary gland to hormonal exposures and changes in gene expression patterns resulting in increased proliferation and reduced differentiation, and include early age at menarche, later age at menopause, nulliparity, late age at first birth, and fewer children.[1,2,8] Exogenous hormone intake (as oral contraceptive and hormone replacement therapy) is also closely associated with overall BC risk due to hormonal exposure.[1,2] Other known risk factors include family history of BC, dense breasts on mammography and radiation exposure, which correlates to either inherent or acquired genetic alterations that potentiate BC.[1,2] In general, lifestyle factors such as alcohol consumption, obesity and unhealthy diet are also associated with increased risk of developing BC.[1,8]

In opposition, late menarche, early menopause, parity, early age at first birth and breastfeeding are known as protective factors, since it reduces a woman's lifetime exposure to hormones like estrogen, which can promote BC cell growth. In particular, lactation induces hormonal changes that delay a woman menstrual period, thus decreasing the overall BC risk.[1,8] The population attributable risk percentage (PAR%) is used to estimate the percentage of disease that could be prevented if a risk factor was removed from the population. The PAR% is dependent on the magnitude of the association between the exposure and outcome, as well as the prevalence of the risk factor in the population. A recent study that combined data from two large cohorts has concluded that considering all risk factors, the PAR% for invasive BC was 70%, meaning that if all women were in the lower risk categories, the incidence of invasive BC would be reduced by 70%. When considering only modifiable risk factors, namely reduced weight gain, no alcohol consumption, high physical activity, ever breastfeeding, and no current hormone usage, BC was associated a PAR% of 34.6%.[1,14]

1.1.2. Classification and Pathophysiology

The use of a standardized cancer pathology report with a synoptic checklist of relevant information is highly recommended and indispensable for optimal management of BC.[15] Consensually, such report should provide a complete characterization of the tumor analyzed. Various classification systems are simultaneously used, based on histologic type according to the WHO classification system,[16] grade of differentiation and clinical stage assessed by the **TNM** classification system (**T**umor size, presence of **N**odal metastasis, and presence of distant **M**etastasis).[17,18]

Despite the inherent molecular heterogeneity of BC, groundbreaking work by Perou & Sorlie [19,20] established an intrinsic classification system based on distinctive gene expression profiles. The use of **P**rediction **A**nalysis of **M**icroarray within a **50**-gene set (**PAM50**) shifted clinical management of BC to biology-centered approaches. The expression levels of these 50 genes in the BC tissue is analyzed by hierarchical clustering and thus classified in the specific subgroups [21,22]

Currently, both research and clinical practice use a molecular classification where breast tumors fall primarily into three BC classes: Luminal, Human Epidermal Growth Factor Receptor 2 (HER2) overexpressed and Triple Negative Breast Cancer (TNBC), according to the detection of key receptor proteins (Table 1.1) accessed by immunohistochemistry (ER, PR and HER2).[23]

Table 1.1. Breast Cancer molecular subtypes based on the detection of receptors for hormones and growth factors. Estrogen Receptor (ER) is expressed only on the luminal subtypes while the Progesterone Receptor (PR) has varied expression on the same subtypes. Human Epidermal Growth Factor Receptor 2 (HER2) is expressed on Luminal B and HER2-overexpressed breast cancers.[23]

	ER	PR	HER2
Luminal A	+	+/-	-
Luminal B	+	+/-	+/-
HER2 Overexpressed	-	-	+
Triple Negative (Basal)	-	-	-

1.1.2.1. Luminal Breast Cancer

Approximately 70% of invasive BC belong to the luminal class (accounting for Luminal A and Luminal B subtypes). These tumors are categorized as hormone receptor positive (HR^+) tumors and express either the estrogen receptor, the progesterone receptor (PR), or both.[23] Estrogen receptor alpha (ER) is a steroid hormone receptor and transcription factor that, upon estrogen binding, and activation of ER controlled genes, promotes breast development, growth and maturation, mainly during puberty, menstrual cycles, and pregnancy. During the menstrual cycles, an imbalance between estrogen and progesterone enhances cell proliferation and may cause DNA damage accumulation.[24] With the repetition of this process at each cycle, a defective repair process can occur, by which the usual mechanisms are not enough to repair the DNA damage accumulated, leading to preserved mutations in pre-malignant and then in malignant cells. At this stage, estrogen activates oncogenic growth pathways in ER^+ BC cells, while by a paracrine mechanism orchestrates proliferation and morphogenesis, affecting nearby cells in the mammary epithelium, namely stromal cells that support cancer development.[2,25]

ER ligand binding can modulate gene expression (Figure 1.1) by interacting with estrogen response elements (ERE) located in the promoter region of specific genes: [26,27]

- Trefoil Factor 1 (TFF1) is an important autocrine factor involved in neoplastic progression and tumor invasion;[28]
- Amphiregulin (AREG) is a critical autocrine growth factor and mitogen of fibroblasts and important factor for ductal development in the mammary gland;[27]
- Progesterone Receptor (PR) is an important steroid sex hormone involved in several key aspects of mammary gland development, namely regulation of proliferative signaling pathways in the breast.[29]

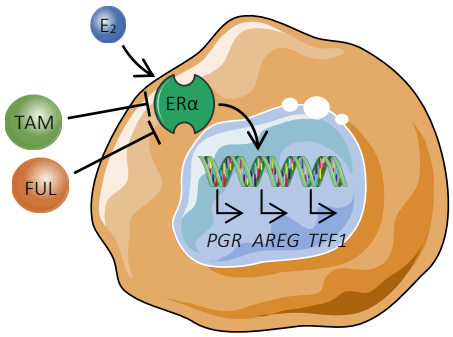

Figure 1.1. Estrogen receptor signaling by estrogen and inhibition by tamoxifen and fulvestrant. Based on *Peterson et al., 2015* [26] and *Zhu et al., 2006*.[27] (Image created with Servier Medicar Art ©)

The use of endocrine agents to downregulate ER signaling is the primary systematic therapy for ER^+ or PR^+ BC.[29]

1.1.2.2. HER2-Overexpressing Breast Cancer

Patients with amplification or overexpression of *HER2* are classified as HER2-overexpressing BC, which account for approximately 20% of BC.[3,4] *HER2* encodes for a transmembrane receptor tyrosine kinase (RTK) of the epidermal growth factor receptor (EGFR) family, and consequent aberrant amplification leads to

abnormal cell growth, inhibition of apoptosis, cellular invasion, among others.[3,4] $HER2^+$ BC are associated with a poorer prognosis than HR^+ BC. The HER2 signaling activates proliferation, cell survival, metastasis and adhesion through different pathways, such as the rat sarcoma - RAS, phosphatidylinositol 3-kinase / protein kinase B - PI3K/AKT and mitogen-activated protein kinase / extracellular signal-regulated kinases - MAPK/ERK pathway, thus promoting cancer progression. HER2 activation occurs through receptor dimerization after ligand binding, although no HER2-specific ligand has been identified. Even though, tumors that overexpress *HER2* can benefit from HER2-targeted therapy, including anti-HER2 antibodies and small-molecule tyrosine kinase inhibitors (which will be further addressed in section 1.2.2.3).[30,31]

1.1.2.3. Triple Negative Breast Cancer

Triple negative tumors represent the most heterogeneous BC class and are comprised largely by the basal subtype. TNBC is characterized by the lack of ER, PR or *HER2* expression. These tumors account for approximately 15% of all BC and have a high risk of distant relapse in the first 3 to 5 years following diagnosis and treatment.[2,23] These tumors are particularly aggressive, usually large in size, showing rapid growth and chemoresistance. Despite recent success with immunotherapies. TBNC currently lacks any form of targeted systemic therapy (endocrine and cell-targeted therapies), leaving chemotherapy, at the moment, the only option. For all these reasons, TNBC are associated with a lower disease-free survival.[23]

1.1.3. The Case of Male Breast Cancer

Male breast cancer (MBC) is a rare malignant form of cancer in men (1 out of 100 cancers diagnosed in men) and it represents less than 1% of all BC cases. Its annual prevalence in Europe has been estimated in 1 out of 100 000 men, and BRCA mutations might be responsible for up to 40% of MBC. In relation to the histopathology classification, over 90% of tumors are ER^+ and PR^+, even though these steroid hormones are usually deemed to be particular of women. As such, MBC follows the standard postoperative regimen (adjuvant) therapy of BC, namely estrogen receptor antagonists, that will be further addressed in the endocrine therapy section (1.2.2.2). Prognostic indicators rely mainly in stage at diagnosis and lymph node status, but overall 5-year survival estimates is around 40–65%.[16,32]

1.2. Breast Cancer Therapy

BC therapeutic management (Figure 1.2) is dependent on the BC subtype and it is classified as either locoregional therapy or systemic therapy, according to whether it is focused on site-directed approaches or non-directed bloodstream delivery. In early BC without metastases, women with tumors that are deemed operable undergo surgical tumor resection with or without radiation therapy. However, a combined treatment with systemic therapy (chemotherapy, endocrine therapy or cell-targeted therapy), is most often required.[2,3]

For metastatic BC, therapeutic goals are: (1) extend life expectancy and (2) symptom palliation. Currently, metastatic BC remains incurable in virtually all affected patients. Although the same categories of systemic therapy are used in metastatic BC, local therapy modalities (surgery and radiation) are typically used for palliation only in metastatic disease.[2,4,33]

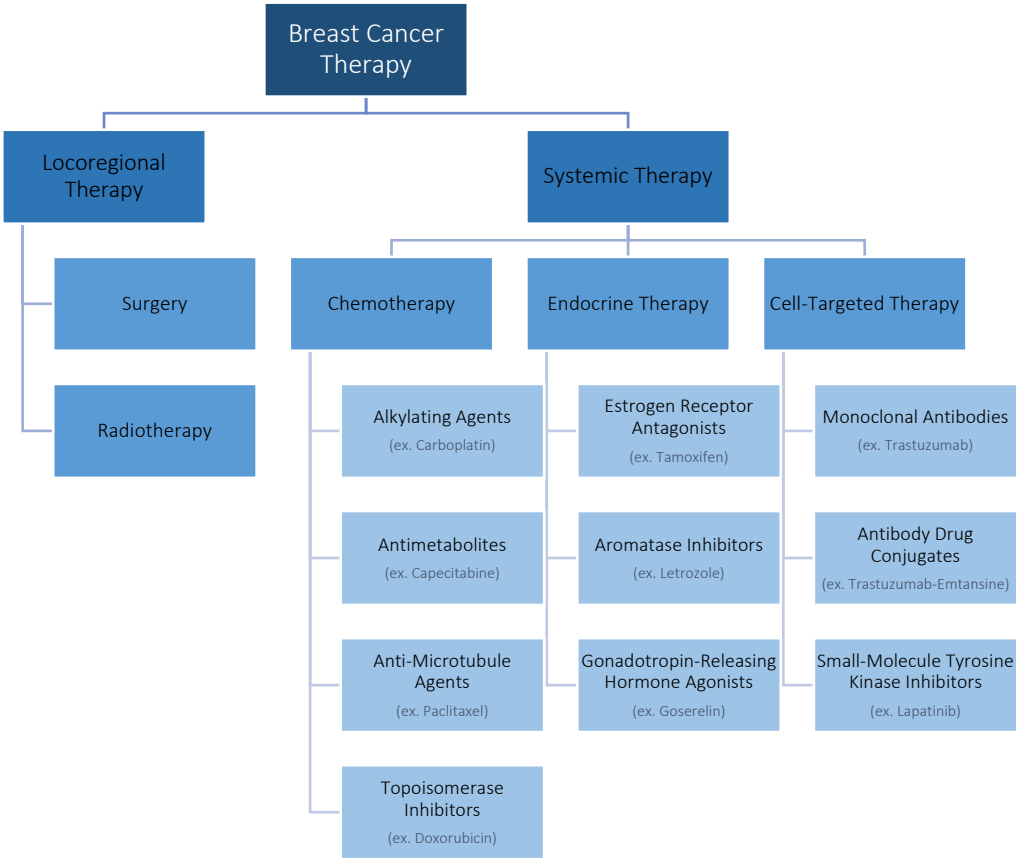

Figure 1.2. Schematic diagram of breast cancer therapy types and subtypes.
Based on *Karen et al., 2010* [34] & *Radice & Redaelli, 2003* [33]

1.2.1. Locoregional Therapy

Locoregional therapy is a therapeutical modality focused on localized approaches targeted to the site of the primary tumor and encompasses both surgery and radiotherapy.

1.2.1.1. Surgery

Surgery of primary BC provides locoregional control of the disease and consists in resection and removal of the tumor, and evaluation of axillary lymph nodes for TNM staging and classification of the extent of cancer spread using an alphanumeric code: (T) describes the size of the primary tumor and whether it has invaded nearby tissues, (N) describes involvement of regional lymph nodes and (M) describes existence of distant metastasis. Based on the determined cancer stage, possibly excision of the affected nodes might be needed.[2,18]

Standard operative approaches are either (1) a partial excision of the breast, in which only the tumor and surrounding tissue is removed (lumpectomy), assuming that no cancer cells are seen at the rim of the tissue that was removed upon microscope evaluation (clear margins), or (2) a complete removal of the breast tissue (mastectomy).[4] However, there has been a trend recently for more conservative procedures (less women-body disfiguring), i.e., breast-conserving surgery in which as much as possible of the healthy breast tissue is retained.[2]

Surgical removal of axillary lymph nodes serves both for diagnostic purpose (determining the anatomic extent of the BC) and therapeutic purpose (removal of cancerous cells that may evolve to distant metastasis). Surgical decision-making is based on whether axillary lymph node involvement is evident at diagnosis and whether preoperative regimen (neoadjuvant) systemic therapy is administered.[3,4]

1.2.1.2. Radiotherapy

Radiotherapy is a treatment that, by the use high doses of radiation, kills cancer cells and shrink tumors. It has been applied to BC as a local therapy, generally adjuvant to surgery, to control or prevent growth of residual tumor cells after surgery and to control metastatic disease. Radiation after surgery is usually preferred for patients with the highest risk of locoregional recurrence, with studies showing that it significantly reduces the local recurrence rate and mortality.[4] Post-operative radiation therapy in BC may be delivered to the whole breast, to a portion of the breast (after lumpectomy), to the chest wall (after mastectomy), or to regional lymph nodes.[4,34]

1.2.2. Systemic Therapy

Systemic therapy is the general designation for the treatments using drugs that, after administration, are distributed through the bloodstream, reaching and affecting target cells all over the body. It might be prescribed by itself or in combination with locoregional therapy, either neoadjuvant, adjuvant, or both.[3] Neoadjuvant therapy is advised for patients with large tumors, to reduce the tumor burden, or if pre-operative therapy has prognostic value regarding further treatments to pursue (such as in HER2-positive disease or TNBC). The prognostic value derives from information of pathological complete response (pCR) which is an absence of all signs of invasive cancer cells in tissue samples removed during surgery or from biopsy after systemic therapy.[2] Moreover, systemic therapy can be given after surgery (adjuvant) if the surgical result or biomarkers indicate increased risk of recurrence.[2,4]

BC subtype guides the standard systemic therapy administered, which consists of endocrine therapy for all HR^+ tumors (with some patients requiring chemotherapy as well), HER2-directed antibody therapy (trastuzumab) plus chemotherapy for all $HER2^+$ tumors (with endocrine therapy given in addition, if concurrent HR^+), and chemotherapy alone for TNBC.[2,4]

Chemotherapy, endocrine therapy, and tissue-targeted therapies enhance definitive local therapy (surgery, radiation therapy, or both), substantially decreasing cancer recurrence and disease-specific death.[2–4] These therapies will be described in the following subsections.

1.2.2.1. Chemotherapy

Chemotherapy regimens rely on the use of cytotoxic and cytostatic drugs for cancer treatment, and may be used before, after, or as an alternative to surgery for those cases in which surgical interventions are considered unsuitable.[3] Chemotherapy is justified for cancers with poor prognosis after surgery, such as triple negative breast cancer.[4]

Chemotherapy remains an essential treatment also for preventing recurrence in many BC patients. It is the only systemic therapy with demonstrated efficacy in TNBC and an important adjunct to endocrine therapy and HER2-targeted therapy.[35] Nevertheless, alongside surgery and radiotherapy, cytotoxic chemotherapy is non-directed, and as such, strong side-effects are a major drawback. These may include

pain, nausea, cardiotoxicity, hair loss, and myelosuppression. Several categories of chemotherapy are available, being classified as it follows.[36]

Alkylating Agents

Originated from the mustard gas used in World War I, alkylating agents are the oldest group of chemotherapeutics. These agents bind covalently to DNA via their alkyl group, either twice to one of the DNA strands (intra-strand crosslink) or once to both DNA strands (inter-strand crosslink). During cell division, DNA strands break leading to apoptosis (programmed cell death).[35]

The subtypes of alkylating agents mainly considered are the nitrogen mustards, nitrosoureas, tetrazines, aziridines, platinum agents, and non-classical alkylating agents. Within the scope of BC management, nitrogen mustards include cyclophosphamide and platinum agents include cisplatin and carboplatin (Paraplatin®).[37,38]

Antimetabolites

Antimetabolites are chemicals that impair the use of the monomeric units of DNA upon cell replication, thus having toxic effects, such as halting cell division and consequently cell growth, which lends them application as chemotherapeutics. These compounds generally impair DNA replication machinery by one of these two mechanisms: incorporation of chemically altered nucleotides, nucleosides or nucleobases or depletion of deoxynucleotides needed for DNA replication and cell proliferation.[38,39]

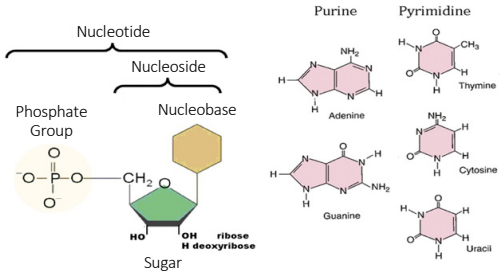

Figure 1.3. Nucleic Acids: Nucleobases, Nucleosides and Nucleotides. Adapted from *Sagar Aryal, 2018* [40] (Microbe Notes ©)

In the first mechanism these drugs may be analogs of the monomeric units of nucleic acids, either nucleobases, nucleosides or nucleotides, that will misincorporate endogenous nucleotides in DNA or RNA, leading to nucleic acid synthesis damage that results in induction of apoptosis.[38,39] On the second mechanism we can find antifolates, chemicals that block the action of folic acid (vitamin B9), a cofactor to various methyltransferases involved in serine, methionine, thymidine and purine biosynthesis. Since folic acid is required for cell replication, inhibition by these chemicals during the S phase of the cell cycle, impairs DNA synthesis.[37,39]

In the context of BC chemotherapy, fluoropyrimidines analogues include capecitabine (Xeloda®), a prodrug of 5-fluorouracil, and deoxynucleoside analogues include gemcitabine (Gemzar®). [37,39]

Anti-Microtubule Agents

Microtubules are hollow, rod-shaped, cellular structures composed of two proteins: α-tubulin and β-tubulin. They are required for cell division, among other cellular functions. These filaments are not static structures as they undergo constant disassembly into their protein subunits and reassembly into filaments. The permanent assembly and disassembly of microtubules serves to link or bundle the filaments or to move cytoplasmic organelles along them.[40] Anti-microtubule agents are plant-derived drugs (as from *Taxus baccata* and *Catharanthus roseus,* known also as *Vinca*) that block cell division by stabilizing microtubules

and disrupting the organization and dynamics of the mitotic spindle formed during cell division to separate sister chromatids between daughter cells. As a consequence, progression towards M phase of the cell cycle, which is responsible for chromosome segregation and cell division, is prevented.[37]

Vinca alkaloids and taxanes are the two main groups of anti-microtubule agents, and although both groups of drugs cause microtubule dysfunction, their mechanisms of action are opposite. The vinca alkaloids prevent the formation of the microtubules, whereas the taxanes prevent the microtubule disassembly. By doing so, they prevent cells in division from completing mitosis, however since cancer cells normally divide more quickly than other cells, inhibiting cell division harms tumor cells more than other cells. Following this, cell cycle arrest occurs, which induces programmed cell death (apoptosis). Additionally, these drugs can affect blood vessel formation (angiogenesis), an essential process that tumors rely on in order to grow and metastasize. The most common anti-microtubules used in BC management are taxanes, namely, paclitaxel (Taxol®) and docetaxel (Taxotere®).[37,41]

Topoisomerase Inhibitors

Topoisomerases are the enzymes that control the unwinding of the DNA double helix during replication or transcription. They introduce single and double strand breaks in the DNA (topoisomerase I and II, respectively)[36] Drugs that block the action of topoisomerase II can be divided into topoisomerase II poisons and topoisomerase II inhibitors, whether they increase topoisomerase II bound to DNA and induce excessive DNA strand breaks, or block the activity of topoisomerase II restraining proper DNA unwinding. The most common topoisomerase II inhibitors are anthracyclines, which are cytotoxic antibiotics that by DNA intercalation form a stable anthracycline-DNA-topoisomerase II ternary complex that hampers the rewiring of double-stranded DNA breaks. In addition, anthracyclines are also known to generate free radicals, which can induce oxidative stress to cellular proteins and induce cell death. Anthracyclines used in BC therapy include doxorubicin (Adriamycin®) and epirubicin (Ellence®).[42,43]

Currently, taxane- and anthracycline-based combination chemotherapy remains the most widely used treatment approach for early-stage TNBC patients although, to date, there are no specific guidelines for chemotherapeutic management of TNBC. The European Society for Medical Oncology (ESMO) states that cytotoxic chemotherapy is the standard of care for the treatment of TNBC and that the choice of the regimen should be made after consideration of disease-related factors (previous therapies and response, tumor burden, and need for rapid disease/symptom control) and patient-related factors (patient preferences, biological age, menopausal status, comorbidities, performance status, and socioeconomic or psychological factors).[33,36]

1.2.2.2. Endocrine Therapy

Endocrine therapy is a hormone-based targeted modality for oncology treatment that involves manipulation of the endocrine system for the pursuit of either inhibition of hormone synthesis or blockage of the associated hormone receptors (hormone antagonists), thereby preventing stimulation of a hormone positive tumor.[4] Endocrine therapy is not effective against cancers lacking hormone receptors but is usually considered the standard choice for patients with advanced ER^+ BC and non-life-threatening disease, or for older patients who are unfit for aggressive chemotherapy regimens.[44] Nevertheless, either intrinsic (primary) or acquired (*de novo*) resistance to endocrine therapy occurs in most patients, and significant risk of relapse represent a major obstacle to optimal clinical management.[3]

Hormonal therapy relies on three major categories, described as it follows.

Estrogen Receptor Antagonists

Estrogen Receptor Antagonists are compounds with variable activity, ranging from a spectrum of mixed agonists-antagonists to pure ERα antagonists. The firsts are designated as selective estrogen receptor modulators (SERMs) and work by competing with estrogen to bind and modulate ER subunits, resulting in dimerization and structural changes of ERα, thus blocking estrogen action and simultaneously inhibiting estrogen-responsive gene transcription. The pure antagonists are designated as selective estrogen receptor degraders (SERDs) that destabilize ER by binding and inducing ER proteasomal degradation, abolishing the ER signaling pathway.[29] While SERMs regulation is reversible upon discontinuation of treatment, SERDs cause irreversible ER degradation. As such SERMs, as tamoxifen (Nolvadex®) are advised for both early and advanced BC in pre- and post-menopausal women as well as men, while, in contrast, SERDs, as fulvestrant (Faslodex®) are preferred for metastatic BC of post-menopausal women.[4,45]

Aromatase Inhibitors

Aromatase inhibitors (AI) are drugs that hamper estrogen production by inhibition of estrogen synthase, (also known as aromatase), an enzyme responsible for a key step in the biosynthesis of estrogens: conversion of the enone ring of testosterone, to a phenol, completing the synthesis of estrogen. The rationale behind the development of such drugs is that in postmenopausal women estrogen production in the ovaries ceases, but in other tissues androgen to estrogen conversion through the action of aromatase is still detectable, which is responsible for oncogenic BC cell growth in these patients.[44]

When the action of aromatase is blocked, estrogen levels in post-menopausal women can drop to extremely low levels, causing growth arrest and apoptosis of hormone-responsive cancer cells.[46] Letrozole (Femara®) and anastrozole (Arimidex®) are the first line of treatment of BC in postmenopausal women, while exemestane (Aromasin®) is an irreversible aromatase inactivator.[47]

Gonadotropin-Releasing Hormone Agonists

Gonadotropin-Releasing Hormone Agonists are analogs of gonadotropin-releasing hormone (GnRH) used to suppress the synthesis and secretion of estrogen and progesterone from ovaries, achieved by continuous inhibition of the anterior pituitary gland (GnRH receptor) in premenopausal women. These analogs suppress the release of luteinizing hormone (LH) and follicle stimulating hormone (FSH), which, in turn, reduce the main source of estrogen production in the ovaries forming a hypothalamus–pituitary–ovarian axis. Goserelin (Zoladex®) in particular is the most relevant drug within this category applied to BC.[48,49]

1.2.2.3. Cell-Targeted Therapy

Cell-targeted therapies comprise molecular targeted therapeutics with the ability to precisely identify cancer cells with molecular abnormalities responsible for malignant progression of the tumor. A clear example is the use of anti-HER2 monoclonal antibodies (mAb) for the treatment of $HER2^+$ BC. Small inhibitor molecules have also emerged as a promising therapeutic modality, allowing for cell-targeted delivery of anticancer therapeutic agents to the desired tissues with reduced systemic toxicity.[50,51]

Anti HER2-targeted therapy might be highlighted in three major categories, described as it follows.

Monoclonal Antibodies

Antibodies (Ab) are glycoproteins belonging to the immunoglobulin (Ig) superfamily that are secreted by B cells and play an important role in the immune system to identify and neutralize foreign organisms or antigens. Antibodies (Abs) consist of two heavy and two light chains (HC and LC respectively) arranged in different isotypes dependent on the heavy chain they contain. Therapeutic monoclonal antibodies (mAb) in particular are usually of the γ-immunoglobulin (IgG) isotype.[50,52]

An IgG antibody is a large protein of approximately 150 kDa formed by one isotype with two heavy and two light chains linked by disulfide bridges (Figure 1.4). The heavy chains comprise a variable domain (V_H), a hinge region and three constant domains (C_H1, C_H2 and C_H3), while the light chains comprise one variable (V_L) and one constant (C_L) domain. The structure can also be divided into the fragment antigen binding (Fab) region that is composed of one constant and one variable domain of both the light (V_L and C_L) and the heavy (V_H and C_H1) chain and the fragment crystallizable (Fc) domain that is composed of two constant domains from both heavy chains (C_H2 and C_H3).[50,52]

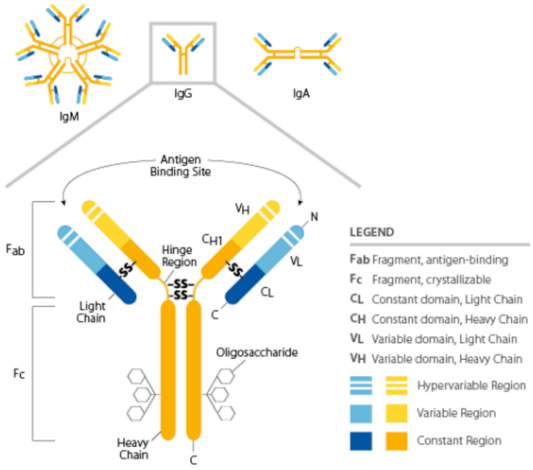

Figure 1.4. Structure of an immunoglobulin. (ThermoFisher Scientific ©)

The specificity of Abs is mediated by their variable domains and represented by the Fab region. The variable domains can be further subdivided into hypervariable regions (or complementarity-determining regions - CDR) which bind to the antigen directly and framework regions which serve as a scaffold for the CDR to contact the antigen. Circulating antibodies protect the host organism in two ways: by directly binding and neutralizing toxins, or by activating the host immune response, mainly through two pathways: (1) binding and activation of complement C1q on the Fc region resulting in the formation of the membrane attack complex lysing the target cell ("complement dependent cytotoxicity" - CDC); or (2) initiation of a cellular response ("antibody dependent cellular cytotoxicity" - ADCC) occurring through binding of Fc receptors (CD16, CD32, and CD64) on natural killer cells, monocytes and macrophages to the opsonized target.[50,52]

The ability of mAb to bind to specific antigenic epitopes allowed them to be utilized not only as a biological tool for diagnosis but also as cancer therapeutics that specifically target a tumor antigen predominantly overexpressed in target cells while having minimal expression on healthy cells.[50] As of December 2020, over 80 therapeutic monoclonal antibodies were approved in the EU, and 100 in the US, 13 of which approved in 2020, a record for a single year.[53] The anti-HER2 mAb trastuzumab (Herceptin®) is a recombinant humanized monoclonal antibody. It was developed by grafting just the murine hypervariable regions from the mAb 4D5 clone onto a human kappa IgG1, resulting in molecules that are approximately 95% human. Trastuzumab is specific against the extracellular domain (ECD) of the HER2 protein. It was first approved by the Food and Drug Administration (of United States of America) in 1998 and is one of the major achievements in BC therapy, being the standard-of-care drug for $HER2^+$ BC management.[51] Nevertheless, the mechanism of its anti-tumor action has not yet been fully elucidated. Several molecular and cellular effects have been observed in experimental models, and the most accepted mechanisms include:

- Inhibition of HER2 extracellular domain (ECD) shedding, that reduces activation of HER2 ECD and lower serum levels which are associated with increased responsiveness to endocrine therapy;[51,54]
- Suppression of angiogenesis and downregulation of vascular endothelial growth factor (VEGF) pathway that support tumor growth by formation of new blood vessels;[51]

- Induction of antibody-dependent cell-mediated cytotoxicity (ADCC) via recruitment of natural killer (NK) cells targeted to the tumor;[51]
- Downregulation of PI3K/AKT, MAPK/ERK or phosphatase and tensin homolog - PTEN pathways that result in cell cycle arrest and inhibition of tumor growth.[51]

The high response rates prolonged the time to disease progression and lowered the risk of death when compared to standard chemotherapy. Nonetheless, cardiac dysfunction has been reported as the main toxic side-effect upon trastuzumab treatment, as explained by the essential role of HER receptors for cardiac development.[51] Other antibodies approved for BC therapy include pertuzumab (Omnitarg®) and extumaxomab (Rexomun®).[52]

Antibody Drug Conjugates (ADCs)

Antibody Drug Conjugates (ADCs) are designed to selectively deliver toxic small molecules specifically to cancer cells. A mAb is covalently conjugated via a molecular linker to one or more cytotoxic agents (also called "payload"), which dictates the administered dose. The ratio of conjugated cytotoxic molecules per antibody is known as Drug-Antibody Ratio (DAR).[55]

The mechanism of action of an ADC is represented in Figure 1.5. An ADC in circulation (Figure 1.5. Step 1) binds to a specific antigen on the surface of a cancer cell (Figure 1.6. Step 2) and is internalized through endocytosis (Figure 1.5. Step 3), following cleavage by proteases in the lysosomes (Figure 1.5. Step 4). Here, the cytotoxic payload is released in a bioactive form (Figure 1.5. Step 5) to exert its function and kill the malignant cell (Figure 1.5. Step 6), usually disrupting DNA or microtubules (as auristatins and maytansines), or inhibiting RNA polymerase or topoisomerase (as exatecans).[55]

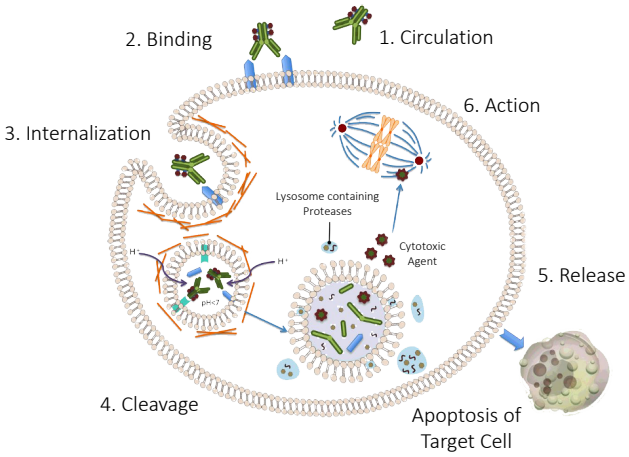

Figure 1.5. Mechanism of action of an Antibody Drug Conjugate (ADC). Adapted from *Peters & Brown, 2015* [55]

The selective delivery of ADCs to a specific target cell represents a clear improvement in respect to untargeted chemotherapy, as it lowers the minimum effective dose by increasing the amount of drug effectively reaching the tumor (typically, less than 2% of the systemically administered dose of small-molecule chemotherapeutics is reported to reach the intracellular target [56]), and it increases the maximum tolerated dose (MTD) by decreasing the amount of free drug reaching normal tissues. As such, affinity and specificity of ADCs for the target antigen are critical points to achieve highly efficient therapies. However, this is only accomplished when a stable linker prevents releasing of the toxic payload to non-target cells. As such, the linker must be strong enough to allow the circulation of the ADC through the bloodstream without being prematurely released off target, for instance upon cleavage by circulating proteases.[57]

Cleavable linkers are organized in **acid labile** (stable in blood at neutral pH but cleavable at acidic pH found in lysosomes), **protease cleavable** (stable in plasma but designed to be cleaved by specific proteases found in lysosomes) or **disulfide linked** (that are conjugated through disulfide linkage and exploit the high level of intracellular reduced glutathione to release the free drug).[55,57]

Non-cleavable linkers consist of stable bonds that are resistant to proteolytic degradation, ensuring greater stability than cleavable linkers. Non-cleavable linkers rely on complete degradation of the antibody component of ADC by cytosolic and lysosomal proteases, which eventually liberates a payload molecule linked to an amino acid residue derived from the degraded antibody. As such, when coupled with a non-cleavable linker, the payload structure must be carefully selected and designed so that the payload itself can exert comparable or even better anti-tumor potency in such a modified form.[55,57]

Moreover, the conjugation strategy also dictates important properties of an ADC, namely if it results in a Heterogeneous or Homogeneous ADC. Heterogeneous ADCs are a mixture of different immune conjugates that differ in the site and stoichiometry of payload conjugation. These first-generation ADCs are synthetized using conventional conjugation methodologies, using solvent accessible amino acids such as lysine or cysteine derived from the reaction of the interchain disulfide bonds in the antibody. Heterogeneous ADC production affords a mixture of ADC species with broad distribution of the DAR and different conjugation sites that may lead to reduced efficacy and higher potency whether naked antibodies or high-loaded species are produced. Additionally, a high DAR is correlated to a more hydrophobic environment and as such there is an increased risk of ADC aggregation that leads to instability and potential premature release of the cytotoxic drug. Despite these inherent drawbacks, heterogeneous conjugation has yield some of the first ADCs approved by the Food and Drug Administration (of United States of America). Nevertheless, many of these weaknesses have been overcome by the new ADC generation, next described.[55,57,58]

Homogeneous ADCs represent an advance over heterogeneously conjugated ADCs. These second-generation ADCs were developed employing technology innovations that allowed for novel conjugation strategies. Homogeneous ADCs contain a specific number of conjugated drug molecules at defined sites of the antibody, achieving increased potency, safety and stability over heterogeneous conjugated ADCs. Recently, some homogeneous ADCs have been approved, paving the way for the implementation of more homogeneous ADC-based therapies. Several are currently undergoing clinical trials. Homogeneous ADCs can be obtained through different methodologies: [55,57,58]

- Thiomabs, where a genetically modified antibody contains a single point mutation to a cysteine where the cytotoxic drug is conjugated in a selective manner.
- Unnatural amino acids, where non-canonical amino acids, as selenocysteine or acetylphenylalanine, are added similarly to thiomabs allowing conjugation in specific locations.
- Enzymatic conjugations, where site-directed conjugations are driven by enzymes that selectively modify antibodies with unique functional groups.
- Linker-based approaches, where site-directed conjugations are achieved by chemically driven processes through linker. [55,57,58]

Due to the vast advantages associated, ADCs represent one of the most intensely developed biologic drugs by biopharma companies recently, and it is anticipated to grow at a large pace in the upcoming years. Currently there are two ADCs approved by the Food and Drug Administration (of United States of America) commercially available for $HER2^+$ BC treatment: T-DM1 and T-DXd, both produced following heterogeneous conjugation strategies.[55,58]

The first, trastuzumab emtansine (Kadcyla®), approved in 2013, consists of the anti-HER2 humanized mAb trastuzumab covalently linked to DM1, a maytansinoid derived microtubule inhibitor. DM1 is linked via the non-reducible thioether SMCC linker of the sulfhydryl groups and primary amines of the antibody lysines (Figure 1.6), with a DAR of 3.5.[55,58] DM1 is a thiol-containing maytansinoid-derived, also named emtansine, or mertansine in its free form; it was initially isolated from the plant *Maytenus ovatus*, but with the increasing interest on its anti-tumorigenic properties, has been synthetized by several published reactions.[59,60]

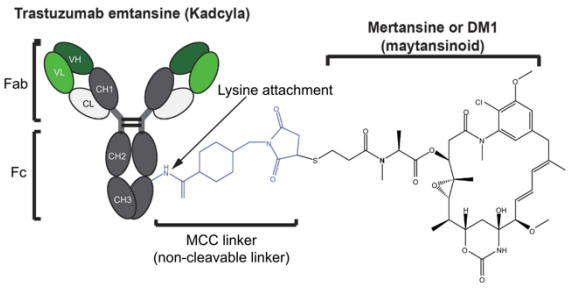

Figure 1.6. Representation of structural components of the antibody drug conjugate trastuzumab-emtansine. *Cruz & Kayser, 2019*[55]

According to the European Medicines Agency (EMA), Kadcyla® is indicated for early breast cancer adjuvant treatment of adult patients with HER2⁺ BC who have residual invasive disease, in the breast and/or lymph nodes, after neoadjuvant taxane-based and HER2-targeted therapy. In metastatic breast cancer, Kadcyla®, is indicated for the treatment of adult patients with HER2⁺ BC, or with unresectable locally advanced BC who previously received trastuzumab and taxanes and which have developed resistance to adjuvant therapy.[61]

Most recently, in 2019, trastuzumab deruxtecan (Enhertu®) was approved. It consists of the same anti-HER2 humanized monoclonal antibody, trastuzumab, covalently linked to the exatecan-derived topoisomerase I inhibitor (deruxtecan, DXd), via a protease-cleavable maleimide tetrapeptide-based linker, with a 7.8 DAR.[58] Currently, Enhertu® has a conditional authorization of EMA for the treatment of adult patients with unresectable or metastatic HER2⁺ BC who have priorly received two or more anti-HER2 based regimens.[62]

Trastuzumab-vcMMAE (T-MMAE) is another trastuzumab derived ADC that uses the cytotoxic payload monomethyl auristatin E (MMAE), a mitotic inhibitor that inhibits cell division by disrupting microtubules.[63] This ADC has been used in clinical trials since 2015 with promising results, but it has not yet been approved.[58]

Small-Molecule Tyrosine Kinase Inhibitors

Small-Molecule Tyrosine Kinase Inhibitors (TKI) are small membrane-permeable synthetic compounds that block or compete with the ATP binding site of the catalytic domain of several oncogenic tyrosine kinases, thus inhibiting the intracellular downstream signaling cascade stimulated by a receptor, blocking tumor growth. Although tyrosine kinase inhibitors can target both intra- and extracellular domains of EGFRs, they show a lower specificity when compared to mAbs, which can translate in a higher toxicity. Additionally, TKIs were found effective to target different cell-signaling pathways associated with BC, as the MAPK/ERK, PI3K/AKT, signal transducer and activator of transcription 3 - STAT3 and protein kinase C - PKC pathway. Hence, TKI treatment also reduces the chances of eventual drug resistance development due to cross-signaling of the referred pathways.[34,51,64]

TKIs are often used as adjuvant therapy to chemotherapy and trastuzumab as it lowers recurrence rate in HER2⁺ BC. The most used TKIs in BC are lapatinib (Tykerb®), neratinib (Nerlynx®) and tucatinib (Tukysa®).[65]

1.3. The Role of Tumor Microenvironment

Treating cancer has been challenging, partly because of the complexity and phenotypic heterogeneity of tumors, often leading to resistance to standard therapies. This complexity reflects the interaction between the tumor cells and their microenvironment (Figure 1.7).[66,67] The tumor microenvironment (TME) consists of stromal cells (such as fibroblasts and mesenchymal cells), endothelial cells (EC), and immune cells (both adaptative immune cells such as lymphocytes and innate immune cells, such as macrophages and dendritic cells). The complex interaction and molecular crosstalk between these different cell types influence and support the physiopathology, structure, development and progression of the tumor.[68,69]

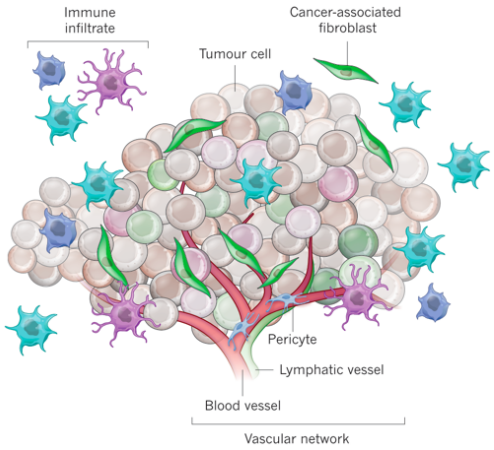

Figure 1.7. Cellular heterogeneity of the tumor microenvironment. *Junttilla & De Sauvage, 2013*[70]

Besides the expansion of neoplastic cells, non-transformed cell types dynamically co-evolve with the tumor cells, so that both continuously participate in the changes inherent to the process of tumorigenesis. The orchestration of these changes involves recruitment of fibroblasts, matrix remodeling, development of vascular networks by endothelial cells and migration and activation of immune cells. Additionally, an adaptive, continuous molecular crosstalk exists between tumor cells and their surroundings, mediated not just by direct cell contact with stromal and immune components, but also through secreted signaling factors such as cytokines, chemokines and growth factors.[70] These interactions, together with other selective pressures such as hypoxia, acidity and nutrients availability, actively shape the tumor development.[70]

Next, an overview of some of the most relevant TME components is presented.

1.3.1. Tumor Stroma

Fibroblasts are an abundant mesenchyme-derived cell type that maintains the structural framework in tissues. Quiescent fibroblasts differentially respond to damage, such as wounding, and become activated to support tissue repair. Although normal fibroblasts typically suppress tumor formation, cancer-associated fibroblasts (CAFs) can significantly promote tumorigenesis through provision of various growth factors, hormones and cytokines. CAFs are the most prominent cell type within the tumor stroma of many cancers; they are reported to stem from resident local fibroblasts, bone marrow-derived progenitor cells or trans-differentiating epithelial cells.[67] Compared with normal tissue fibroblasts, CAFs have increased proliferation, enhanced extracellular matrix production and unique cytokine secretion (for example stromal cell derived factor 1 - SDF1, vascular endothelial growth factor - VEGF, platelet derived growth factor - PDGF and hepatocyte growth factor - HGF). In addition, CAFs have been associated with extensive tissue remodeling mediated by augmented expression of proteolytic enzymes, deposition of extracellular matrix and induction of pathogenic angiogenesis by liberating pro-angiogenic factors within the matrix. As such, the abundance of stromal cells correlates with increased aggressiveness and poor prognosis.[70,71]

1.3.2. Vasculature

The tumor vascular network is dynamic and can either limit or support tumor growth. Vascular networks are derived through formation of new vessels (angiogenesis), modification of existing vessels within tissue,

or recruitment and differentiation of endothelial precursors from bone marrow (vasculogenesis), all of which contribute to vascular heterogeneity. Uneven vascularization and differences in vascular maturity combined with a lack of drainage due to poor lymphatic vessel coverage contributes to the complex topography and variable interstitial pressure within tumors. Inadequate function of poorly organized tumor vasculatures results in areas of hypoxia and limited nutrient supply that promote oncogenic pathways. Moreover, distance from blood vessels generates a gradient that is crucial in the impairment of drug distribution to all cells within the tumor.[68,70]

1.3.3 Tumor Immune Component

Usually, the immune cells cooperate to recognize foreign substances (e.g., pathogens) and protect tissues from infection and damage. However, both the innate and adaptive immune systems have been implicated not only in preventing but also, if dysregulated, in promoting tumor growth through different mechanisms.[72] Immune cell recruitment and localization within the tumor vary widely and are influenced by various cues, including factors secreted by CAFs, the extent and permeability of the vasculature, and the tumor cells themselves.[67] These clues can lead to the generation of an immunosuppressive microenvironment and continuous engagement of inhibitory receptors on T-cells, preventing antitumor T-cell response.[70] B-cells may either suppress or support T-cell function, resulting in differential effects on tumorigenesis. B-cells also promote tumor progression by enhancing pro-tumoral inflammation.[70] At this point, recruitment of immunosuppressive myeloid lineages (such as neutrophils, dendritic cells and monocytes) to the tumor site, not only suppresses adaptive immunity but also fosters angiogenesis through the secretion of VEGF, basic fibroblast growth factor - bFGF and transforming growth factor batea - TGF-β. Furthermore, mast cell recruitment has been implicated in tumorigenesis and angiogenesis, and tumor-associated macrophages can also drastically support tumor progression once polarized into an M2 phenotype.[70]

1.4. Experimental Models in Cancer Research

Cancer is a complex heterogeneous disease that encompasses diverse cell types, ECM components, and numerous soluble factors. To recapitulate the TME is not easy and indeed is one of the most challenging tasks in experimental cancer modeling, but simultaneously one of the most relevant ones to assure the representativeness of the model.

The models classically used in cancer biology and drug discovery are generally highly reductionist and do not represent accurately the drug response observed in the patient.[73] These cancer models do not incorporate the complexity or heterogeneity of a human tumor *in situ*. As such, around 95% of new anticancer drugs eventually fail in clinical trials, showing lack of efficacy (despite robust indications of activity in existing *in vitro* and *in vivo* pre-clinical models), which is the major motive for failure in phase 2.[74,75]

Innovative models that better capture human tumor biology are thus required. Here, a summary of the characteristics, with both advantages and limitations, of classical and innovative cancer models are described, namely 2D and 3D models, *ex vivo* and *in vivo* patient-derived models and a description of controlled culture systems.

1.4.1. 2D and 3D Cancer Models

1.4.1.1. 2D Cancer Models

Since HeLa cell line establishment in 1951, cell culture was introduced as a tool to screen *in vitro* compounds with antitumor activity, using cells grown and passaged indefinitely on plastic surfaces, in semisynthetic medium. However, the correlation between *in vitro* culture, *in vivo* results, and clinical responses was very poor.[73] Nevertheless, the introduction of a panel of 60 cell lines by National Cancer Institute (NCI-60) and the sequencing and characterization of human genome in recent decades has led to the establishment of more comprehensive panels of cell lines that could be used by researchers around the globe. It has been shown that cancer cell lines retained the genetic properties of the original cancers, and that most of the oncogenic alterations identified in tumor tissues are also present in cancer cell lines.[76] Experimental data generated using these lines allowed for more coherent and systematic studies that deepened the mechanistic knowledge on cancer.[77]

To date, monolayer 2D tumor cell cultures growing in plastic remain a valuable tool to dissect molecular pathways. However, as referred above, the tumor is described by a complex and heterogeneous environment that is not only composed by tumor cells, but also immune cells, stromal cells, endothelial cells, and others. As such, co-cultures with other tumor-associated cells as fibroblasts, macrophages or endothelial cells allowed for the introduction of tumor stroma components, with increasing model complexity and recapitulation of the tumor microenvironment.[73]

1.4.1.2. 3D Cancer Cell Models

Without neglecting that current 2D models still have their space, even complex 2D co-culture models still ignore an important feature, which is that solid tumors grow in three dimensions (3D).[77]

While migration in 2D is governed by classic polarized signaling and mechanical patterns that are often not crucial for effective migration, in 3D there are more modes of motility that are very complex and take into consideration ECM stiffness and geometry.[78] As a consequence, it has been shown that 2D systems result in cell metabolism and physiology that is different from the *in vivo* response.[73] For instance, some important cancer cell features (such as morphology, genetic profile or tumoral heterogeneity, or even ER signaling in the specific case of BC) are not correctly modeled in 2D cultures. The 3D cell culture platforms help to circumvent these limitations by preserving the tridimensional arrangement of cancer cells.[69]

Over the years, several techniques have been developed to cultivate cells in 3D (Figure 1.8), which include:

- Liquid overlay technique, which prevents cells from attaching to the vessel surface using a non-adherent coating (ex. ultra-low attachment plates with round bottom), [73]
- Aggregating cells by gravity, at the bottom of a drop ("hanging drop"), [73]

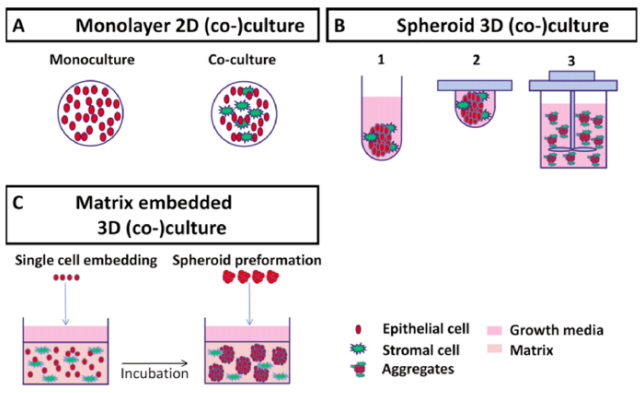

Figure 1.8. Two- and three-dimensional cell culture systems. (A) Conventional 2D monolayer (co-) culture. (B) Spheroid 3D (co-) cultures: (1) Non-adhesive coating; poly hema, ultra-low attachment or agarose, (2) hanging drop method, (3) stirred tank-based culture. (C) Matrix embedded 3D (co-)cultures either derived from single cells or pre-formed spheroids. Adapted from *Hickman et al., 2014.* [73]

- Creating spheroids in stirred-tank culture systems, such as spinner flasks, or stirred-tank bioreactors, by preventing cells in suspension from settling and by promoting cell-to-cell collisions via constant stirring. [73]

After initial aggregation, cells generally start to secrete extracellular matrix (ECM) components and upregulated proteins mediating cell–cell interactions and contacts.[73] Resultant 3D spheroids are relatively compact and stable microstructures with gradients of proliferating cells, oxygen levels, and nutrition supplies decreasing from the periphery toward the spheroid center. These physiological characteristics of the 3D spheroids closely resemble avascular tumor nodules, micro-metastases, and inter-vascular regions of large solid tumors.[79,80]

A spheroid mono-culture system, however, still lacks the aforementioned diversity of cell types present in TME. Investigators have addressed this issue by mixing tumor cell spheroids with fibroblasts, monocytes, endothelial cells, among others. This resulted in cell-to-cell communication, either by paracrine (secretion of hormones, pro-inflammatory cytokines or ECM components and remodeling enzymes) or by juxtacrine signaling, thus altering cell behavior and recreating an invasive and immunosuppressive TME.[73,81,82] Among several studies, *Singh et al., 2016* [79] have shown that heterotypic cell–cell and cell-ECM crosstalk promote 3D spheroid formation and affect inter-cellular signaling and gene expression of tumor cells, resulting in altered tumor cell proliferation and migration. Nevertheless, extensive characterization and validation of the 3D spheroid models for different cancer pathologies is still required in order to understand how closely they resemble the biological properties of *in vivo* tissue, including growth kinetics, gene expression, the architecture of signaling cascades, and drug treatment responses.[73,74]

Although the referred arguments might suggest that 3D culture should always be used, the lack of a universal 3D model appropriate for every application, together with the ease of manipulation of 2D culture are the main reasons why the platform of choice is most often dictated by the specific application intended and the object of interest. [69]

1.4.1.3. Scaffold-Based Approaches

As aforementioned, ECM represents a key aspect of TME.[82] As such, models based on tumor cell spheroids freely floating in liquid medium are unable to accumulate ECM produced and remodeled by the different cell types of the TME.[83]

Scaffolds are 3D structures produced from materials with tunable porosities, permeability, surface chemistry, and mechanical properties to serve as a surrogate of the ECM and 3D architecture. Due to their porosity, scaffolds provide a mechanical support for single cells or spheroids and provides support for accumulation of secreted ECM. A particular class of scaffolds, the hydrogels, are comprised of networks of cross-linked polymer chains or complex protein molecules of natural or synthetic origin.[83,84] Due to their significant water content, hydrogels possess biophysical characteristics similar to natural tissue, and serve as effective matrices that were shown to affect stem cell differentiation, tumor progression, invasion and drug sensitivity.[82,85]

Assays including ECM components such as collagen may be performed in 2D, by coating plates with the ECM proteins, or in 3D, with spheroids embedded into scaffolds, or sitting on top of a gel matrix. Due to the above outlined advantages of growing cells in three dimensions, and the impact of matrix stiffness on cell growth and differentiation, 3D scaffold-based approaches are nowadays preferred by some.[74,79] Commonly used matrices in 3D cell culture are animal derived as collagen I and Matrigel® or similar, laminin-rich

basement membrane extracts (BME) purified from Engelbreth–Holm–Swarm (EHS) mouse sarcoma, composed mainly of laminin-111, collagen IV, and heparan sulfate proteoglycans.[73]

Regarding matrices of non-animal origin, alginate is among the most used matrices for 3D culture applications.[86] Alginate is an inert polysaccharide derived from brown algae that has been applied in industries as food, textiles and pharmaceuticals.[87] Alginate consists of β-D-mannuronic acid M units and α-L-guluronic acid G units assembled as block copolymers. Alginate is notable for its ability to form hydrogels via ionic crosslinking. The crosslinks of alginate are formed using divalent cations such as calcium, magnesium, or barium to promote the formation of ionic bridges between alginate G units. Ion chelation with an isotonic solution, allows easy hydrogel dissolution and cell harvesting for downstream applications.[85,86] Due to the outlined advantages, these models are therefore excellent tools to bridge the gap between oversimplified 2D systems and unrepresentative animal models.[84] Indeed, *Cavo et al.*[88] have reported dramatic morphological differences between cells cultured in a 3D alginate model *versus* flat 2D conditions, namely exhibiting a circular, spheroid-organized conformation within the hydrogel, similar to those *in vivo*. Moreover, it was described a strict correlation between substrate elasticity and cell viability and proliferation, highlighting the need for realistic incorporation of original tissue stiffness for correct recapitulation of BC cell activity that dictates therapy response. Another example is the work by *Thakuri et al.*[89] on a 3D hybrid hydrogel system composed of collagen and alginate to examine the invasive capability of BC, where the authors demonstrated its application for migration studies with mammary fibroblasts and BC cell co-cultures. In the host Lab, *Estrada et al.*[82] have reported that alginate-microencapsulated 3D co-cultures of breast cancer cells with fibroblasts shows phenotypic features of TME as loss of cell polarity, increased cell migration and angiogenic features, which are characteristic of BC disease progression.

1.4.2. *Ex vivo* Patient-Derived Models

Ex vivo culture of patient-derived tumor tissues provides the opportunity to study the molecular and phenotypic heterogeneity of cancer cells in the context of a preserved TME that faithfully recapitulate a patient tumor. The maintenance of other cell types of the particular tissue as well as the ECM, results in the conservation of naturally occurring interactions between tumor and non-tumor cells in the TME.[85]

Given the influence of the tumor heterogeneity and environment on several aspects of tumor biology and drug sensitivity, these models appear more suitable to study patient tumors than established immortalized cell lines. In fact, tumor tissue culture has the potential to cover the whole clinical spectrum of solid tumors including all stages and grades from well-differentiated slow growing to poorly differentiated fast-growing subtypes. In contrast, most cell lines represent only high-stage, metastatic and poorly differentiated tumors. Consequently, short-term cultivated tumor tissue could mirror more closely the typical intra- and inter-tumoral variability of solid tumors typically, including proliferative aspects as well as the response to drug treatment, stepping into the personalized medicine field.[73,75]

1.4.2.1. Organoids

Patient-derived organoids (PDO) are derived from patient tissue cells or tumor specific stem cells and have the capacity to self-organize into 3D tissue-resembling cellular clusters.[92] In comparison to other culturing techniques, organoids allow cell expansion, and as such, they are feasible for medium to high-throughput drug screening on personalized medicine. By mimicking tumor characteristics such as tumor cell heterogeneity and tumor cell intrinsic mechanisms of resistance, they can aid in the prediction of treatment response by functional *ex vivo* assays and patient stratification.[75,92,93] However, organoid models still fail to

fully capture tumor-stromal interactions which influence drug sensitivity and resistance and are important for immune-oncology research. As such resistance mechanisms derived from TME are not recapitulated in these models.[92,93] Culturing techniques of PDOs can include static or dynamic systems.[93–95]

1.4.2.2. Patient-Derived Explants (PDEs)

PDEs have been in use since the 1950s[96] and correspond to fragments of freshly resected human tumors without deconstruction of the tumor, thus retaining the histological features of the original tumor. This model represents a bridge between *in vitro* and *in vivo* models, combining the *in vivo* features of microenvironment, original tissue architecture and possibly impaired diffusion of oxygen and nutrients, with the feasibility and ease of manipulation and analysis of *in vitro* models.[97]

By using PDEs, it is also possible to investigate drug penetrance into the original tumor tissue using mass spectrometry imaging (MSI).[96] Additionally, the generation and culture of PDEs is also relatively inexpensive compared with the production and maintenance of mouse models or the isolation and culture of organoids, which often require costly cell culture reagents and matrices for their maintenance. However, perhaps the most significant downside relates to the limited material and unfeasibility for expansion, as well as intrinsic patient heterogeneity. In addition, some concerns have been raised, namely regarding maintenance of tissue architecture, viability and ER signaling for longer periods.[96] These disadvantages should be address by optimizing culture conditions as it previously demonstrated by *Muraro et al.,*[90] where by using a perfusion-based bioreactor combined with a collagen scaffold, BC tissue was cultured for 14 days with maintenance of viability and ER^+ cells. Most recently, published work from the host Lab by *Cartaxo et al*.[91] has described successful culture of PDEs for one month, while retaining ER signaling and original tumor architecture.

1.4.2.3. Organotypic Tumor Tissue Slices

Organotypic tumor tissue slices are obtained through the use of microtomes (specifically designed precision cutting instruments), without interfering with the morphology of the tissues.[73] This model retains the complexity of tumors without the need of extensive manipulation. Short-term culture of organotypic tissue slices could serve as a model to examine response of the tumor to anti-cancer compounds *ex vivo*. Tumor tissue slices are usually cultured statically on the bottom of a dish, freely floating in culture medium or frequently grown on membrane supports (air-liquid interface) such as filters or collagen coatings. Moreover, agitation improved diffusion of oxygen and nutrients, which was able to redeem breast tumor slices vital for 7 days, in comparison to 48h for slices cultured in static conditions.[75] Indeed, preservation of tumor slices for extended periods without losing tumor viability, has proven difficult and leads to significant alteration of several stress pathways and loss of tissue integrity.[75]

1.4.3. Animal Models

The inability of the previous models to examine complete pathophysiological interactions between the tumor site and distant organs represent a major limitation of the *in vitro* and *ex vivo* models.[72] The use of animal models to study cancer overcomes this limitation as it allows to recreate tumor development and progression in a systemic model.[69] Consequently, their use has greatly impacted our understanding of the processes governing initiation, progression and metastasis and allowed the discovery and pre-clinical validation of novel cancer treatments.

Distinct animal models can be used in cancer research. Over the last decades the most common specie used was the mouse (*Mus musculus)*. However, other models have also been applied, including the zebrafish (*Danio rerio*), and the common fruit fly (*Drosophila melanogaster)*. A variety of approaches can be applied depending on the aim of the study. Importantly, mice and human genomes share a high degree of homology, and there is an overlap in the function of their genes. Moreover, as mice have a shorter lifespan, it makes possible to study development and progression of diseases such as cancer in a feasible period of time.[98]

Within mice models, we can summarize them in 5 classes: (1) Cell Line-Derived Xenografts (CDX), (2) Patient-Derived Xenografts (PDX), (3) Syngeneic mouse models, (4) Chemically Induced Mouse Models (CIMM), and (5) Genetically Engineered Mouse Models (GEMM). In the context of this thesis, only the Patient-Derived Xenografts will be addresses, due to their similarity with previously mentioned patient-derived models, here *in vivo*.[98]

1.4.3.1. Patient-Derived Xenografts (PDXs)

PDX models involve implanting a piece of fresh tumor removed from a patient at primary surgical excision into immunodeficient or humanized mice allowing tumor amplification and *in vivo* testing. PDXs have been shown to reliably preserve genetic, histological and phenotypical characteristics of the primary tumor with a 60 to 80% graft success rate, while reflecting histopathology, tumor behavior, and the metastatic properties of the original tumor.[72,99] As such, PDX models provide a valuable platform for culture of rare tumor subtypes allowing to study its biological mechanisms and to assess subtype-specific responses rates of anti-cancer agents validating preclinical studies.[97]

Subcutaneous heterotopic implantation (tumor implanted into an area unrelated to primary tumor site) is the most common method of PDX used in cancer with advantages that tumor growth can be monitored by visual inspection or examination avoiding the need for imaging techniques, although it is not representative of the original tumor localization and environment which can impact the observed effects.[98] Orthotopic transplantation (tumor implanted into site of primary tumor) have the advantage of mimicking invasion and metastatic spread and therefore recapitulate disease natural history as well as tumor characteristics. They therefore strengthen the utility of PDX models in pre-clinical studies aimed at evaluating molecular pathways and drug responses in advanced disease.[75,97]

Nevertheless, the requirement of immunodeficient mouse strains impairs the study of the anti-tumor host immune response, constituting a problem when the aim of a particular study is focused in immunomodulatory mechanisms, one of the major players of the tumor microenvironment.[98]

1.4.4. Bioreactors and Controlled Culture Systems

In order to increase the relevance of the *in vitro and ex vivo* tumor modeling approaches discussed above, a more complex recreation of the TME composition and architecture could be achieved through utilization of controlled culture systems that combine fluidic motion with a 3D setup. [73,100]

Bioreactors are computer-controlled culture systems designed to provide efficient mass transfer and automated control of culture variables such as temperature, pressure, pH, or dissolved oxygen. Furthermore, the use of perfusion

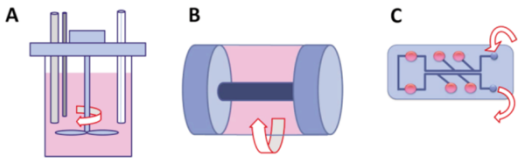

Figure 1.9. Bioreactor systems for culture of in vitro tumor models. *(A) Stirred culture vessels; (B) Rotary cell culture systems; (C) Microfluidic devices. Hickman et al., 2014*[73]

operation modes allows control of nutrients and O_2 levels, supply and clearance of metabolites, cytokines, growth factors and ECM components.[73,101]

In recent years, bioreactor development has been towards improved accuracy in control of cellular microenvironment with reduced shear stress and reduced working volumes. Currently, the range of bioreactor types (Figure 1.9) with potential application in cancer *in vitro* models is wide: from classical stirred-tank culture vessels to rotary cell culture systems (RCCS) and last-generation microfluidic devices.[73]

1.4.2.1. Stirred-tank Culture Systems

Cell culture in stirred-tank systems have two main objectives: cell expansion and improved cell functionality.[83] This technology includes spinner vessels and computer-controlled stirred-tank bioreactors, and provide a dynamic environment, control of substrate consumption/metabolite production, cell growth, pH, temperature, and gas transfer limitations, as well as culture heterogeneity.[73,79,83]

Manipulation of parameters such as vessel and impeller design and stirring rate allow applicability to an array of cell types with distinct aggregative capabilities and sensitivities to shear stress. Indeed, bioreactor-engineered cancer tissue-like structures have been described to more closely mimic phenotypes, gene expression profiles and drug resistance patterns observed *in vivo* than static cultures, providing an interesting platform for BC therapy studies.[102] Another important feature is the feasibility to perform non-destructive sampling along time, enabling continuous monitorization as well as retrieval of material for further applications. [73,81,103] Importantly, stirred-tank bioreactors are highly flexible, and can accommodate different 3D culture strategies, from freely floating spheroids, to scaffold-based mono- and co-cultures.[73,82,104]

The main limitations of stirred-culture vessels are the hydrodynamic shear force-related cellular stress, promoted by stirring, and the culture volumes associated with these systems (typically a minimum of 50 to 80 mL). Microencapsulation and scaffold strategies can minimize cell shear-stress and improve TME recapitulation by accumulation of secreted factors and ECM components, as previously described.[85,105]

1.4.2.2. Organs-on-a-Chip

Recent advances on microfluidic devices have led to the development of organs-on-a-chip. These models are based in tissue engineering and microfluidics, enabling the design of customized cellular microenvironments with precise fluidic, mechanical and structural control.[106] These translates in specific architectures within a microfabricated device, facilitating the creation of 3D models that allow culture of cells under continuous perfusion, exhibiting functional hallmarks of native tissues (for example, contractile properties of cardiomyocytes or albumin secretion of hepatic cells).[73,84,107]

Organ-on-a-chip technologies aim to replicate key aspects of human physiology as 3D cell-cell and tissue-organ interactions, crucial for the understanding of drug effects, improving pre-clinical safety and efficacy testing. The primary focus of this technology is the re-creation of three key aspects of human physiology: the multicellular vascular or epithelial interfaces of organs (which function as barriers in tissues), the tissue-level organization of parenchymal cells (which are responsible for the key functional properties of an organ), and the systematic interaction of multiple organs (which determine drug pharmacokinetics: absorption, distribution, metabolism and elimination).[107,108]

1.5. Thesis Aim

Within the scope of the increasing BC resistance and the continuing failure of most drugs in clinical development due to lack of efficacy (despite robust indications of activity in existing pre-clinical models), the urging need for improvement of BC models for drug testing served as motivation for this work. Specifically, the need for cell models more recapitulative of the TME to serve the discovery and development of novel BC therapies. Improved *in vitro* and *ex vivo* models and their application in drug development will contribute to the implementation of the 3R's (replace, reduce and refine policy)[109] for animal experimentation in medical research. Bearing this in mind, the main aim of this thesis was to assess the amenability of 3D BC models developed in the host Laboratory for pre-clinical evaluation of targeted therapies has a proof-of-concept. For this end, two distinct objectives were purposed:

- The first objective comprised the assessment of the therapeutic potential of HER2-targeted drugs, namely of trastuzumab-derived Antibody-Drug-Conjugates (ADCs), using a 3D BC model, previously established in the host Lab. [82]
  BC spheroids were generated and microencapsulated using a hydrogel scaffold (alginate). Assay conditions, such as challenge duration, drug concentrations and readouts were established. The 3D BC model was challenged with the standard of care anti-HER2 targeted therapy, trastuzumab, and its ADC derivatives to evaluate the effect of these drug conjugates, by using cell viability, metabolic activity, apoptosis and cytotoxicity assays.

- The second objective consisted in the assessment of endocrine therapy compounds, such as standard-of-care anti-ER drugs, employing an *ex vivo* ER^+ BC patient-derived explant model recently established in the host Lab. [91]
  For this, tumor tissues from ER^+ BC patients were obtained by surgical resection, processed, encapsulated in a hydrogel scaffold, and cultured under agitation. Explant cultures were stimulated with the estrogen agonist 17β-estradiol and maintenance of *ER* signaling evaluated by protein and mRNA levels. Effect of endocrine drugs tamoxifen and fulvestrant was assessed by *ER* and downstream effector gene analysis.

Chapter 2. Materials & Methods

2.1. *In Vitro* 3D BC Cell Model

2.1.1. Cell Line 2D Culture

Established cell lines of triple negative breast cancer HCC1806 (ATCC® CRL-2338™) and HER2 overexpressed HCC1954 (ATCC® CRL-2338™) were cultured in Roswell Park Memorial Institute (RPMI) 1640 medium, supplemented with Fetal Bovine Serum (FBS), HEPES Buffer, 2-Mercaptoethanol and Penicillin-Streptomycin, according to Table 2.2.

Cells were cultured in a humidified incubator at 37 °C and 5% CO_2 (Nuaire Autoflow IR Water-Jacketed CO_2 Incubator). Cells were subcultured twice a week at a seeding concentration of 15 000 cell/cm^2 (HCC1806) or 8 000 cell/cm^2 (HCC1954).

Table 2.2. Culture media composition for cancer cell lines.

Medium Component	Concentration	Brand	Cat. Number
RPMI 1640 Medium [–] Phenol Red	[1X]	Gibco™	#11835-063
Fetal Bovine Serum	10% (v/v)	Gibco™	#A3160801
HEPES Buffer	6 mM	Gibco™	#31350-010
2-Mercaptoethanol	50 µM	Gibco™	#31350-010
Penicillin-Streptomycin	1% (v/v)	Gibco™	#15140-122

2.1.2. Primary Cell 2D Culture

Human Dermal Fibroblasts (hDF) isolated from neonatal foreskin samples (Innoprot, #P10856) were grown in Iscove's Modified Dulbecco's Medium (IMDM) with GlutaMAX™ Supplement, and additional supplementation of FBS and Penicillin-Streptomycin, according to Table 2.3. Cells were subcultured every 2 weeks, at a seeding concentration of 4 300 cell/cm^2 and total medium changed by new every week. Cells were cultured in a humidified incubator at 37 °C and 5% CO_2 (Nuaire Autoflow IR Water-Jacketed CO_2 Incubator).

Table 2.3. Culture media composition for primary fibroblast cultures.

Medium Component	Concentration	Brand	Cat. Number
IMDM + GlutaMAX™	[1X]	Gibco™	#31980-022
Fetal Bovine Serum	10% (v/v)	Gibco™	#A3160801
Penicillin-Streptomycin	1% (v/v)	Gibco™	#15140-122

2.1.3. Cancer Cell Aggregation

Adherent cultures of HCC1806 and HCC1954 cells were trypsinized, counted with Trypan Blue Solution, 0.1% (Gibco, #15250-061) in a Fuchs-Rosenthal counting chamber (Karl Hecht, #40449712), centrifuged 5 min at 300x g in a 5810R Centrifuge equipped with a A-4-81 rotor (Eppendorf), resuspended in an appropriate volume of culture medium for the conditions described below, and filtered through a 70 µm cell strainer (Falcon, #352350) to obtain a single cell suspension.

HCC1806 cells were plated in AggreWell™400 microwell culture plates (Stemcell Technologies, #34425), previously treated with Anti-Adherence Rinsing Solution (Stemcell Technologies, #07010), to reduce surface tension and prevent cell adhesion to culture plates and washed with culture medium. Cells were plated at a seeding density of $3.5x10^6$ cell/well (500 cell/microwell) in 4 mL of culture medium and incubated in static conditions in a humidified incubator at 37 °C and 5% CO_2 (Nuaire Autoflow IR Water-Jacketed CO_2 Incubator) for 3 days to induce spheroid formation.

HCC1954 cells were inoculated into 125 mL Glass Spinner Vessels with 70 mm flat center cap, two 32 mm angled sidearms and three side baffles to enhance aeration and agitation of flask contents (Corning, #4500-125), at a final cell concentration of 200 000 cell/mL, and cultured for 4 days at a stirring rate of 80 rpm to induce cell aggregation, using a bioMIXdrive 1 single point stirring drive (2mag AG) with bioMIXcontrol 4MS external control unit (2mag AG) set in a humidified incubator at 37 °C and 5% CO_2 (Nuaire Autoflow IR Water-Jacketed CO_2 Incubator).

The glass surface of the spinner vessels was previously subjected to a silanization procedure with the purpose of reducing surface hydrophobicity and consequently cell attachment. Silanization consisted in a cleaning step with 1M potassium hydroxide, KOH (Merck, #105033) in ddH_2O, overnight, followed by dichloromethylsilane (Merck, #803452) coating and excess solution removal with toluene (Merck, #108325).

The polytetrafluoroethylene (PTFE) impeller of spinner vessels was coated with polydimethylsiloxane (PDMS) to avoid cell infiltration into the impeller's fenestrations during aggregation procedure, by preparing a two components mixture of Elastosil RT601 A (Wacker, #124690) and B (Wacker, #124691) at a ratio of 9:1, and applying the mixture to fill the interior and coat the lateral fenestrations of the impeller. Solidification of Elastosil A and B mixture was obtained by placing the impeller at 37 °C in an ED115 Drying Chamber (WTC Binder), until achieving a smooth surface.

Once aggregation was achieved, cell viability was assessed by FDA/TO-PRO®-3 staining as described in the corresponding section ahead.

2.1.4. Microencapsulated Cancer 3D Spheroid Cultures

Once compact and spherical spheroids were obtained, spheroids were collected, centrifuged at 50x g for 2 min, washed in Dulbecco's phosphate-buffered saline [-] Calcium [-] Magnesium, DPBS $^{(-/-)}$ (Gibco, #14190-094), centrifuged again at 50x g for 2 min and resuspended at a concentration of 20 000 spheroid/mL in 1.1% (w/v) PRONOVA UP MVG Sodium Alginate (NovaMatrix, #4200101), dissolved in 0.9 % (w/v) NaCl (Merck, #106404), which was transferred to a 5 mL luer lock syringe without needle (Terumo, #SS-05L) and assembled on a Syringe Infusion Pump KDS-100 (KDScientific) set at a flow rate of 10.0 mL/h, pumping the alginate solution containing the spheroids, in a controlled manner into the nozzle.

For the co-cultures, hDFs were centrifuged similarly to the tumor cells and resuspended in the alginate solution. This suspension was then used to resuspend the HCC1954 spheroids which were transferred to the syringe. In co-cultures, a ratio of 1 : 1 tumor cells to hDFs was used. To count the number of tumor cells in

the spheroids, these were trypsinized and cells counted with Trypan Blue Solution, 0.1% (Gibco, #15250-061) in a Fuchs-Rosenthal counting chamber (Karl Hecht, #40449712).

Microencapsulation was performed using an electrostatically-driven Encapsulation Unit VarV1 (Nisco). The alginate solution containing the spheroids was passed through a holder arm set to a height of 3 cm, coupled to a 0.7 mm nozzle suspended over a 100 mm petri dish (Corning, #CLS430165) containing the gelling bath (to keep a distance of 1.2 cm from the nozzle to the bath surface).

The gelling bath is composed by a crosslinking solution of 20 mM $BaCl_2 \cdot 2\ H_2O$ (Merck, #101717) / 115 mM NaCl, 5 mM L-Histidine (Sigma-Aldrich, #H9511) in ddH_2O (pH 7.4, 300 mOsm), with a 4.7 kV electrode submerged, that produces an electrostatic force, pulling the droplets and inducing alginate polymerization. A magnetic stirrer bar is placed in the gelling bath to keep encapsulated spheroids separated during alginate polymerization. The obtained microcapsules were washed three times in 0.9 % (w/v) NaCl and equilibrated in culture medium before being transferred to 125 mL Erlenmeyer flasks with 0.2 µm vented caps (Corning, #431143) and cultured under orbital agitation, at 80 rpm, in a humidified incubator shaker at 37 °C and 5% CO_2 (Infors HT Multitron).

2.1.5. Challenge with Antibody Drug Conjugates (ADCs)

A set of monoclonal antibodies and derived ADCs, composed by trastuzumab, heterogeneous conjugated trastuzumab-DM1 (DAR 3), heterogeneous conjugated trastuzumab-MMAE (DAR 4), homogeneous conjugated trastuzumab-MMAE (DAR 8), trastuzumab_cys114 and homogeneous conjugated trastuzumab_cys114 -MMAE (DAR 2), was kindly provided by Dr. Jordi Joan Cairó Badillo and Dr. Joan Miret Minard, from Universitat Autònoma de Barcelona, and sterile-filtered through an Acrodisc Syringe Filter Low Protein Binding 0.2 µm Supor® Membrane (Pall Corporation, #4602). Serial dilutions of each ADC were prepared in culture medium, to get the final concentrations between 0.001 to 10 µg/mL. Twice a week, half of the spent medium was removed and replaced with new culture medium supplemented with fresh compounds and at the required drug concentration.

2D Cell Culture

Cells were plated at the described seeding concentration, in quadruplicates, in standard flat bottom 96-well tissue culture plates (Falcon, #353072), in 100 µL culture medium per well and cultured, under static conditions in a humidified incubator at 37 °C and 5% CO_2 (Nuaire Autoflow IR Water-Jacketed CO_2 Incubator). Exposure to ADCs was started at 24h after plating, for a total of 3 days (HCC1808 and HCC1954 cell lines) or 2 weeks (hDFs). Metabolic activity was assessed after plating and at the end of drug challenge, cell viability and cell apoptosis were assessed at the end of drug challenge.

3D Spheroid Culture

One week after encapsulation, capsules were plated in quadruplicate in standard flat bottom 96-well tissue culture plates (Falcon, #353072), at approximately 25 to 30 capsules *per* well (300 µL capsule suspension), in 100 µL of culture medium, and cultured, under orbital agitation, at 80 rpm, in a humidified incubator shaker at 37 °C and 5% CO_2 (Infors HT Multitron). Metabolic activity was assessed, and drug challenge performed for up to 2 weeks. Metabolic activity and cell viability were assessed before and after drug challenge, up to 2 weeks post challenge.

2.1.6. Metabolic Activity Assessment

Cellular metabolic activity was assessed by PrestoBlue™ Cell Viability Reagent reduction assay (Invitrogen, #A13262), according to the manufacturer's instruction. PrestoBlue™ assay is based on resazurin reduction, a blue, non-toxic, membrane-permeable compound. Once it is reduced to resorufin, a red fluorescent compound, by aerobic respiration within mitochondria by NADH or NADPH dehydrogenase, it serves as an assessment of metabolic activity and indicator of cell viability.

Cells were washed in DPBS $^{(-/-)}$ and incubated with PrestoBlue™ diluted 1/10 in culture medium for either 30 mins (2D cultures) or 4 h (3D cultures) at 37 ºC. A control with only diluted reagent was kept in the same conditions. After incubation, 100µL of culture medium containing PrestoBlue™ [1X] was transferred to a flat-bottom 96-well Black Plate (Costar, #3603), and resazurin fluorescence was read at 560 nm excitation with 590 nm emission wavelength on an Infinite® 200 PRO Micro Plate Reader (Tecan Life Sciences). The mean fluorescence of the only medium control was subtracted from each replicate and condition, and the mean value of each day of each condition was normalized by day 0 (before ADCs challenge). Metabolic activity is represented as percentage of each condition relative to untreated condition (control).

When repeated cycles of challenge were applied, the remaining medium with PrestoBlue™ reagent was removed from cells, which were washed in DPBS $^{(-/-)}$ and returned to culture conditions,

2.1.7. Cell Viability Assessment in 2D Cell Culture

In 2D cell cultures, cell viability was assessed through the crystal violet assay, that identifies live cells and removes dead ones in washing steps. After exposure to ADCs, medium was removed, cells were fixed in Formalin Solution 10% Neutral Buffered (Sigma-Aldrich, #HT5012) for 10 min, repeatedly washed with DPBS $^{(-/-)}$ and stained with 10% Crystal Violet (Merck, #115940) in 20% Methanol (Merck, #106018), for 20 min, under orbital agitation. After staining, excess dye was removed by repeated washes with ddH_2O and the plate was let to dry. After complete drying, crystal violet crystals were dissolved in 10% Acetic Acid (Glacial) (Merck, #100063) under orbital agitation, until obtaining a homogeneous solubilized crystal violet solution. Plate absorbance was measured spectrophotometrically at 595nm, in an Infinite® 200 PRO Micro Plate Reader (Tecan Life Sciences). Cell viability is represented as percentage, of each condition relative to untreated condition (control).

2.1.8. Cell Viability Assessment in 3D Cell Culture

In encapsulated spheroid cultures, cell viability was assessed through a fluorescent membrane integrity assay to discriminate live from dead cells. Spheroids (either encapsulated or non-encapsulated) were incubated with 5 µg/mL Fluorescein Diacetate, FDA (Sigma-Aldrich, #F7378) from 5 mg/mL FDA in acetone (Sigma-Aldrich, #32201) and 1 µM TO-PRO®-3 Iodine (Invitrogen, #T3605) in DPBS $^{(-/-)}$ and observed in a DMI6000B fluorescence microscope (Leica Microsystems).

Fluorescein diacetate (FDA) is a cell-permeant viability probe, an esterase substrate which is hydrolyzed by intracellular esterase in live cells, generating a fluorescent compound. As such, cell-membrane integrity is required for FDA-fluorescent product retention. TO-PRO-3® Iodide is a carbocyanine monomer nucleic acid, impermeant to live cells but that penetrates dead cells with compromised membranes. Cells that accumulated the fluorescent green metabolized product of FDA were considered live and red cells, stained with TO-PRO-3® Iodide, were considered dead.

2.1.9. Cell Apoptosis Assessment

In encapsulated spheroid cultures from both cancer cell lines, apoptosis was assessed trough the NucView® 488 Caspase-3 Apoptosis Assay Kit (Biotium, #30062). The methodology used to assess apoptosis in culture is based on a green non-fluorescent caspase-3/7 recognition sequence DEVD that, when cleaved by activated caspases during the apoptosis process, binds DNA and becomes fluorescent. At the same time, live cells were visualized through MitoView™ 633. This is a cell membrane permeable far-red fluorescent mitochondrial dye, that becomes brightly fluorescent after accumulation in mitochondria. Cells presenting far-red fluorescence, from MitoView™ 633, were considered alive and cells presenting green fluorescence, from NucView® 488, were considered late apoptotic cells.

Cultures were incubated in culture medium with [1X] NucView® 488 Caspase-3 Substrate (Biotium, #99949) and [1X] MitoView™ 633 Mitochondrial Dye (Biotium, #99950) for 15 min at 37 °C before observation under a DMI6000B fluorescence microscope (Leica).

2.1.10. Cytotoxicity Assessment

In encapsulated HCC1954 spheroid cultures, cytotoxicity was analyzed by the CyQUANT™ LDH Cytotoxicity Assay (Invitrogen, #C20301) which quantifies the release into cell culture medium of a cytosolic enzyme, lactate dehydrogenase (LDH), upon damage of the plasma membrane. The extracellular LDH is quantified by a coupled enzymatic reaction in which LDH catalyzes the conversion of lactate to pyruvate via NAD^+ reduction to NADH. Oxidation of NADH by diaphorase leads to the reduction of iodonitrotetrazolium (INT) salt to a red formazan product that can be measured spectrophotometrically at 490 nm.

LDH leakage was measured in medium collected from cultures and maximum LDH activity was measured from the same samples after total cell lysis, obtained through exposure to Triton™ X-100 (Sigma-Aldrich, #T-8787) 10% (w/v) in ddH_2O for 24 h. Samples for either spontaneous LDH or maximum LDH activity assessment were centrifuged at 1 000x g for 5 min, and 50 µL of supernatant transferred to a 96-well culture plate (Falcon, #353072). An equal volume of Reaction Mixture (50 µL, composed of Substrate Mix combined with Assay Buffer reconstituted in ddH_2O according to the supplier's protocol) was added and the reaction was incubated under orbital agitation, for 30 min, protected from light. An equal volume of Stop Solution (50 µL) was added and the absorbance at 490 nm and 680 nm (background signal from instrument) measured.

LDH activity was determined by subtracting the 680 nm (background) to the 490 nm absorbance value. The mean differential absorbance of the control was subtracted to each replicate and condition, assayed in quadruplicate. LDH activity represents the ratio of LDH leakage activity over the total LDH activity (maximum + leakage). Each value is represented as fold change of each condition relative to untreated condition (control), which was set as 1.

2.1.11. Immunofluorescence in 2D Cultures

Fixation

HCC1954 cells and hDFs were cultured as monolayers on 13 mm glass coverslips (VWR, #631-1578) in a 24-well culture plate (Falcon, #353047), according to the adherent culture systems section. After four days, medium was removed, and cells fixated for 20 min with 4% (v/v) paraformaldehyde (PFA) (Fluka, #762470) + 4% (v/v) sucrose (Sigma-Aldrich, #S9378) prepped from 8% (w/v) PFA, 40% (w/v) sucrose in ddH_2O with DPBS (-

$^{/-)}$ [10X] (Invitrogen, #14200067), pH 7.2, and sterile-filtered through an Acrodisc Syringe Filter Low Protein Binding 0.2 µm Supor® Membrane (Pall Corporation, #4602).

Permeabilization

Cells were washed with DPBS $^{(-/-)}$ and permeabilized for 10 min with 0.1% (v/v) Triton™ X-100 in DPBS $^{(-/-)}$ prepped from Triton™ X-100 (Sigma-Aldrich, #T-8787) 10% (w/v) in ddH_2O.

Blocking

Cells were washed with DPBS $^{(-/-)}$, followed by blocking for 20 min with 0.2% (v/v) Fish Skin Gelatin (FSG) in DPBS $^{(-/-)}$ prepped from gelatin from cold water fish skin (Sigma-Aldrich, #S4521) 10% (w/v) in ddH_2O.

Antibody Incubation

Incubation of antibodies was performed on a dark chamber humidified with soaked filter paper. Primary antibody described in Table 2.4 was diluted in 0.125% (v/v) FSG and added directly to the parafilm. Coverslips with cells were washed with DPBS $^{(-/-)}$ and transferred facing primary antibody solution placed on parafilm, and left to incubate overnight at 4 °C. As a control DPBS $^{(-/-)}$ was used instead of antibody. Cells were washed with DPBS $^{(-/-)}$ by dilution / aspiration and coverslips transferred to new parafilm containing the secondary antibody described in Table 2.5, diluted in 0.125% (v/v) FSG and left for incubation for 1 h.

Table 2.4. Primary antibody used for immunofluorescence.

Primary Antibody	Brand	Cat. Number	Host	Dilution
Anti-Human c-erbB-2 [HER2]	Dako	#A0485	Rabbit – IgG (Polyclonal)	1 : 200

Table 2.5. Secondary antibody used for immunofluorescence.

Secondary Antibody	Brand	Cat. Number	Host	Dilution
Anti-Rabbit Alexa Fluor 488	Invitrogen	#A11008	Goat – IgG (Polyclonal)	1 : 500

Mounting

Cells were washed with DPBS $^{(-/-)}$ and coverslips mounted on microscope slides (VWR, #631-1559) with ProLong™ Antifade Mountant with DAPI (Invitrogen, #P36941). Slides were left to dry at RT covered from light and then stored at 4 °C. Image acquisition was performed at a DMI6000B fluorescence microscope (Leica).

2.1.12. Statistical Analysis

Data from N independent experiments (or technical replicates if N=1) are expressed as mean ± SD. Data sets were analyzed using GraphPad Prism 9 (GraphPad Software), and within each replicate tested for presence of outliers using Grubb's Test, alpha 0.05. Area under the curve (AUC) was used as a cumulative measurement of a drug effect in pharmacokinetics. Half maximal effective concentration (EC50) was used as a quantitative measurement of a drug concentration in pharmacokinetics. For determination of AUC and EC50, Log10 [compound] was represented on a linear axis and 4 parameter logistic (4PL) regression was employed using the nonlinear regression (curve fit) of "Log_{10} [compound] vs. response -- Variable slope (four parameters)" function in GraphPad. Linear regressions were performed to assess dependence of data to one independent variable, and fitness evaluated by R^2 value.

Two-way ANOVA analysis with a correction for multiple comparisons (to a control, either trastuzumab or Tcys114) using Dunnett's post-hoc statistical hypothesis test was performed. Significances are depicted as: n.s.: not significant, *p < 0.05, **p < 0.01, ***p < 0.001, ****p < 0.0001.

2.2. *Ex vivo* BC PDE Model

2.2.1. Primary Explant Handling and Culture

Patient-derived BC explants were provided by Instituto Português de Oncologia de Lisboa Francisco Gentil (IPOLFG) through a collaboration with Dr. Saudade André. The use of patient material was approved by the IPOFLG ethics committee and all patients have signed an informed consent form to agree to donate the material for research purposes. All tissues were anonymized before transfer to the Laboratory for further processing.

Once collected, tissue was kept in a 1:1 mixture of Dulbecco's Modified Eagle Medium (DMEM) / Nutrient Mixture F-12 (Ham), supplemented with FBS and Penicillin-Streptomycin, according to Table 2.6, and transported to the Lab, within 1 to 3 h after surgery. In the Lab, tissue was weighted, washed with DPBS $^{(-/-)}$ and thoroughly minced with scalpels, obtaining a mixture or fragments of approximately 1 - 1.5 mm^3. Minced samples were transferred to a Digestion Media composed by DMEM/F-12 medium supplemented with FBS, Penicillin-Streptomycin, Benzonase® Endonuclease and Collagenase A, according to Table 2.7.

Primary explants were mildly digested for 12 h, under continuous motion on a GyroMini™ Nutating Mixer (Labnet) in a humidified incubator with 5% CO_2 at 37 °C (Nuaire Autoflow IR Water-Jacketed CO_2 Incubator). For subsequent encapsulated explant culture, Human Mammary Epithelial Cells (HMEC) Medium was used, either with complete supplementation, as described in

Table 2.***8***, or with Insulin, Hydrocortisone and Epidermal Growth Factor (EGF) depletion when under estrogen stimulation, as explained in Section 3.1.

Table 2.6. Composition of Collection Media.

Medium Component	Concentration	Brand	Cat. Number
DMEM/F-12 Medium [+] L-Glutamine [+] 15 mM HEPES [–] Phenol Red	[1X]	Gibco™	#11039-021
Fetal Bovine Serum	10% (v/v)	Gibco™	#A3160801

Penicillin-Streptomycin	1% (v/v)	Gibco™	#15140-122

Table 2.7. Composition of Digestion Media.

Medium Component	Concentration	Brand	Cat. Number
DMEM/F-12 Medium [+] L-Glutamine [+] 15 mM HEPES [–] Phenol Red	[1X]	Gibco™	#11039-021
Fetal Bovine Serum	10% (v/v)	Gibco™	#A3160801
Penicillin-Streptomycin	1% (v/v)	Gibco™	#15140-122
Benzonase® Endonuclease	30 U/mL	Merck	#101654
Collagenase A	0.09 U/mL	Roche	#1010358

Table 2.8. Composition of Human Mammary Epithelial Cells (HMEC) Culture Media.

Medium Component	Concentration	Brand	Cat. Number
DMEM/F-12 Medium [+] L-Glutamine [+] 15 mM HEPES [–] Phenol Red	[1X]	Gibco™	#11039-021
Penicillin Streptomycin	1% (v/v)	Gibco™	#15140-122
Human Apo-Transferrin	0.5 µg/mL	Sigma-Aldrich	#T1147
Isoproterenol	0.1 mM	Sigma-Aldrich	#I5627
Ethanolamine	0.1 mM	Sigma-Aldrich	#E0135
O-Phosphoethanolamine	0.1 mM	Sigma-Aldrich	#P0503
Bovine Pituitary Extract	70 µg/mL	Sigma-Aldrich	#P1476
Primocin™	0.1 mg/mL	InvivoGen	#ant-pm
Insulin	10 µg/mL	Sigma-Aldrich	#I6634
Hydrocortisone	0.5 µg/mL	Sigma-Aldrich	#H2270
Recombinant Human EGF	5 ng/mL	PeproTech	#AF-100-15

2.2.2. BC Explant Encapsulation

BC explants were obtained after digestion, centrifuged at 100x g for 2 min, washed in DPBS $^{(-/-)}$ and centrifuged again at 100x g for 2 min. Explants were then resuspended in 2.1% (w/v) PRONOVA UP MVG Sodium Alginate, dissolved in 0.9 % (w/v) NaCl, which was transferred to a 5 mL luer lock syringe without needle (Terumo, #SS-05L) and assembled on a Syringe Infusion Pump KDS-100 (KDScientific) set at a flow rate of 10.0 mL/h, pumping the alginate solution containing the spheroids, in a controlled manner into the nozzle.

Microencapsulation was performed using an electrostatically-driven Encapsulation Unit VarV1 (Nisco). The alginate solution containing the BC explants, were feed to a holder arm set to a height of 3,8 cm, coupled to a 1 mm nozzle suspended over a 100 mm petri dish (Corning, #CLS430165) containing the gelling bath (to keep 1.2 cm from the nozzle to the bath surface).

The gelling bath is composed by a crosslinking solution of 100 mM $CaCl_2 \cdot 2\ H_2O$ (Merck, #102382) / 10 mM HEPES (Sigma-Aldrich, #H3375) in ddH_2O (pH 7.4), with a 5.3 kV electrode submerged and a magnetic stirrer bar as described above (Section 2.1.4.). Microcapsules were washed three times in 0.9 % (w/v) NaCl and equilibrated in culture medium before being distributed in 6-well tissue culture plates (Falcon, #353224) and

cultured under orbital agitation at 80 rpm (IKA KS 260 Control Shaker), in a humidified incubator with 5% CO_2 at 37 °C (Nuaire Autoflow IR Water-Jacketed CO_2 Incubator).

2.2.3. BC Explant Culture

Encapsulated BC explants were plated in 6-well tissue culture plates (Falcon, #353224), and cultured with in 4 mL/well of HMEC complete culture medium, under orbital agitation at 80 rpm (IKA KS 260 Control Shaker), in a humidified incubator with 5% CO_2 at 37 °C (Nuaire Autoflow IR Water-Jacketed CO_2 Incubator). Half of the medium was changed twice a week and replaced with fresh culture medium.

2.2.4. BC Explant Challenge

Encapsulated BC explants were exposed for two weeks to either (Z)-4-Hydroxytamoxifen (Sigma-Aldrich, #579002) or ICI 182,780 (Tocris, #1047) (indicated as tamoxifen or fulvestrant, respectively), at 1 µM final concentration. As vehicle control, encapsulated BC explants were exposed to 0.1% v/v ethanol (molecular biology grade) (Fisher Scientific, #BP2818), the percentage present in the drug incubation wells.

Twice a week, half the medium was replaced with new culture medium supplemented with fresh compounds at the specified drug concentration. After 2 weeks, medium was changed to HMEC depleted medium for 3 days, keeping fulvestrant, tamoxifen and vehicle control as described above. After 3 days in depleted medium, a 24h-stimulus with 10 nM 17β-estradiol (Sigma-Aldrich, #E2758) was applied. Cultures were kept always under orbital agitation, in a humidified incubator with 5% CO_2 at 37 °C.

2.2.5. BC Explant RNA Extraction and Quantification

BC encapsulated explants were collected, centrifuged for 1 min at 50x g and 4 °C and washed with DPBS $^{(-/-)}$ and centrifuged for 1 min at 50x g at 4 °C in a 5810R Centrifuge equipped with a F45-30-H rotor (Eppendorf). The explants were collected and either directly used for RNA extraction or stored in RNAlater™ Stabilization Solution (Invitrogen, #AM7020) at -80 °C until processing, to preserve RNA from RNase degradation. To proceed with the RNA extraction, alginate capsules were dissolved using a chelating solution, composed by 50 mM Sodium Citrate (Sigma-Aldrich, # S4641) / 104 mM Sodium Chloride (PanReac AppliChem, #131659). Alginate capsules were exposed to this solution in a GyroMini™ Nutating Mixer (Labnet) until all alginate dissolved. Solution was removed and BC explants washed with DPBS $^{(-/-)}$, followed by 1 min centrifugation at 50x g and 4 °C.

RNA from tissue lysates was collected by using the RNeasy® PowerLyzer® Tissue & Cells Kit (Qiagen, #15055-50). Explants were resuspended in a lysing buffer of TR1, provided the kit, supplemented by 10% (v/v) β-Mercaptoethanol (Sigma-Aldrich, #M6250), transferred to PowerBead 2.8 mm Ceramic Tubes (Qiagen, #13114-50) and lysed using a Precellys Evolution tissue homogenizer (Bertin Technologies). Tissues were homogenized for 2 cycles at 4500 rpm for 40 s each with 30 s dwells between cycles. Briefly, after lysates elution into the provided MB RNA Spin Columns, a DNase I (Qiagen, #79254) incubation step was performed to eliminate genomic DNA contamination. For each sample, 40 Kunitz DNase diluted 1:7 in RDD Buffer (Quiagen) was added to each column and incubated for 15 min at RT. RNA collecting columns were washed according to manufacturer's instruction with appropriate provided buffers. At the end of the washing steps, RNA was finally eluted in 30 µL of UltraPure™ DNase/RNase-Free Distilled Water (Invitrogen, #10977-035), by a final centrifugation for 1 min at 11 000x g.

RNA was used directly for RT-qPCR or stored at -80 °C. RNA concentration was quantified by a NanoDrop ND-2000C spectrophotometer (Thermo Scientific™) using UltraPure™ DNase/RNase-Free Distilled Water as blank. Amount or RNA extracted was very variable, ranging from bellow 2 ng/µL to 115.8 ng/µL.

2.2.6. Reverse Transcription Quantitative Polymerase Chain Reaction (RT-qPCR)

The reverse transcription reactions were performed using Sensiscript® Reverse Transcription Kit (Quiagen, #205213), and 10 U/µL Protector RNase Inhibitor (Roche, #3335399001), following the supplier's protocol. Reaction was carried over a 2 h incubation at 37 °C (Lid at 105 °C and heated at a 2 °C/s slope) in SimpliAmp Thermal Cycler (Applied Biosystems). cDNA was either immediately used or stored at -20 °C.

For qPCR reactions, the LightCycler® 480 SYBR Green I Master (Roche, #04887352001) strategy was followed, with 8 µL of PCR mix (composed by 2 µL UltraPure™ DNase/RNase-Free Distilled Water, 1µL Forward Primer [10X] + 1 µL Reverse Primer [10X] and 5 µL Master Mix [2X]), added to each reaction with 2 µL cDNA template in a 384-well plate, in triplicate for each condition. Plate was sealed with Light Cycler 480 Sealing Foil (Roche, # 64729757001) and reaction carried out in a LightCycler® 480 II (Roche). Sequences of primers used in this study are listed in Table 2.9 and were manufactured by IDT (Integrated DNA Technologies).

Cycle threshold (Ct) and melting curves were determined using LightCycler 480 Software version 1.5 (Roche). All data was analyzed using the $2^{-\Delta\Delta Ct}$ method described by *Livak & Schmittgen, 2001* [110] for relative gene expression analysis. Geometric mean of replicates and 2 housekeeping genes (RPL22 and 36B4) was determined for each condition and subtracted for the same condition within other assessed genes (ΔCt). Fold Change of Ct was assessed relative to control, either untreated or estrogen challenged condition, (ΔΔCt) and normalized to control set as 1 ($2^{-\Delta\Delta Ct}$). For each individual qPCR analysis, error propagation of the standard deviation was calculated in parallel by Formula 1. For the representation of relative gene expression relative to estrogen stimulus, a Log_2 transformation was performed to convert values bellow one to negative values.[111] Error propagation of the standard deviation associated with Log_2 transformation was determined by Formula 2.

(1) $$SD = relative\ gene\ expression \times ln2 \times \sqrt{\sqrt{SD_{condition}{}^2 + SD_{housekeeping\ genes}{}^2}^2 + \sqrt{SD_{control\ condition}{}^2 + SD_{control\ housekeeping\ genes}{}^2}^2}$$

(2) $$SD_{Log_2} = \frac{SD_{relative\ gene\ expression}}{\ln(2) \times relative\ gene\ expression}$$

Table 2.9. List of primers used in RT-qPCR. Description of gene acronym, protein encoded by the gene, and primer sequence used for RT-qPCR. Primer sequence indicates the 5' - 3' nucleotide sequence of the forward primer (top) and reverse primer (bottom).

Gene	Protein Encoded	Primer Sequence	
ER	Estrogen Receptor Alpha (ERα)	CCACCAACCAGTGCACCATT	FW 5' - 3'
		GGTCTTTTCGTATCCCACCTTTC	RV 5' - 3'
PGR	Progesterone Receptor (PR)	CGCGCTCTACCCTGCACTC	FW 5' - 3'
		TGAATCCGGCCTCAGGTAGTT	RV 5' - 3'
TFF1	Trefoil Factor 1 (TFF1)	TCGGGGGTCGCCTTTGGAGCAG	FW 5' - 3'
		GAGGGCGTGACACCAGGAAAACCA	RV 5' - 3'
AREG	Amphiregulin (AREG)	TGGAAGCAGTAACATGCAAATGTC	FW 5' - 3'
		GGCTGCTAATGCAATTTTTGATAA	RV 5' - 3'

RPL22	60S Ribosomal Protein L22 (RPL22)	CACGAAGGAGGAGTGACTGG TGTGGCACACCACTGACATT	FW 5' - 3' RV 5' - 3'
36B4	60S Ribosomal Phosphoprotein P0 (RPLP0)	GTGTTCGACAATGGCAGCAT GACACCCTCCAGGAAGCGA	FW 5' - 3' RV 5' - 3'

2.2.7. Protein Extraction and Quantification

BC encapsulated explants were collected, centrifuged for 1 min at 50x g and 4 °C and washed with DPBS $^{(-/-)}$ and centrifuged for 1 min at 50x g at 4 °C in a 5810R Centrifuge equipped with a F45-30-H rotor. Alginate capsules were exposed to a 50 mM Sodium Citrate / 104 mM Sodium Chloride chelating solution in a GyroMini™ Nutating Mixer (Labnet) until all alginate dissolved. Solution was removed and BC explants washed with DPBS $^{(-/-)}$, followed by 1 min centrifugation at 50x g and 4 °C. Explants were resuspended in Laemmli Lysis Buffer (composition described in Table 2.10), transferred to PowerBead 2.8 mm Ceramic Tubes (Qiagen, #13114-50) and lysed using a Precellys Evolution tissue homogenizer (Bertin Technologies). Tissue was homogenized for 2 cycles at 4500 rpm for 40 s each with 30 s dwells between cycles.

Lysates were transferred to new 1.5 mL micro tubes (Sarstedt, #72.706.600) and centrifuged again for 1 min at 13 000x g. Supernatant was transferred to new micro tubes and stored at -80 °C until further use (within one month).

Table 2.10. Laemmli Buffer Composition used for Protein Extraction of BC Explants.

Buffer Component	Concentration	Brand	Cat. Number
Tris-Base (pH 6.8)	1.0 M	Calbiochem	#648311
Sodium Dodecyl Sulfate 20%	80 mg/mL	Invitrogen	#0077027
Glycerol	40%	BioXtra	#G66279
β-Mercaptoethanol	20%	Sigma-Aldrich	#M3148

2.2.8. Western Blot

Sample Preparation

Protein samples extracted from BC explants (Section 2.2.7.) were thawed and denatured by boiling for 15 min at 95 °C in a ThermoMixer C (Eppendorf). Sample protein concentration was quantified with a NanoDrop ND-2000C spectrophotometer using Laemmli Lysis Buffer as blank. Samples (28 µg each) were prepared for gel loading adjusting final volumes with Laemmli Buffer. NuPAGE™ LDS Sample Buffer [4X] (Invitrogen, #NP0007) and NuPAGE™ Sample Reducing Agent [10X] (Invitrogen, #NP0009) were added at required dilutions.

Gel Electrophoresis

XCell SureLock Mini-Cell Electrophoresis System (Thermo Fisher) was assembled using a NuPAGE™ 4-12% Bis-Tris Gel (Invitrogen, #NP0321) and chambers were filled with a NuPAGE™ MES SDS Running Buffer [20X] (Invitrogen, #NP0002) in ddH_2O. Protein samples were heated for 10 min at 70 °C and centrifuged for 5 min at 10 000x g before loading 25 µL/well (28 µg protein). SeeBlue™ Plus2 Pre-Stained Protein Standard (Invitrogen, #LC5925) was used as ladder. NuPAGE™ Antioxidant (Invitrogen, #NP0005) was added to inner chamber; electrophoresis was run at 200 V, for 50 min, with a PowerPac Universal Power Supply (Bio-Rad). When the stained migration front gets to the end of the gel, this was removed from the electrophoresis cassette.

Wet Transfer

The gel was transferred to a wet blotting cassette assembled with three blotting papers (Whatman, #GB003) on each side, soaked in transfer buffer (composition in Table 2.11), and a PVDF membrane (GE Healthcare, #RPN1416F), previously activated in methanol (Merck, #106018) for 3 min, washed in ddH_2O and equilibrated in transfer buffer. The transfer apparatus was assembled, and the protein transferred overnight, at 30 V at 4 °C under magnetic agitation in a RCT basic Magnetic Stirrer (IKA), with a PowerPac Universal Power Supply (Bio-Rad). After protein transfer, gels were stained for 30 min with InstantBlue™ Coomassie Based Staining Solution (Expedeon, #ISB1L) to verify of the non-transferred protein.

Table 2.11. Composition of Wet Transfer Buffer for Protein Blotting.

Buffer Component	Concentration	Brand	Cat. Number
Tris-Base	3 mg/mL	Calbiochem	#648311
Glycine	14 mg/mL	Sigma-Aldrich	#104169
Methanol	20% (v/v)	Merck	#106018
Sodium Dodecyl Sulfate 20%	10% (v/v)	Invitrogen	#0077027

Immunoblot

Membranes were incubated with blocking solution for 1 h, under agitation, to prevent unspecific binding of the antibodies. The composition of the blocking solution was 5% Non-Fat Milk (PanReac AppliChem, #A0830) in Tris Buffered Saline Tween (TBST) Buffer; TBST was prepared from pre-packed Tris Buffered Saline, pH 8.0 (Sigma, #T-6664), dissolved in ddH_20, supplemented with 0.1% (v/v) Tween 20 prepared from 20% Tween 20 (w/v) (Merck, #9005-64-5)).

The primary antibodies, described in Table 2.12, were incubated in blocking solution in the presence of 0.1% Sodium Azide (Merck, #6688), to prevent microbial contamination. Detection of β-tubulin was used as a loading control. Membranes were incubated overnight at 4 °C in a SRT6 Tube Roller (Stuart). Membrane washes were performed in TBST, followed by 2 h incubation with secondary antibody (Table 2.13), at RT, under agitation. Secondary antibodies were prepared in blocking solution. Membranes were washed in TBST buffer, followed by $DPBS^{(-/-)}$ and incubated for 5 min with Amersham ECL Select Western Blotting Detection Reagent (GE Healthcare, #RPN2235), covered from light. Detection was performed in a ChemiDoc XRS+ Imaging System (Bio-Rad); analyzes was performed in ImageLab (Bio-Rad), using Chemi Hi Sensitivity protocol for Blots.

Table 2.12. Primary antibodies used for western blot.

Primary Antibody	Brand	Cat. Number	Host	Dilution
Anti-Estrogen Receptor α (1D5)	Invitrogen	#MA5-13191	Rabbit – IgG (Monoclonal)	1 : 500
Anti-Progesterone Receptor (1E2)	Ventana	#790-2223	Mouse – IgG (Monoclonal)	1 : 100
Anti-β Tubulin (H-235)	Santa Cruz Biotechnology	#SC-9104	Mouse – IgG (Polyclonal)	1 : 1 000

Table 2.13. Secondary antibodies used for western blot.

Secondary Antibody	Brand	Cat. Number	Host	Dilution

ECL Anti-Mouse HRP-Linked	GE Healthcare	#NA931	Sheep – IgG (Monoclonal)	1 : 20 000
ECL Anti-Rabbit HRP-Linked	GE Healthcare	#NA934	Donkey – IgG (Monoclonal)	1 : 20 000

2.2.9. Statistical Analysis

Data from independent biological sample experiments or technical replicates is expressed as mean ± SD. Data sets were analyzed using GraphPad Prism 9 (GraphPad Software).

The nonparametric Mann-Whitney U Test was applied to analyze significance in statistical hypothesis of biological independent experiments. Significances are depicted as: n.s.: not significant, *$p < 0.05$, **$p < 0.01$, ***$p < 0.001$, ****$p < 0.0001$.

Chapter 3. Results and Discussion

The main aim of this thesis was the pre-clinical evaluation of therapeutic potential of targeted therapies using 3D *in vitro* and *ex vivo* BC models previously established in the host Lab. For this purpose, methodologies already implemented were applied to generate and maintain two distinct tumor cell models (*in vitro* and *ex vivo*). These models were then used to assess the effect of endocrine (tamoxifen and fulvestrant) and anti-HER2 cell-targeted therapies, specifically ADCs, as proof-of-concepts.

Following a reconstruction approach of the tumor microenvironment using a 3D cell line-derived model different trastuzumab-derived ADCs were applied and their therapeutic potential assessed (Section 3.1). Encapsulated spheroids allow, as described in Section 1.4.1.3. (Scaffold-Based Approaches), to accumulate ECM [85], protect cell spheroids from shear stress generated by the continuous agitation and avoid spheroid fusion. Cell encapsulation also allow a better ease of manipulation without compromising spheroid integrity. This method thus tackles the two most described challenges of working with 3D spheroids in agitation: sheer stress and spheroids fusion, without any impact on the advantages but even increasing the *in vivo* features recapitulated (ECM accumulation).

In parallel, and pursuing a maintenance approach, encapsulated microstructures of patient-derived explants were stimulated with estrogen and challenged with endocrine therapy and ER downstream signaling assessed (Section 3.2).

3.1. Pre-clinical assessment of the therapeutic potential of ADCs using an *in vitro* 3D BC model

For the assessment of the effect of trastuzumab-derived ADCs (T-ADCs) on $HER2^+$ BC, experiments were conducted using the HCC1806 and HCC1954 cell lines. HCC1954 is a $HER2^+$ cell line characterized by resistance to monoclonal antibody trastuzumab. HCC1954 cells contain a mutation (H1047R) of *PIK3CA,* the gene encoding the p110a catalytic subunit of PI3K, resulting in aberrant activation of the PI3K/AKT pathway that translates on a HER2-PI3K-FoxO-Survivin Axis that has previously been described as a mechanism of adaptation or resistance to trastuzumab.[112] Since patients resistant to trastuzumab are the primary candidates to use HER2-ADCs, as second-line treatment, this cell line was chosen as cell model, due to its intrinsic resistance to trastuzumab. HCC1806 is a TNBC cell line (ER^-/PR^-/$HER2^-$) which served as negative control for the specificity of the ADCs targeting HER2.

Drug challenge comprised mAb and ADCs (Figure 3.5) developed by Dr. Jordi Badillo and Dr. Joan Minard, from Universitat Autònoma de Barcelona which were kindly provided as part of a collaborative project:

- Monoclonal antibody, trastuzumab
- Heterogeneous conjugated trastuzumab-DM1 (DAR 3) **(T-DM1)**
- Heterogeneous conjugated trastuzumab-vcMMAE (DAR 4) **(T-MMAE4)**
- Homogeneous conjugated trastuzumab-vcMMAE (DAR 8) **(T-MMAE8)**
- Trastuzumab_cys114 **(Tcys114)**, a genetically modified antibody (thiomab) with substituted alanine for cysteine at position 114 that allows for site-directed conjugation.
- Homogeneous conjugated trastuzumab_cys114-vcMMAE (DAR2) **(Tcys114-MMAE2)**

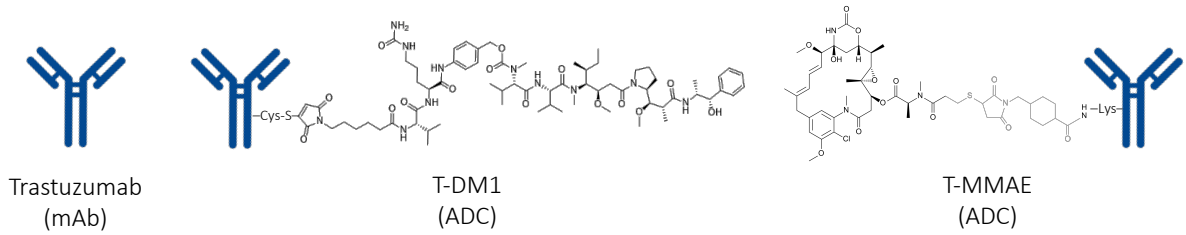

Figure 3.5. Schematic representation of the monoclonal antibody trastuzumab (T) and antibody drug conjugates (ADC) trastuzumab-emtansine (T-DM1) and trastuzumab-monomethyl auristatin E (T-MMAE).

3.1.1. Assessment of the effect of T-ADCs in 2D BC cell line models

To establish a control of the relevance of a 3D cell model, and determine the range of concentrations to use, a preliminary experiment was performed in HCC1806 and HCC1954 cells, cultured in 2D, consisting of drug challenge with trastuzumab and T-ADCs. A schematic representation of the experimental workflow is presented in Figure 3.6. Drug challenge was conducted for 3 days, using 10-fold serial dilutions (0.001 to 10 µg/mL) and the effect was assessed by metabolic activity, measured by resazurin reduction (Presto Blue™ assay, Figure 3.7), and cell number, measured by crystal violet assay (Figure 3.8).

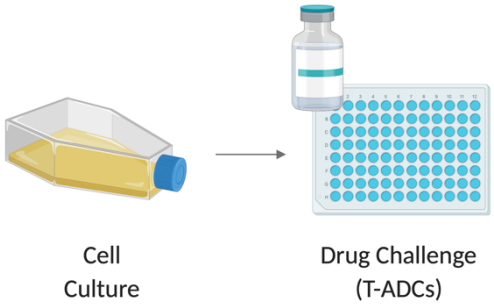

Figure 3.6. Schematic representation of the experimental design used for the 2D cell culture model and the drug challenge. Drug challenge with trastuzumab-derived antibody drug conjugates (T-ADCs), on HCC1806 and HCC1954 cells, performed 24 hours post-platting of cells. Image created with BioRender©.

The effects of T-ADCs on HCC1806 and HCC1953 2D cultures were analyzed by measuring metabolic activity (Figure 3.7.) and cell viability (Figure 3.8.) after three days of drug challenge. When both cell lines were exposed to trastuzumab or Tcys114, no differences were observed in both parameters relatively to the vehicle control (Figure 3.7. and Figure 3.8.). This result is in accordance with H1806 being described as a TNBC cell line, that do not express HER2, and HCC1954 as a trastuzumab-resistant cell line, due to an activating *PIK3CA* mutation.[112] An additional mechanism of action of trastuzumab is through ADCC [50,52], but this would only be observed in the presence of NK cells. Moreover, the data suggests that the Cys114 modification did not confer cytotoxicity properties to T.

In contrast T-DM1 and T-MMAE 8 induced a significant decrease in HCC1806 cell metabolic activity (Figure 3.7. A, B) and viability (Figure 3.8. A, B, E), when applied at 1 µg/mL or higher concentrations, as well as T-MMAE 4 and Tcys111-MMAE2 at the highest concentration tested, 10 µg/mL. Considering that HCC1806 are TNBC cells, this result suggests that at high concentrations (10 µg/ml) these T-ADCs may have untargeted toxic effects (Figure 3.7. A, B and Figure 3.8. A, B, E).

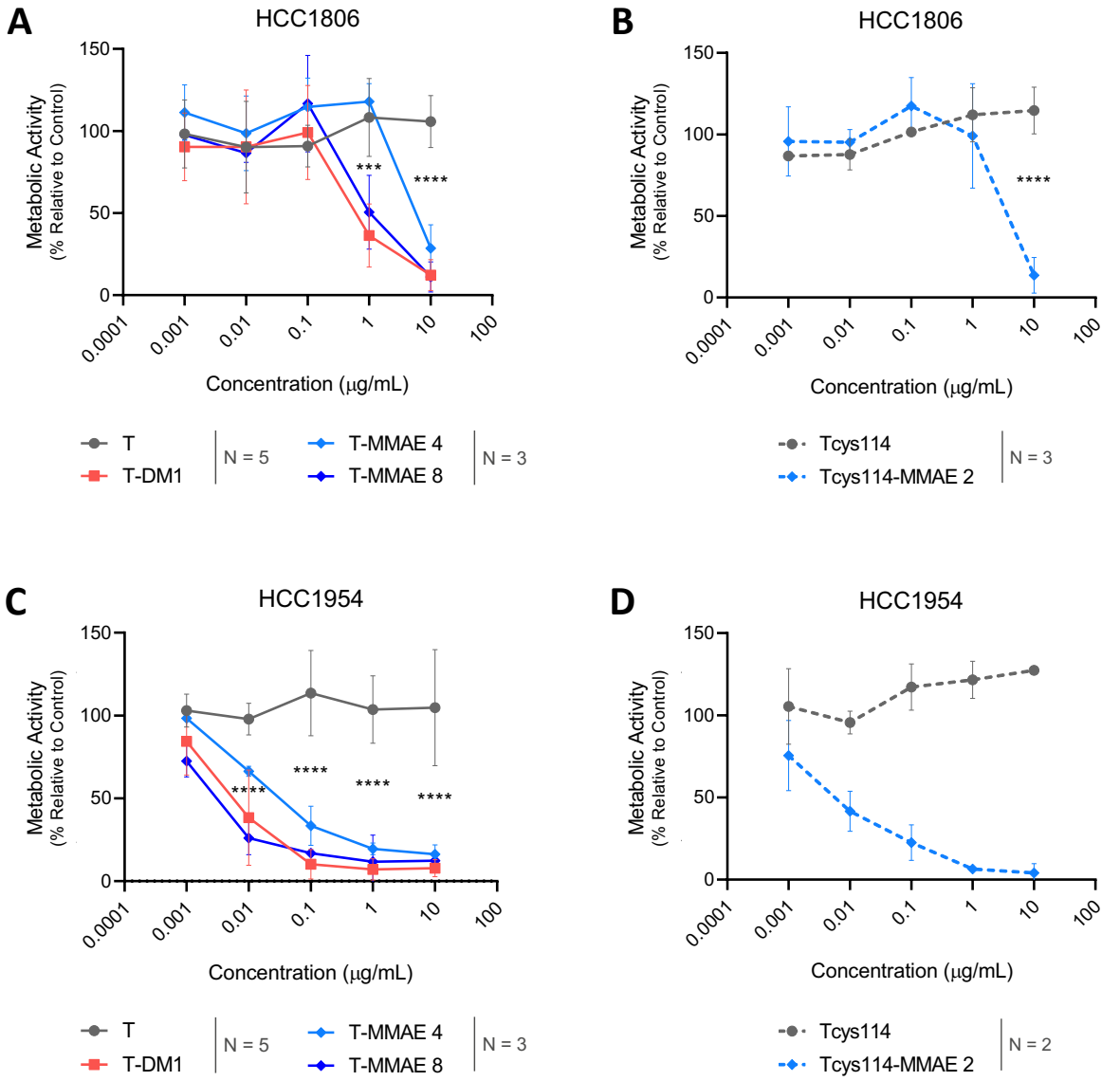

Figure 3.7. Effect of trastuzumab-derived antibody drug conjugates (3-day challenge) on the metabolic activity of HCC1954 [HER2⁺] and HCC1806 [TNBC] cells in 2D cultures. (A & B) Effect on HCC1806 cell metabolic activity. (C & D) Effect on HCC1954 cell metabolic activity. Metabolic activity assessed by resazurin reduction, normalized to day 0 and represented as percentage relative to vehicle control. Data shown as mean ± SD of N independent experiments, as indicated in the figure. Presence of outliers tested using Grubb's Test, alpha 0.05; two-way ANOVA analysis with a correction for multiple comparisons (to a control, either T or Tcys114) using Dunnett's post-hoc statistical hypothesis test was performed when N ≥ 3. Significances are depicted as: n.s.: not significant, *p < 0.05, **p < 0.01, ***p < 0.001, ****p < 0.0001. T = trastuzumab, T-DM1 = trastuzumab-emtansine, T-MMAE 4 = trastuzumab-monomethyl auristatin E (DAR 4), T-MMAE 8 = trastuzumab-monomethyl auristatin E (DAR 8), Tcys114 = modified trastuzumab with substituted alanine for cysteine at position 114, Tcys114-MMAE 2 = modified trastuzumab with substituted alanine for cysteine at position 114 conjugated with monomethyl auristatin E (DAR 2).

As for HCC1954, a decrease in metabolic activity and cell concentration relatively to the vehicle control was observed even at low concentrations of the T-ADCs (0.1 µg/mL), whereas for HCC1806, only 1 µg/mL or higher concentrations were cytotoxic (Figure 3.7. C, D and Figure 3.8. C, D, F); this suggests that there may be a concentration range in which ADCs exert specific effects. Interestingly, Tcys114-MMAE 2 induced a reduction of cell viability at 0.01 µg/mL (22.5%), higher than T-MMAE 4 (13.3%), which has a higher payload (DAR).[113]

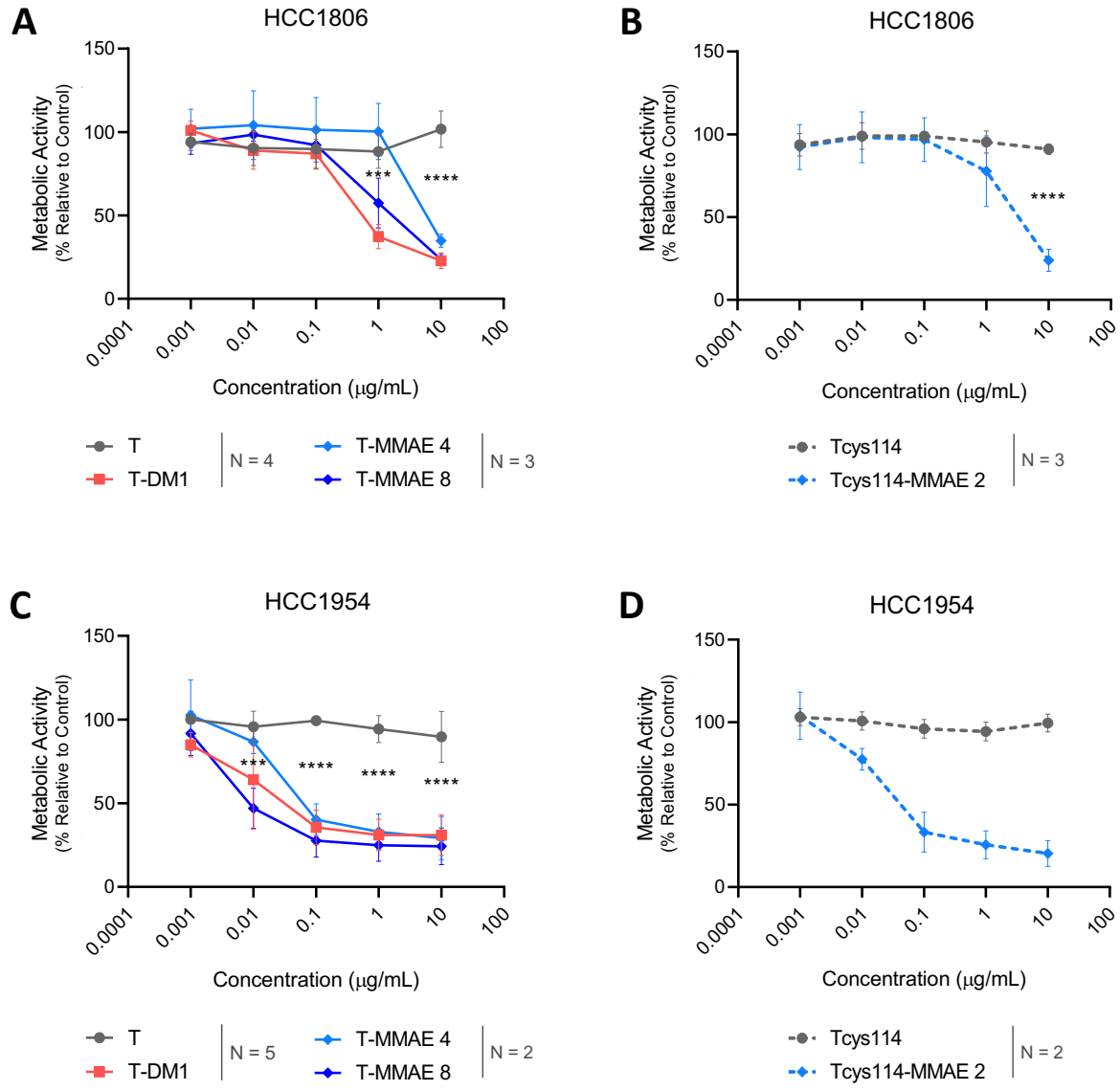
A
HCC1806
Metabolic Activity (% Relative to Control)
Concentration (μg/mL)
T
T-DM1
N = 4
T-MMAE 4
T-MMAE 8
N = 3
B
HCC1806
Tcys114
Tcys114-MMAE 2
N = 3
C
HCC1954
N = 5
N = 2
D
HCC1954
N = 2

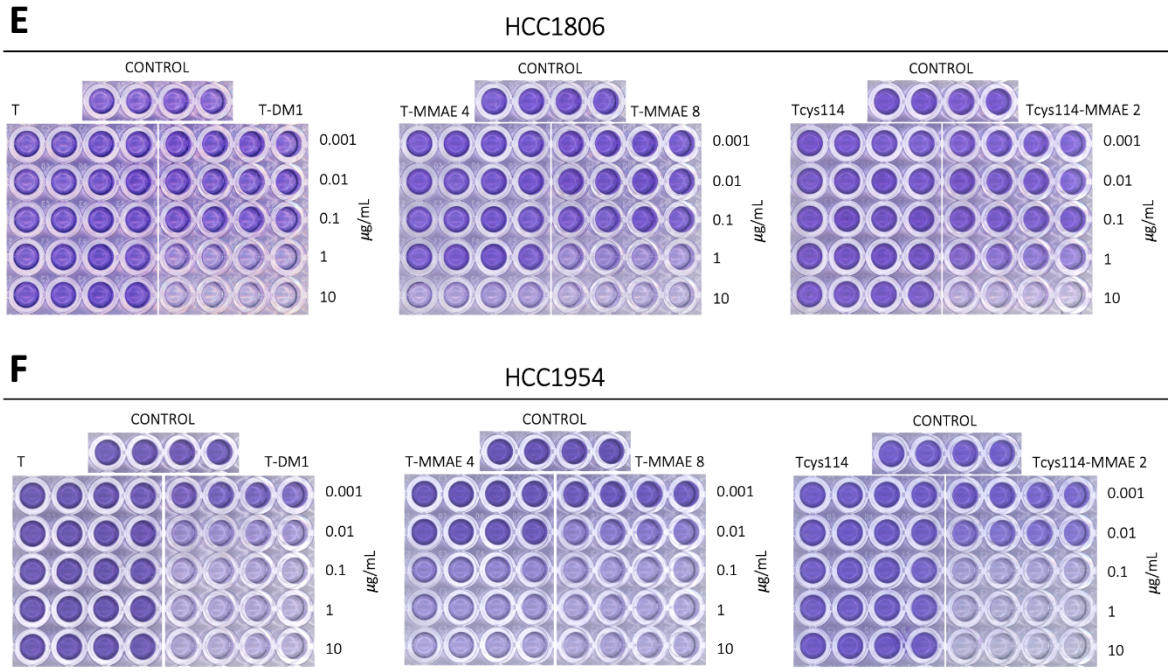
E
HCC1806
CONTROL
T
T-DM1
T-MMAE 4
T-MMAE 8
Tcys114
Tcys114-MMAE 2
0.001
0.01
0.1
1
10
μg/mL
F
HCC1954

◀ **Figure 3.8. Effect of trastuzumab-derived antibody drug conjugates (3-day challenge) on the viability of HCC1954 [HER2$^+$] & HCC1806 [TNBC] cells in 2D cultures.** (A & B) Effect on HCC1806 cell viability. (C & D) Effect on HCC1954 cell viability. (E & F) Picture of representative culture plates: cells were fixed, and nuclei stained with crystal violet; crystals were dissolved in acetic acid and optical density values measured (Abs 595 nm). Cell viability is represented as percentage relative to vehicle control. Data shown as mean ± SD of N independent experiments, as indicated in the figure. Presence of outliers tested using Grubb's Test, alpha 0.05; two-way ANOVA analysis with a correction for multiple comparisons (to a control, either T or Tcys114) using Dunnett's post-hoc statistical hypothesis test was performed when N ≥ 3. Significances are depicted as: n.s.: not significant, *p < 0.05, **p < 0.01, ***p < 0.001, ****p < 0.0001. T = trastuzumab, T-DM1 = trastuzumab-emtansine, T-MMAE 4 = trastuzumab-monomethyl auristatin E (DAR 4), T-MMAE 8 = trastuzumab-monomethyl auristatin E (DAR 8), Tcys114 = modified trastuzumab with substituted alanine for cysteine at position 114, Tcys114-MMAE 2 = modified trastuzumab with substituted alanine for cysteine at position 114 conjugated with monomethyl auristatin E (DAR 2).

Taken together, these results showed that the data obtained from both endpoints, metabolic activity (Figure 3.7) and cell viability (Figure 3.8) were in accordance and corroborating each other, namely in the lack of effect observed for trastuzumab or Tcys114 in both cell lines. It was also shown that T-DM1 and T-MMAE were highly effective and that their effect increased with concentration and DAR number. In addition, HCC1954 was shown to be more sensitive to T-ADCs than HCC1806. Even so, at higher concentrations, ADCs induced toxicity even on HCC1806, suggesting that there is a therapeutic window to be explored.

The observations here reported are supported by previous results described by *Phillips et al., 2008.*[114] In this study, trastuzumab-sensitive SKBR3 [HER2$^+$] cells cultured in 2D were challenged for 3 days with trastuzumab-SMCC-DM1 ADC (DAR 3.2), and viability assessed by Cell Titer-Glo (ATP content). Similar to our findings, major reduction in viability was observed at 0.01 µg/mL. MDA-MD-468, a TNBC cell line, was challenged in parallel showing reduction in viability above 1 µg/mL in a result very close to the one here reported. Recently, *Saatci et al., 2018* [115] have also reported T-DM1 challenge for 3 days on SKBR3 [HER2$^+$] and BT-474 [Luminal B with HER2$^+$] cells grown in 2D; the effect was assessed on cell viability (measured by ATP levels) and apoptosis (measured by quantification of caspase -3/7 activation). Yet, in the referred work single cells were plated in Matrigel, a previously described animal-derived active matrix with higher variability than the inert alginate scaffolds as described in the next section within the 3D model.

The results published report an EC50 of 0.01 µg/mL for SKBR3 [HER2$^+$] cells and 0.43 µg/mL for BT-474 [Luminal B] cells, a 43-fold increase. This finding is corroborated by the trend described here, with major reduction of viability in HER2$^+$ cells after 3 days challenge at 0.01 µg/mL and a higher concentration required for T-DM1 to be effective in HER2$^-$ cells.

Another study by *Abdollahpour-Alitappeh et al., 2019* [116] conducted drug challenges in trastuzumab-sensitive SKBR3 [HER2$^+$] and insensitive MDA-MB-468 [TNBC] cells. Trastuzumab-vcMMAE ADC (DAR 5.12) was applied for 3 days and a major reduction in cell viability/proliferation (MTT assay) was observed for 0.01 µg/mL of ADC, with 70% decrease in SKBR3 cells, in a result comparable to the one we are reporting for HCC1954 [HER2$^+$] cells and within the reduction of cell viability (crystal violet assay) observed at the same concentration (Figure 3.8) with T-MMAE 4 (33.7%) and T-MMAE 8 (74.0%). In MDA-MB-468 [TNBC] cells, at the highest concentration tested (1 µg/mL), reduction in metabolic activity was only of 35%, a result in line with what we observed in HCC1806 [TNBC] cells; for the same concentration (0.01 µg/mL of ADC, Figure 3.7) we have found no decrease in metabolic activity (resazurin reduction assay) with T-MMAE4 and a 50% reduction with T-MMAE 8.

3.1.2. Assessment of the effect of T- ADCs in encapsulated 3D spheroids of BC cell lines

Having observed that ADCs resulted in decreased metabolic activity and viability of HCC1954 cells cultured in 2D but did not impacted significantly HCC1806 TNBC cells (except at the highest T-ADCS concentration), we moved to assess whether this effect could also be observed in 3D cell cultures. To this purpose, 3D cancer cell spheroids were employed. In 2D monolayer, proliferation genes and morphology are modified compared to the human tumors. As alternative, 3D cultures of cancer cell lines successfully reproduce the tumor cell cluster organization and morphology observed in tumors, presenting increased similarity to the *in vivo*, as discussed in the Introduction Section of this thesis. The host Lab has previously established a 3D cancer cell model based on alginate encapsulation of tumor cell spheroids, eventually in co-culture with other cell types present in the TME.[82] Considering the future use of these models more recapitulative of the TME to evaluate T-ADCs, the assay setup included the encapsulation of 3D cancer cell spheroids to avoid spheroid fusion, promote accumulation of ECM and protect spheroids from agitation-derived sheer-stress.

The experimental layout of the drug assays in 3D cultures is represented in Figure 3.9. The same cell lines and drug concentration range (0.001 to 10 µg/mL) used in the drug challenges in 2D were employed in 3D; as for the incubation period, it was extended from 3 to 7 days. The drug exposure period was longer since DM1 and MMAE are microtubule inhibitors that prevent cells in division from completing mitosis, and the cell growth rate in the 3D setting is lower [80]. This slower cell growth is derived from two factors: contact inhibition, a well-known regulatory mechanism by which proliferation rate of mammalian cells is dictated by the space available, with induction of cell cycle arrest to stop proliferation once the available space is occupied[69]; cellular response to environment stiffness and consequently elasticity. Therefore, cells in spheroids grow slower than in 2D due to contact inhibition and dependent on the stiffness of the alginate matrix.[69,88] BC tissues have increased matrix stiffness than healthy tissue, which is known to contribute to tumor cell dissemination,[82] and alginate scaffolds contribute to recreate the original *in vivo* TME providing a firm mechanical support with still higher elasticity than 2D substrates.[88] As such, stiffness of alginate scaffolds takes particular relevance in allowing growth and viability of tumor cells in 3D spheroids, and its viscosity must be finely tuned.

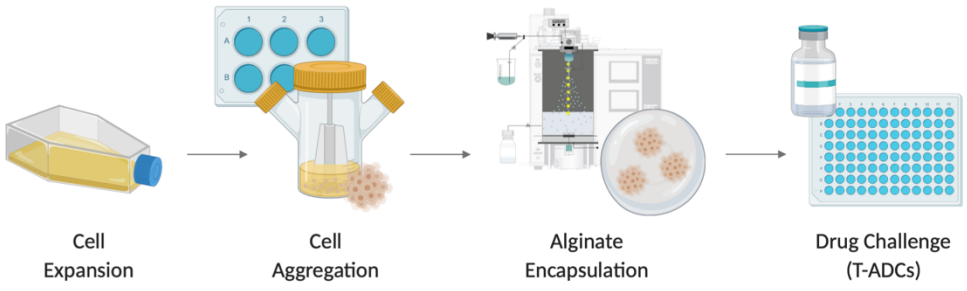

Figure 3.9. Schematic representation of the experimental design used for the encapsulated 3D cell models and for the drug challenge. HCC1806 and HCC1954 cells expanded in 2D cultures systems were inoculated into AggreWell™400 microwell culture plates (HCC1806) or spinner vessels (HCC1954) to induce aggregation into spheroids. Cancer cell spheroids were encapsulated prior to drug challenge with the trastuzumab-derived antibody drug conjugates (T-ADCs). Image created with BioRender ©.

The effect of drug challenge was quantitatively assessed by metabolic activity through resazurin reduction (Presto Blue™ assay, Figure 3.10). T-ADCs had not significant effect on the metabolic activity of the TNBC cell line HCC1806 (Figure 3.10. A, B), although there was a tendency for a decrease at the higher T-ADC concentration, similar to the results obtained in 2D (Figure 3.7. A, B). For the HCC1954 cell line (Figure 3.10. C, D), neither with trastuzumab nor Tcys114 induced a reduction in the metabolic activity. In contrast, a strong reduction of the metabolic activity of HCC1954 cells was observed for all the T-ADCs, as reported above in 2D cultures (Figure 3.7. C, D).

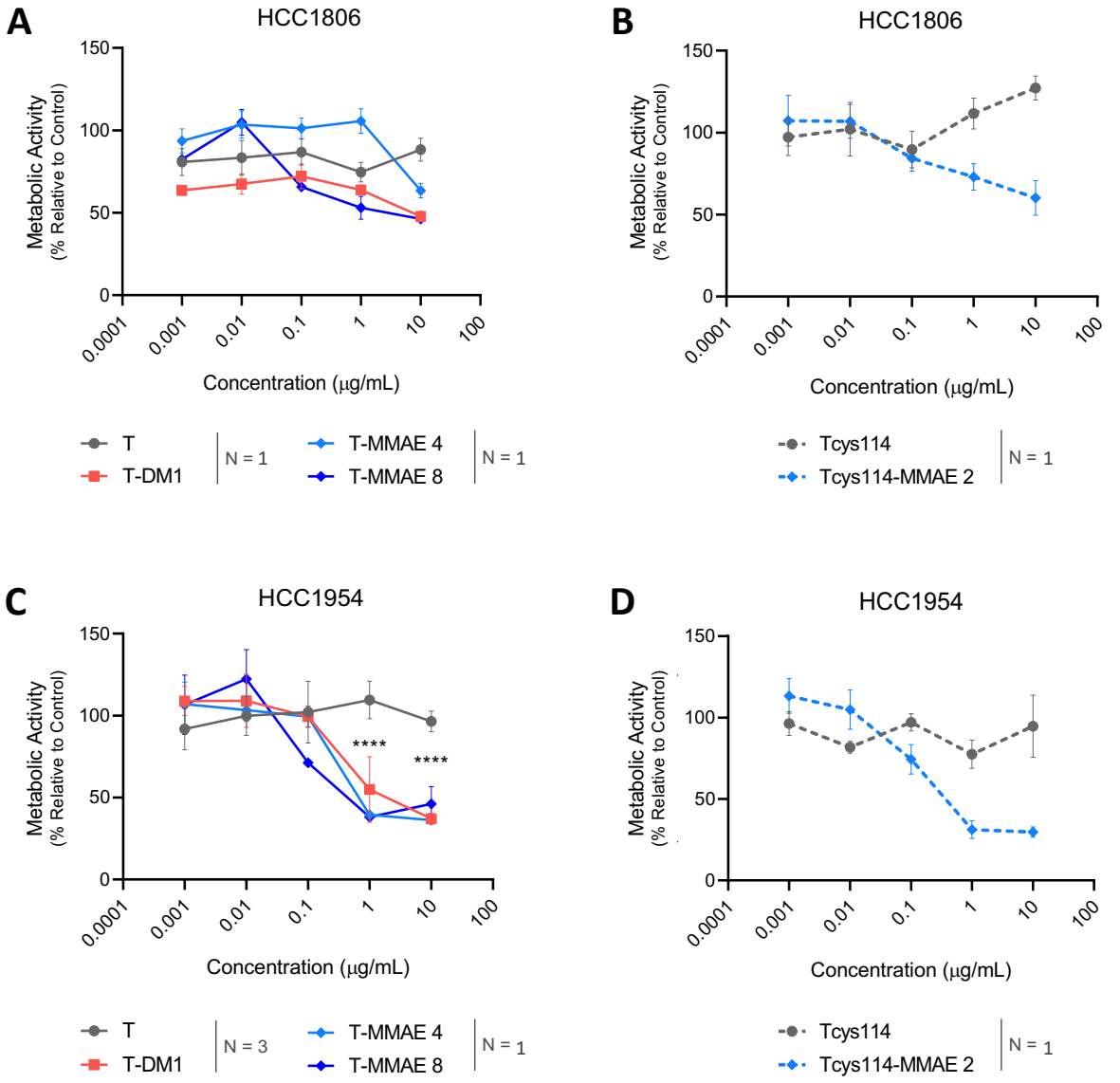

Figure 3.10. Effect of trastuzumab-derived antibody drug conjugates (7-day challenge) on the metabolic activity of HCC1954 [HER2⁺] & HCC1806 [TNBC] cells in encapsulated 3D cultures. (A & B) Effect on HCC1806 cell metabolic activity. (C & D) Effect on HCC1954 cell metabolic activity. Metabolic activity assessed by resazurin reduction, normalized to day 0 and represented as percentage relative to vehicle control. Data shown as mean ± SD of N independent experiments, as indicated in the figure. For N=1, values correspond to mean ± SD of technical quadruplicates. Presence of outliers tested using Grubb's Test, alpha 0.05; two-way ANOVA analysis with a correction for multiple comparisons (to a control, either T or Tcys114) using Dunnett's post-hoc statistical hypothesis test was performed when N ≥ 3. Significances are depicted as: n.s.: not significant, *p < 0.05, **p < 0.01, ***p < 0.001, ****p < 0.0001. T = trastuzumab, T-DM1 = trastuzumab-emtansine, T-MMAE 4 = trastuzumab-monomethyl auristatin E (DAR 4), T-MMAE 8 = trastuzumab-monomethyl auristatin E (DAR 8), Tcys114 = modified trastuzumab with substituted alanine for cysteine at position 114, Tcys114-MMAE 2 = modified trastuzumab with substituted alanine for cysteine at position 114 conjugated with monomethyl auristatin E (DAR 2).

In what concerns the effect of T-MMAE 4 and T-MMAE 8, at 0.1 μg/mL, a reduction of 2.7% and 30.9% relatively to vehicle control, respectively, was observed, whereas in the higher and lower concentrations there was not a marked difference between both ADCs (Figure 3.10. C, D). Although preliminary, these results suggest that increasing the DAR of the T-ADCs results in a higher toxicity to $HER2^+$ cells, mainly at intermediate concentrations. Nevertheless, this represents the result of a single independent experiment (performed with technical quadruplicates), and therefore further experiments are required to determine statistical significance and confirm this hypothesis.

Furthermore, when applied at 0.1 μg/mL, Tcys114-MMAE 2 induced a reduction in metabolic activity of 25.7% relatively to the vehicle control condition, whereas T-MMAE 4 induced no significant reduction (2.7%). Only when employed at 1 μg/mL, T-MMAE 4 induced a similar level of toxicity of Tcys114-MMAE 2, but even at this concentration, Tcys114-MMAE 2 was more effective (68.8% *vs* 60.5%) in terms of reduction of metabolic activity (Figure 3.10. C, D). Unconjugated Tcys114 showed no effect. These data suggests that Tcys114-based ADCs may be more effective even with reduced payloads.

Finally, the Area Under the dose-response Curve (AUC) was calculated for the 2D and 3D drug assays (Figure 3.11). AUC has been described as a more accurate metric than EC50 (half maximal effective concentration) for analysis of four parameter logistic (4PL) regression of dose response curves, namely when comparing and ranking different compounds.[117,118] Being an integrated measurement, AUC has the best performance when classifying different curves, since it has the advantage of accumulating information across the entire dose range.

Comparing the AUC results from 2D metabolic activity (Figure 3.11. A) with cell viability (Figure 3.12. B), it is clear how both assays provided a similar result. All T-ADCs have shown to be more effective on HCC1954 cells, with a reduction of viability around 50%, and a reduction of activity around 75%. T-MMAE 8 was the most effective T-ADC in reduction of cell viability (60%) and T-MMAE 4 the less effective on both assays (respectively 40% and 60% decrease compared to T). These observations support the complementarity of the readouts and the reduction of metabolic activity prior to decrease in viability could be assessed. In HCC1806 both T-DM1, T-MMAE 8 and Tcys114-MMAE2 resulted in decreased metabolic activity (10% to 30%) and cell viability as well (15% to 25%), although respectively at lower extent. T-MMAE 4 effect was comparable to trastuzumab. Tcy114-MMAE 2 had an effect more similar to T-MMAE 8, which presents a higher payload, than with T-MMAE 4. As previously described, this might be related to the expected increased effect of homogeneously conjugated ADCs such as the case of the Tcys-MMAE 2.

The AUC of metabolic activity (Figure 3.11. C) revealed a lower effect of T-ADCs in relation to the control mAbs), than it has in 2D (Figure 3.11. A), although a similar trend was observed. Comparing AUC of metabolic activity in 3D, the difference is particularly remarkable for HCC1954, where effect of all T-ADCS was similar and but not surpass a reduction of 17% to 25%, at least 50% less than the previous observations in 2D. As for HCC1806, reduced effect was observed, for T-DM1, T-MMAE 8 and Tcys114-MMAE 2 in reduction of metabolic activity (around 10% to 20%) and, as in 2D, T-MMAE 4 was not effective. Yet, the majority of this assay results from a single independent experiment (performed with quadruplicates) and further studies are required to determine significance of the results.

Even though, these observations suggest that HCC1954 cells were less sensitive to T-ADCs in 3D than in 2D cultures. In 3D cultures, only at the higher drug concentrations the effect was similar to the one detected in 2D at considerably lower concentrations. For therapeutic purposes, the use of higher concentrations is not be the best strategy since it can lead to unspecific off-target effect and the alternatives are cyclic exposure, or prolonged exposure times [116]; it remains to be determined if prolonged drug challenges with intermediate drug concentrations can induce in 3D cytotoxicity similar to that detected in 2D.

Interestingly, T-DM1 (DAR 3.1) shows a similar effect in reduction of cell viability or metabolic activity to the one described for T-MMAE 8 both in 2D and in 3D. Although both cytotoxic molecules, are anti-microtubule agents, DM1 mechanism of action is similar to vinca alkaloids, while MMAE mechanism of action resembles the one exerted by taxanes. Nevertheless, we found that one explanation for the possible increased toxicity of T-DM1 (non-cleavable linker), in relation to T-MMAE 8 (cleavable linker), comes from the observation of *Tsuchikama & An* [57] that in ADCs with non-cleavable linker, the payload structure must be carefully designed so that upon proteasomal degradation it can exert comparable or even better anti-tumor potency.[57]

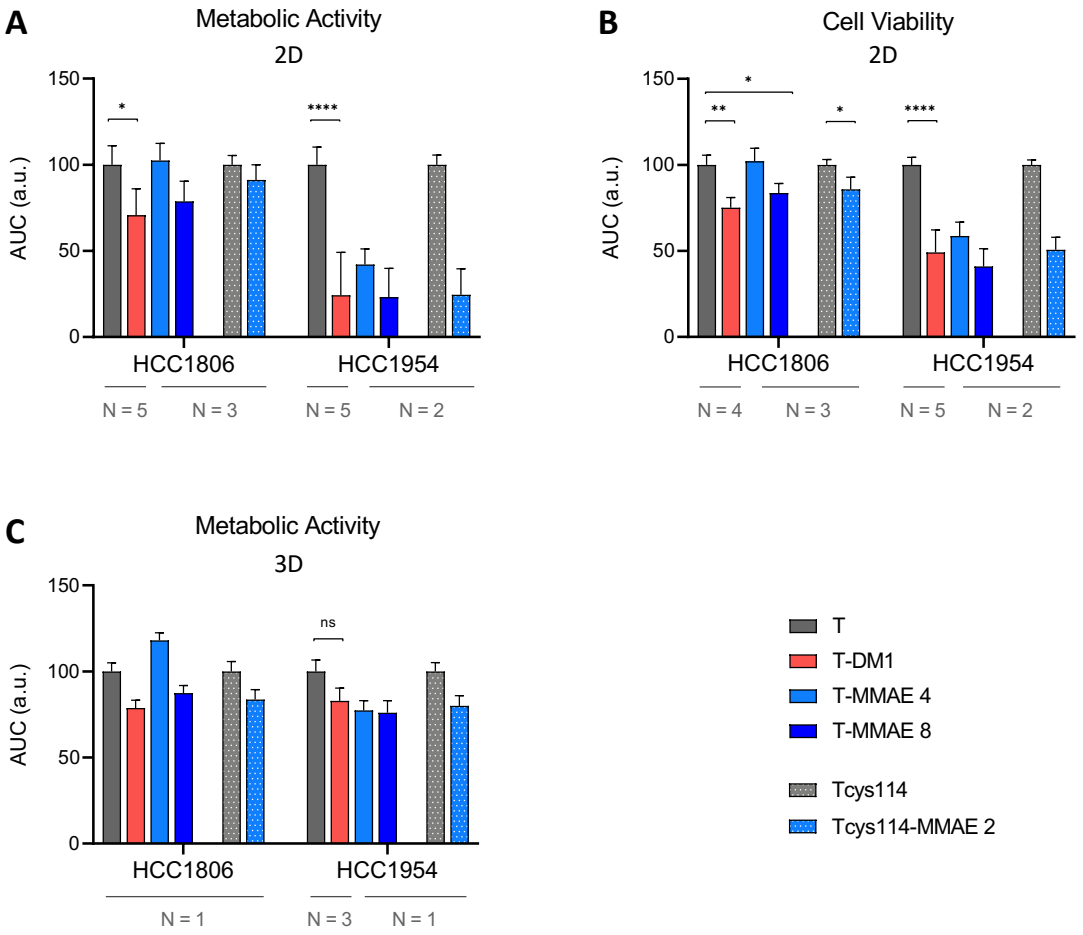

Figure 3.11. Effect of trastuzumab-derived antibody drug conjugates in 2D and encapsulated 3D cultures of HCC1954 [HER2$^+$] & HCC1806 [TNBC] cell lines, assessed by the area under the dose-response curve (AUC) of metabolic activity and viability. Effect in (A & B) 2D and (C) encapsulated 3D cultures. (A & C) AUC of metabolic viability, determined by resazurin reduction. (B) AUC of cell viability, determined by crystal violet staining. Values were determined by mathematical fitting of Log10 [compound] represented on a linear axis with 4 parameter logistic (4PL) regression and are represented as percentage relative to antibody control (T for T-DM1, T-MMAE4 and T-MMAE 8; Tcys114 for Tcys114-MMAE2). Data shown as mean ± SD of N independent experiments, as indicated in the figure. For N=1, values correspond to mean ± SD of technical quadruplicates; two-way ANOVA analysis with a correction for multiple comparisons (to a control, either T or Tcys114) using Dunnett's post-hoc statistical hypothesis test was performed when N ≥ 3. Significances are depicted as: n.s.: not significant, *p < 0.05, **p < 0.01, ***p < 0.001, ****p < 0.0001. T = trastuzumab, T-DM1 = trastuzumab-emtansine, T-MMAE 4 = trastuzumab-monomethyl auristatin E (DAR 4), T-MMAE 8 = trastuzumab-monomethyl auristatin E (DAR 8), Tcys114 = modified trastuzumab with substituted alanine for cysteine at position 114, Tcys114-MMAE 2 = modified trastuzumab with substituted alanine for cysteine at position 114 conjugated with monomethyl auristatin E (DAR 2).

The methods used in this study, such as resazurin reduction (PrestoBlue™ assay), provide a general picture of the variation in cell metabolic activity after drug challenge but does not give spatial information of the cells affected within the spheroids. So, fluorescence microscopy analysis was used to discriminate the cells affected by the T-ADCs in each condition. Cell viability (Figure 3.12) and cell apoptosis (Figure 3.13) were evaluated. For this, encapsulated HCC1806 and HCC1954 spheroids were stained with FDA (live cells) / TO-Pro®-3 (dead cells) and MitoView™ (mitochondrial membrane potential)/ NucView® (apoptosis), after 7 days treatment with 1 µg/mL of each mAb or T-ADC, plus vehicle control. The 1 µg/mL was chosen based on the results described above; at this concentration, a differential effect among the monoclonal antibodies and T-ADCs was observed (Figure 3.10), contrary to the highest dose of 10 µg/mL that induced similar effects in HCC1954 and HCC1806 cells cultured in 3D (Figure 3.10). TO-Pro®-3 and NucView® were used as two measurements of cell death, as the first identifies cells with compromised plasma membranes, and the second identifies late apoptotic cells with activated caspase-3/7.

TO-Pro®-3 staining was more prominent in 3D HCC1954 spheroids (Figure 3.12. B) than in 3D HCC1806 spheroids (Figure 3.12. A). For both cell lines, the reduction in viability upon T-ADC challenge was clear when compared to the mAb- or vehicle- conditions. For HCC1954, it was also observed that T-MMAE 8 had a higher effect than T-MMAE 4, showing once again how increased payload can contribute to increased cytotoxic effect. Nevertheless, it must be taken into consideration that these images are from a single independent experiment (performed with technical quadruplicates), thus further independent experiments will be required to confirm this observation. Upon 7 days of challenge with Tcys114-MMAE at 1 µg/mL, it was observed that the majority of the HCC1954 cells were apoptotic (Figure 3.13), except in the core of the spheroids; on the contrary, under exposure to the same concentration of Tcys114 just a few sparsely distributed apoptotic cells were detected.

These observations corroborate the data obtained when evaluating net metabolic activity of the cultures. It was also observed that T-ADCs induced higher apoptosis levels in HCC1954 (Figure 3.13. B) than in HCC1806 (Figure 3.13. A) but even in the latter, apoptosis was higher with T-ADCs than with the mAb controls (T and Tcys114), or the vehicle control. Comparing the cell viability (Figure 3.12) upon T-ADCs challenge in both cell lines, HCC1806 spheroids (Figure 3.12. A) had a more compact core of live cells (FDA^+) than HCC1954 spheroids (Figure 3.12. B), in which the cells in the core were looser, and many dead cells were detected. The apoptosis staining, (Figure 3.13) allowed a clearer identification of individual dead cells than viability staining (Figure 3.12), both in the outer layer and in the core of the HCC1954 spheroids challenged with the T-ADCs (Figure 3.13. B), in higher amount than in the HCC1806 spheroids exposed to the same challenge (Figure 3.13. A). The increased specificity from apoptosis staining with NucView® 488 derived from specific recognition of the DEVD sequence form caspase-3/7 in discrete regions of the cytoplasm (Figure 3.13), while in viability staining TO-PRO-3® Iodine penetrates compromised membranes and accumulates fluorescence indiscriminately in the cytoplasm (Figure 3.12).

In summary, exposure of alginate-encapsulated 3D spheroids to T-ADCs showed that the drugs induced a less evident reduction of metabolic viability than in 2D assays, with HCC1954 showing higher susceptibility than HCC1806. In fact, even at the highest T-ADCs concentration applied, there was still detectable metabolic activity (35% to 40% of vehicle control), whereas in the 2D cultures the metabolic activity observed after 3 days of challenge was residual (5% to 15% of vehicle control). These results were corroborated by the fluorescence microscopy analysis, as increased loss of cell viability and increased apoptosis were observed in HCC1954 cells, particularly in the outer layer of the spheroids (that retained a viable core), suggesting that the 7 days of exposure were not enough to allow for a homogeneous distribution of the drug. Another hypothesis is that the cells in the core of the spheroids presented a slower proliferation rate than the ones on the spheroid periphery and therefore were less susceptible to the T-ADCs.

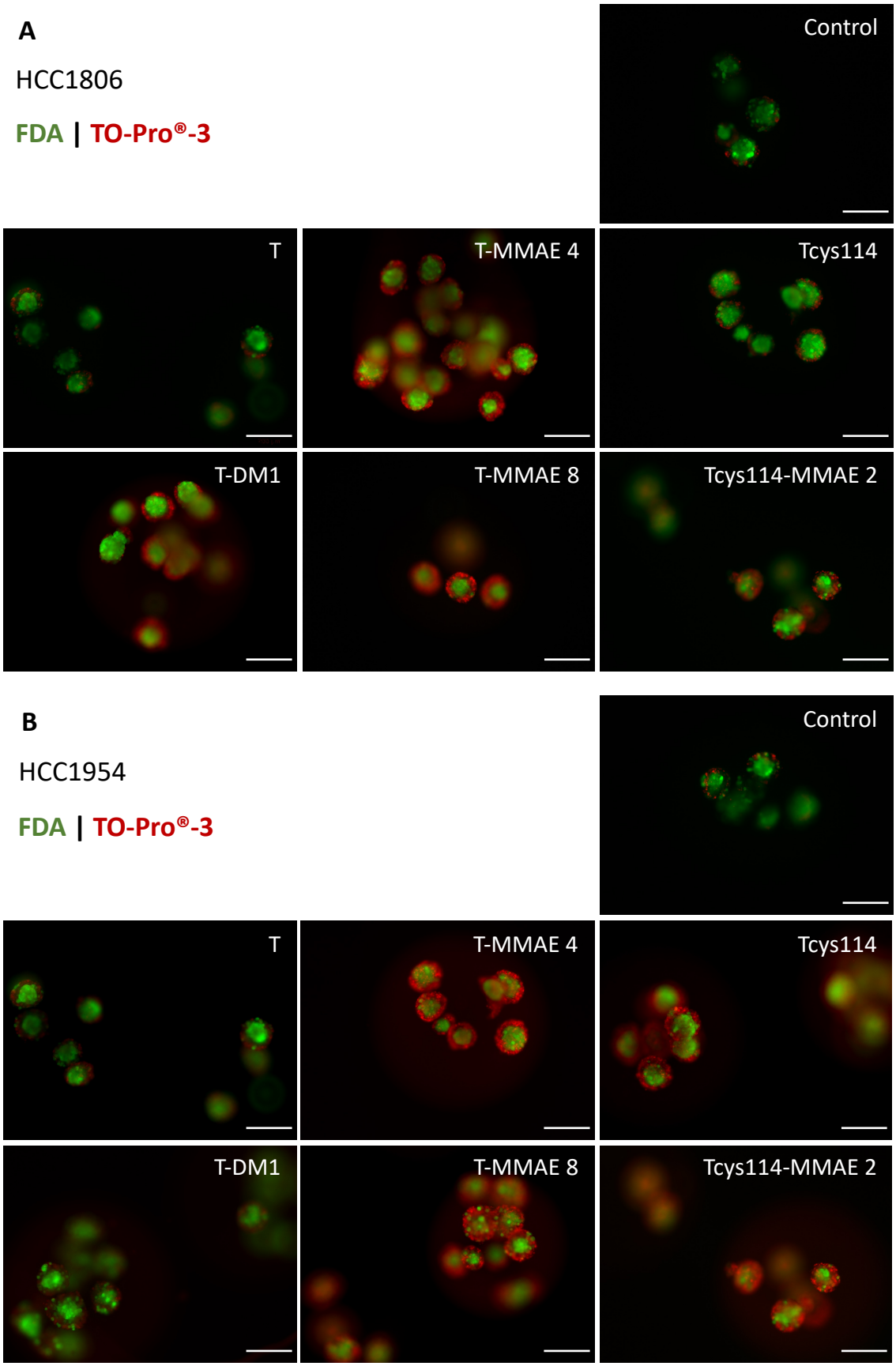

Figure 3.12. Effect of trastuzumab-derived antibody drug conjugates (7-day challenge) in cell viability of HCC1954 [HER2$^+$] & HCC1806 [TNBC] cells in encapsulated 3D spheroids, assessed by fluorescence microscopy. Effect on HCC1806 (A) and HCC1954 (B) cell viability. Drug challenge conducted for 7 days at 1 μg/mL. Staining with FDA (green) shows live cells and staining with TO-Pro®-3 (red) shows dead cells. Scale bars represent 200 μm. Representative images from one experiment with technical quadruplicates.

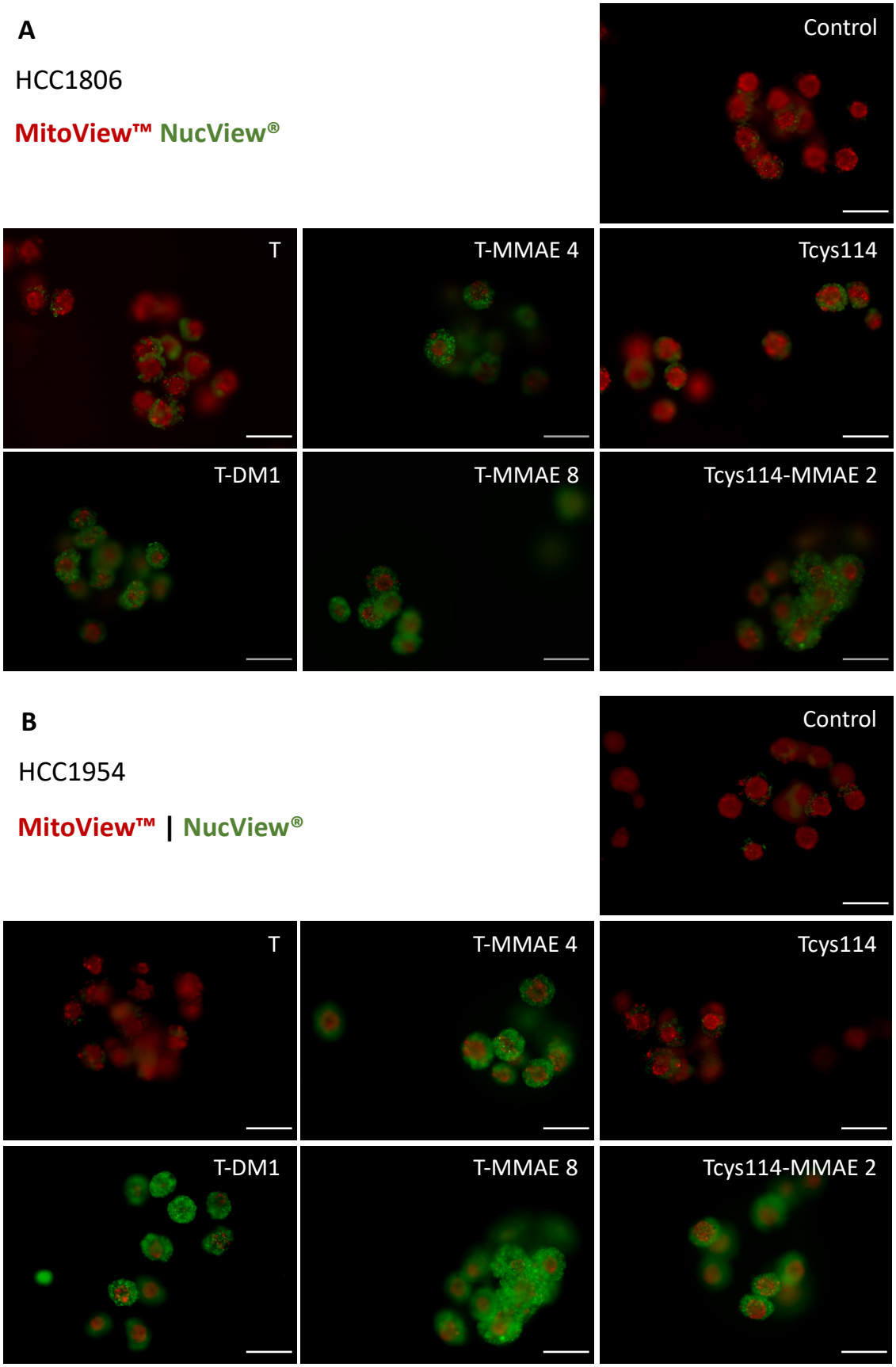

Figure 3.13. Effect of trastuzumab-derived antibody drug conjugates (7-day challenge) in cell apoptosis of HCC1954 [HER2$^+$] & HCC1806 [TNBC] cells in encapsulated 3D spheroids, assessed by fluorescence microscopy. Effect on HCC1806 (A) and HCC1954 (B) cell apoptosis. Drug challenge conducted for 7 days at 1 µg/mL. Staining with MitoView™ (red) shows live cells and staining with NucView® (green) shows late apoptotic cells. Scale bars represent 200 µm. Representative images from one experiment with technical quadruplicates.

As for the first hypothesis, the behavior observed is in accordance with the largely reported difficult tissue penetration and heterogeneous distribution of antibodies within solid tumors.[119,120] Macromolecular compounds such as monoclonal antibodies face particular extravascular distribution difficulties due to their high molecular weights and target-binding affinity, as well as a range of other factor such as vascularity, hypoxia, or drug efflux transporters, thus resulting in slow and often inefficient drug penetration.[121,122] Regarding the biomaterial component of the 3D cell models employed in this thesis, in a previous work from the host Lab, *Cartaxo et al., 2020* have demonstrated penetration and diffusion of a fluorescent antibody in alginate capsules, reaching the tumor cell spheroids [119], therefore we do not expect the encapsulation to affect drug penetration.

The slower growth rate (higher doubling time) of cells cultured in 3D is a well-studied phenomenon that among others derives from space restrains [80] and as the cytotoxic drugs conjugated to trastuzumab are antimitotic agents, it is expected that these take longer time in 3D than 2D to exert their cytotoxic effect. Moreover, it has been largely described that a quiescent center may be formed in tumor cell spheroids, due to diffusional limitations of oxygen and nutrients.[79,80] Also, cell growth has been described to be repressed by collagen physical properties [85] and it is established how encapsulated 3D spheroids promote higher accumulation of ECM proteins such as this, in relation to 2D culture.[82]

These differential cell response within each cell line to the T-ADCs was only possible in 3D models, as in 2D all cells are equally exposed to nutrient, oxygen and drugs and the concentration gradients present in tumors are not recapitulated.[120] Overall, this suggested that more time might be required in 3D culture systems for observation of the same effect.

3.1.3. Assessment of the long-term effect of T- ADCs in 3D BC cell models

As described in Section 3.1.3., when encapsulated 3D spheroids were exposed to T-ADCs for 7 days, there was a proportion of exposed cells that remained alive, suggesting that a longer exposure to the drugs would be required to observe maximum therapeutic effect. To setup longer-term studies, we focused on the HCC1954-based encapsulated 3D spheroid model. We took advantage of the amenability of the 3D cell culture strategy employed in this thesis as, in fact, it is compatible with long-term and cyclic drug exposure regimens.[81] The schematic of the experimental design in represented in Figure 3.14. Microencapsulated spheroids were cultured for one week, under agitation, prior to exposure to the drugs, for one or two weeks (Figure 3.14). The initial 7-day culture period was introduced to promote the molecular crosstalk between tumor cells, establishing paracrine interactions regulated by secreted molecules (growth factors, cytokines) and ECM.[82]

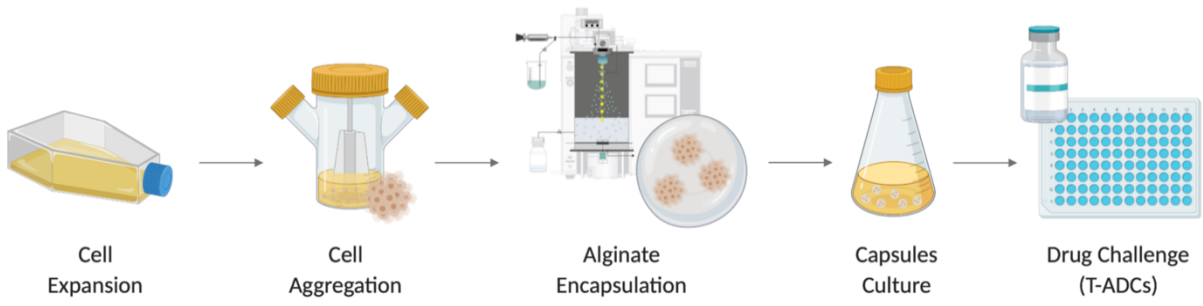

Figure 3.14. Schematic representation of the experimental design used for the for generation of encapsulated 3D cell models and for the long-term drug challenge. HCC1954 cells expanded in 2D cultures systems were inoculated in spinner vessels to induce aggregation into spheroids. Cancer cell spheroids were encapsulated in alginate and cultured for one week under agitation, to generate the 3D cell model, which was subjected to drug challenge with the trastuzumab-derived antibody drug conjugates (T-ADCs). Image created with BioRender ©.

To have a direct quantitative measurement of the cytotoxicity induced by the drugs, the lactate dehydrogenase (LDH) release assay was employed. LDH is a cytoplasmic enzyme that, upon plasma membrane damage, is released to the extracellular space. The LDH release assay consists in the measurement of the enzymatic activity of LDH in the culture supernatant. This assay has been described by *Gordon et al.*[123] or *Fotakis & Timbrell* [124] as a one of the most used methods providing a rapid and reliable detection of cell death following exposure to toxic substances. Other methods described for *in vitro* assessment of drug-induced cytotoxicity are indirect, relying on measurement of cell viability and proliferation such as ATP production or DNA content (e.g., crystal violet), metabolic activity (e.g., MTT, MTS and resazurin reduction assays), cellular uptake and binding (e.g., neutral red uptake) and colony formation ability. Assays that measure apoptosis, such as caspase activity can also be employed if this is the death mechanism induced by the drug.[123,124] One potential benefit of the LDH cytotoxicity assay is the ability to distinguish between cell death and growth inhibition; another advantage is that it is not a destructive assay and cells can be either use for additional readouts or remain in culture. Moreover, it has also advantages for 3D cultures, in which dead cells/cellular remains may be trapped in the 3D structure and accounted as live cells as in other assays such as crystal violet (where dead cells remain encapsulated and therefore the DNA of necrotic cells would also be accounted).[123,124] LDH release is regularly used in the host Lab for assessment of cytotoxicity in drug challenge of 3D cell models with targeted therapies.[125]

Prior to the assessment of cytotoxicity, the linearity range of the assay employing encapsulated HCC1954 spheroids was determined. To this end, different amounts of capsules were plated and the metabolic activity (resazurin reduction assay, Figure 3.15. A) and total LDH activity assessed after membrane disruption of the cells in culture with Triton™ X-100 (Figure 3.15. B). As shown in Figure 3.15. B, the mean values of LDH activity were within the linearity range for all capsule concentrations tested although above 40 capsules *per* well, a higher standard deviation was detected but were similar to the standard deviation obtained for the metabolic activity measurements (Figure 3.15. A). As these results derive from a single independent experiment (performed with technical quadruplicates), this increased standard deviation was probably due to technical issues in the capsule distribution procedure. We continued with the previously used range of 25 to 30 capsules *per* well, that had yielded a good linearity and low standard deviations.

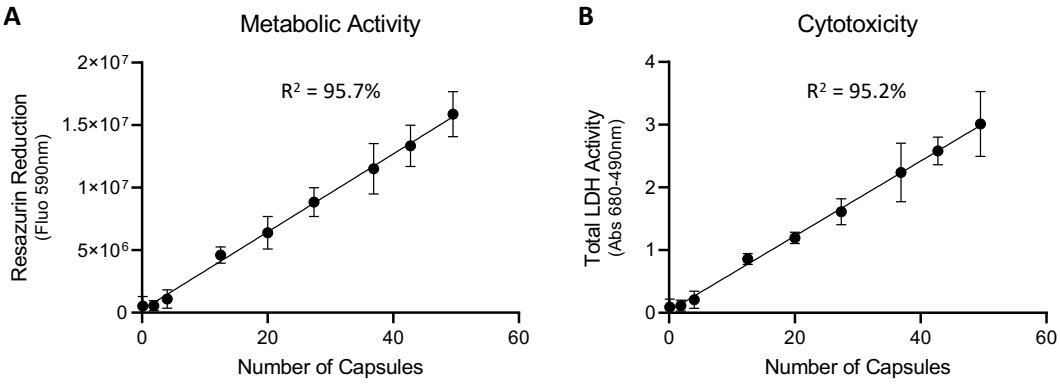

Figure 3.15. Calibration curves of resazurin reduction and LDH activity as a function of the number of capsules containing HCC1954 [HER2⁺] spheroids. (A) Metabolic activity as a function of the number of capsules. Linear regression, with an R^2 of 95.7%. (B) Total LDH activity as a function of the number of capsules. Total LDH activity determined by total cell lysis by exposure to the detergent Triton™ X-100. Linear regression, with an R^2 of 95.2%. Data presented as mean ± SD of technical quadruplicates. Number of capsules plated determined from the calibration curve presented in Figure S.28.

For the next assays, drug challenge comprised only one T-ADC for determination of EC50, so that challenge with the same ADC concentration in future experiments could be performed, thus allowing a more feasible experimental setup and practical comparison of their effects. Tcys114-MMAE 2 at 8 serial concentrations, within the same range applied before (from 0.001 to 10 µg/mL), was the T-ADC of choice. These concentrations yielded good results on the experiments described above, namely a reduction in cell viability and metabolic activity in the same order of magnitude as the other tested T-ADCs, thus being comparable and allowing to extrapolate a correlation to those. This assay would therefore provide a quantifiable assessment of an optimal concentration to apply with all T-ADCS and mAbs used before and determine their effect in further experiments. Although it is expected that EC50 may vary among the tested ADCs, the range of concentration where a more accentuated slope in the variation of metabolic activity or cytotoxicity is observed should be within the same order of magnitude since the above experiments demonstrated a similar effect among them.

A first experiment sought to determine whether the suggested 1- or 2-week drug challenge period could determine effect in metabolic activity and cytotoxicity (Figure 3.16). For assessment of cytotoxicity overtime, only LDH leakage was detected whereas the normalization of LDH activity with maximum LDH release upon membrane permeabilization was not performed in order to assess spontaneous release of LDH over a 2-week period.

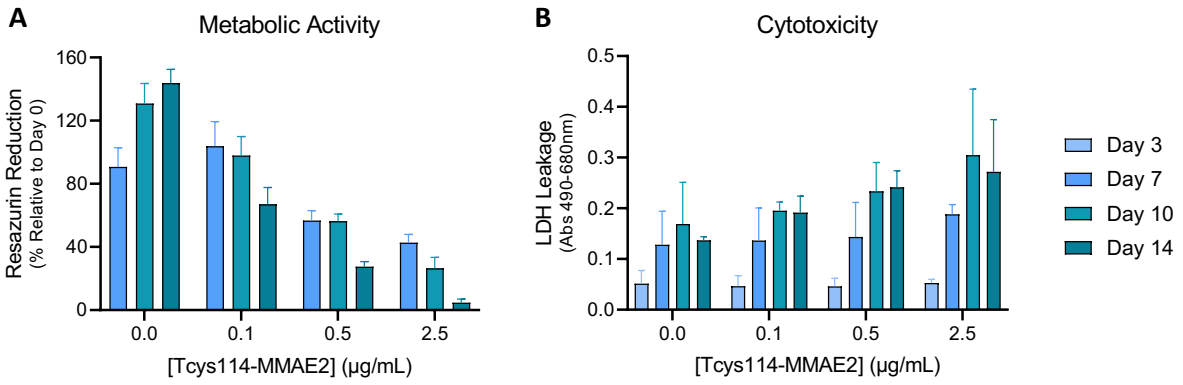

Figure 3.16. Assessment of the overtime effect of trastuzumab-derived antibody drug conjugates on the metabolic activity and cytotoxicity of HCC1954 [HER2$^+$] cells in encapsulated 3D cultures. (A) Effect on metabolic activity (over 2-week challenge) assessed by resazurin reduction and represented as percentage relative to day 0. (B) Effect on cytotoxicity (over 2-week challenge) assessed by LDH leakage. Data shown as mean ± SD of technical quadruplicates. Presence of outliers tested using Grubb's Test, alpha 0.05. Tcys114-MMAE 2 = modified trastuzumab with substituted alanine for cysteine at position 114 conjugated with monomethyl auristatin E (DAR 2).

The evolution of Tcys-MMAE 2 effect overtime in metabolic activity (Figure 3.16. A) and cytotoxicity (Figure 3.16. B) was assessed to determine whether prolonged drug exposure up to 2 weeks would provide a timeframe amenable to observe a potential time-dependent increase in drug effect. For this preliminary assay, only three intermediate drug concentrations (from 0.1 to 2.5 µg/mL) and vehicle control were evaluated (in quadruplicate). Over the 2-week drug challenge, it is observed how metabolic activity increases in the untreated condition, in agreement to expected increased cell proliferation (Figure 3.16. A), by opposition to the three conditions with Tcys114-MMAE2, where metabolic activity decreases, in particular between 10 to 14 days. From 7 to 10 days drug challenge, longer drug challenge does not appear to result in a significant increased effect. Moreover, increased concentration relates to decreased metabolic activity in every timepoint, as expected. A similar behavior is observed at the cytotoxicity level, measured by LDH leakage (Figure 3.16. B). Three-days ADC challenge was not sufficient to induce LDH leakage, so we excluded

this time point from subsequent analysis. LDH leakage was observed starting from 7 days, particularly at the higher drug concentration tested, with increased effect observed at 10 and 14 days. Having this result in mind, it was concluded that the 1- to 2-weeks drug challenge period provides an amenable timeframe to assess the effect of Tcys114-MMAE 2.

Afterwards, Tcys114-MMAE 2 challenge for either 1 or 2 weeks was performed (Figure 3.17). An analysis of the results from metabolic activity (Figure 3.17. A) suggests that the observable effect of Tcys114-MMAE 2 in reducing activity is higher upon 2 weeks of drug challenge than 1 week, as it was anticipated. Nevertheless, in both challenges, higher drug concentrations correlated with lower metabolic activity (Figure 3.17. A), suggesting a decreased cell viability. A longer drug challenge (2 weeks compared to 1 week) also resulted in a more accentuated reduction of cellular metabolism (60% upon 1 week and 80% upon 2 weeks at the highest tested concentration), at the point that, at higher concentrations (above 2.5 µg/mL), the remaining metabolic metabolism is minimal (around 0% to 5% for 2 weeks). Indeed, upon 2-weeks drug challenge, the reduction in metabolic activity (Figure 3.17. A) is accompanied by a parallel 3-fold increase in cytotoxicity (Figure 3.17. B) revealed by a dose-dependent increase in LDH activity in culture medium (LDH leakage normalized to total LDH activity). This fact suggests that both assays are complementary and support each other: while increased drug concentration translates in a reduction of metabolic activity, it also corresponds to increasing cell cytotoxicity. Yet, LDH leakage was not observed at 1 week (Figure 3.17. B), which suggests that reduced mitochondrial metabolism due to ADC exposure, revealed by the resazurin reduction assay, occurs prior to cytotoxicity detection.

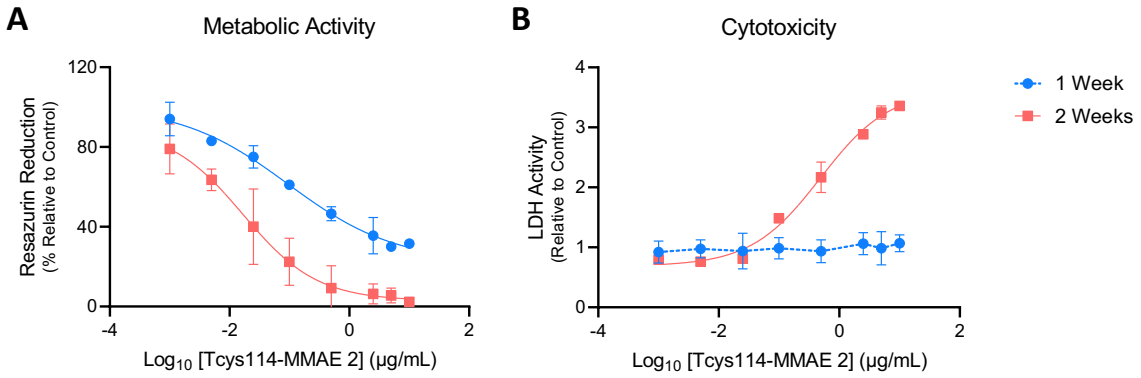

Figure 3.17. Effect of trastuzumab-derived antibody drug conjugates (1- or 2-week challenge) on the metabolic activity and cytotoxicity of HCC1954 [HER2⁺] cells in encapsulated 3D cultures. (A) Effect on metabolic activity assessed by resazurin reduction, normalized to day 0 and represented as percentage relative to vehicle control. (B) Effect on cytotoxicity assessed by LDH activity values (ratio of LDH leakage over total LDH activity) and represented as fold change relative to vehicle control. Data shown as mean ± SD of 2 independent experiments. Presence of outliers tested using Grubb's Test, alpha 0.05. Filled lines represent the nonlinear 4 parameter (4PL) regression of Log [Tcys114-MMAE 2]; values determined are presented in Table 3.14. Tcys114-MMAE 2 = modified trastuzumab with substituted alanine for cysteine at position 114 conjugated with monomethyl auristatin E (DAR 2).

These observations are also supported by the EC50 value provided in Table 3.14. In metabolic activity at 1 or 2 weeks, the EC50 value, yielded by nonlinear fit, was 0.095 or 0.017 µg/mL, respectively, while cytotoxicity corresponded to an EC50 of 0.487 µg/mL at 2 weeks. The decrease in EC50 concentration of metabolic activity from 1 to 2 weeks reflects how a lower concentration has equivalent effect upon prolonged drug challenge than a higher concentration for a shorter period. When comparing both metabolic activity and cytotoxicity values at 2 weeks, the higher EC50 concentration expresses the decreased susceptibility in assessing LDH leakage when compared to metabolic activity assay, such that, at 1 week,

there is no increase in LDH activity (Figure 3.17 B) to determine EC50. As such, in future experiments, the effect of T-ADCs upon 2-weeks drug challenge at a fixed concentration between 0.01 and 0.5 µg/mL would be of interest to evaluate.

Table 3.14. Half effective maximum concentration (EC50) of the effect of trastuzumab-derived antibody drug conjugates (1- or 2-week challenge) on the metabolic activity and cytotoxicity of HCC1954 [HER2+] cells in encapsulated 3D cultures. Values determined by nonlinear 4 parameter (4PL) regression of Log [Tcys114-MMAE 2] of 2 independent experiments represented on Figure 3.17. Tcys114-MMAE 2 = modified trastuzumab with substituted alanine for cysteine at position 114 conjugated with monomethyl auristatin E (DAR 2).

Metabolic Activity	Cytotoxicity
$EC50_{1\ week}$ = 0.095 µg/mL	–
$EC50_{2\ weeks}$ = 0.017 µg/mL	$EC50_{2\ weeks}$ = 0.487 µg/mL

As previously pledged, the improvement in novel BC models for pre-clinical phases of drug development served as motivation for this work. While the growing knowledge and innovation in drug discovery over the last years has provided new molecular targets and therapeutic approaches to address BC, advance on pre-clinical models in use has not, in general, been coincident. To this day, still many drug development assays rely on challenge of cells cultured in monolayer (2D) and a few percentage of papers have evolved to novel and more complex 3D models, with wide advantages in recapitulating TME, such as spheroids cultures [126,127] or tumor organoids [94,128], described and advocated as useful tools for this purpose.

One particular study by *Sachs, et al., 2018* [129] described the generation of a living biobank composed of over 100 BC organoid lines that broadly recapitulate histological and genetic features of original tumors. Blinded histopathological analysis showed preservation of ER/PR in around 75% of organoids derived from ER^+/PR^+ tumors, while HER2 status was retained in 80% of $HER2^+$ tumor-derived organoids.[129] However, IHC analysis was performed with unprocessed pieces from each sample at day 0 and consequently no long-term maintenance of these key biomarkers was assessed. Nevertheless, *in vitro* drug assays revealed some heterogeneity in response of BC organoids to diverse anti-HER2 targeted therapy upon viability analysis (CellTiter-Glo), both between distinct organoids with similar HER2 expression upon the same drug challenge, and between different drugs applied to the same organoid.[129] Although authors consider drug sensitivities obtained *in vitro* to bear physiological significance, we must consider the high degree of processing and selection of samples, which were subjected to isolation of tumor viable cells and do not retain original TME, neither the diversity of non-tumorous cell types, such as stroma.

Remarkably, the use of spheroids (particularly from BC) for the evaluation of the effect of anticancer drugs, and namely ADCs, has yet been scarce, but some publications [130–132] have already reported these models for assessment of ADC efficacy. One of them, *Arhoma et al.*[131] has used both a suspension culture and an alginate-based 3D culture model similar to the one we employ, to assess the therapeutic effect of a ligand protein in multiple myeloma cells, assessing growth inhibition (CellTiter-Glo) and apoptosis (PI fluorescent microscopy and caspase-3 activity). Interestingly, they found 3D cell spheroids to be more sensitive to the drug tested, compared to 3D suspension cultures that did not show significant apoptosis after challenge. This result is in accordance with the differential therapeutic effect of cell spheroids cultured in 3D upon drug challenge similar to what we have also been describing, although in our findings T-ADCs were shown to be less effective in 3D. As such, this observation contributed to the hypothesis that cells cultures using 3D models have distinct expression of signaling pathways that may alter drug sensitivity.

Most recently, *Durbin et al.* [132] have reported the effect of an ADC using MMAE payload (DAR 4) in treating squamous cell carcinoma spheroids, highlighting how various *in vivo* features, such as tumor penetration, cell interactions and increased resistance to therapeutics, can be integrated into a spheroid model. In this work, it was described how the MMAE ADC notably had weaker potency against spheroids compared to cells in monolayer, similar to what we observed. Nevertheless, upon ADC challenge, spheroid volume still decreased following a dose-dependent kinetic, with over 85% volume reduction at the highest concentrations. Moreover, this volume reduction during treatment appeared to occur from the outside-in, likely because cells from the outside were exposed to a higher local concentration of drug than those further towards the core of the spheroids, one crucial observation that we were able to replicate. In addition, it was reported how in large spheroids there is limited access to oxygen and nutrients at the core, which might contribute to lower proliferation of these cells in relation to the ones at the perimeter of the spheroid. Since mitotic cells are more prone to microtubule inhibitors as MMAE, it may be possible that these cells require longer drug challenge for effect to be observed. This remark is indeed in line with the effect we have reported in 3D spheroids challenged with T-ADCs, where we observed a live core surrounded by dead cells and which might provide an additional explanation to this fact.

Finally, even though all of these observations are in accordance with the findings we have reported, to the best of our knowledge, neither these or any other publication has employed suspension culture of spheroids with agitation and the scaffold-based encapsulation for evaluation of BC targeted therapies, namely anti-HER2 ADCs. As such, we believe the work we present paves the way for future pre-clinical assessment of BC targeted therapies using an agitation-based 3D model of encapsulated spheroids.

3.1.4. Preliminary experiments for assessment of the effect of T-ADCs in long-term encapsulated 3D co-cultures of HCC1954 with hDFs

One of the future aims of this project would be to add other relevant TME cells relevant to this model as previously shown by the host Lab and published in the work by *Estrada et al.*[82] This approach will enable us to evaluate the influence of non-tumorous cells on the effect of drugs such as ADCs in a more complex reconstructed TME. In particular, we intended to assess the effect of stromal cells upon response to ADCs, which has been previously described,[82] to influence tumorigenicity *in vitro*, namely by promoting secretion of pro-inflammatory cytokines, deposition of ECM [133] and phenotypic alterations, typical of aggressive and advanced stages of cancer, which were not observed in the mono-cultures. Stromal cells have also been previously reported to promote cell resistance in $HER2^+$ BC,[134] possibly by the described mechanism of EGF-related growth factors production by fibroblasts that constitutively activate EGFR, serving as oncogenic drivers in BC that promote resistance.[135]

For this purpose, and to support the specificity of T-ADCs on $HER2^+$ cells, immunofluorescence of 2D cultures of HCC1954 and hDFs was performed to characterize the presence of HER2 on the cell membrane (Figure 3.18). The result showed HER2 expression on the cell surface of HCC1954 cells, as expected (Figure 3.18. A). Nevertheless, since HER2 also contains an intracellular tyrosine kinase domain,[51] cytosol staining in HCC1954 was also observed. By opposition, no staining was depicted in hDFs (Figure 3.18. B). The specificity of the secondary antibody to c-erbB-2® is shown in Figure 3.18. C where no staining is observed for HCC1954 cells without the primary antibody. Considering this result, it is expected that hDFs do not exhibit any sensitivity to T-ADCs challenge.

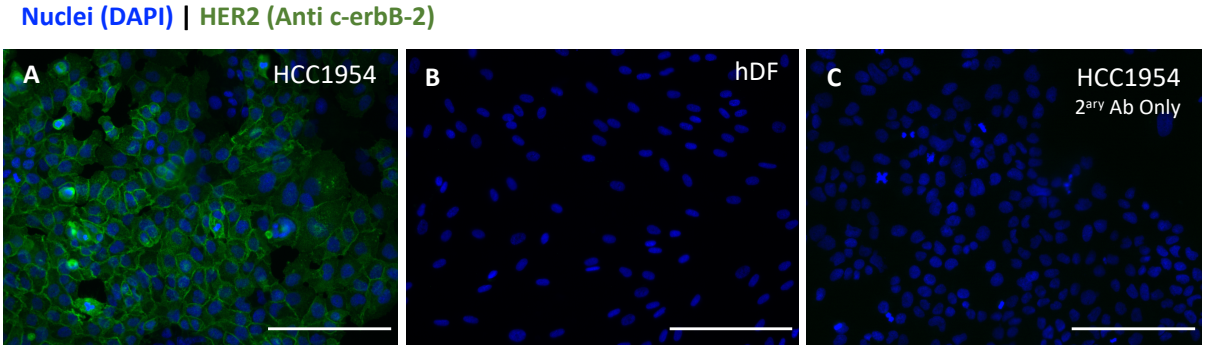

Figure 3.18. Characterization of HER2 detection in HCC1954 cells and hDFs in 2D, assessed by immunofluorescence. HCC1954 cells (A & C) and hDFs (B) were labeled for HER2 (green) with anti c-erbB-2® + AlexaFluor® 488 (A & B), or AlexaFluor® 488 only (C). Cells were counterstained with 4',6-diamidino-2-phenylindole (DAPI, blue) for nuclei identification. Scale bars represents 200 µm. Representative images from one experiment.

A preliminary 2D culture and drug challenge of hDFs, similar to the one described in results section 3.1.1, was applied to further confirm this hypothesis. Drug challenge was conducted with trastuzumab and T-DM1 for 2 weeks (since cell growth ratio is longer for primary hDFs) at 5 serial concentrations (0.001 to 10 µg/mL) and the effect was assessed by cell viability, measured by crystal violet assay (Figure 3.19).

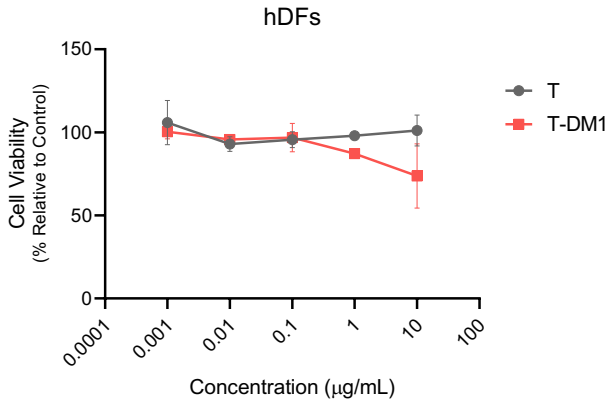

Figure 3.19. Effect of trastuzumab and trastuzumab-DM1 (2-week challenge) on the cell viability of hDFs in 2D cultures. Cell viability is represented as percentage relative to vehicle control. Data shows mean ± SD of 2 independent experiments. Presence of outliers tested using Grubb's Test, alpha 0.05. T = trastuzumab, T-DM1 = trastuzumab-emtansine.

Analysis of cell viability upon drug challenge showed similar behavior between hDFs and HCC1806 2D cultures (Figure 3.8. B). Overall, there is no significant effect on the reduction of cell viability by T-DM1 in comparison to trastuzumab (exception made to 10 µg/mL), similarly to the effect observed in the TNBC cell line. However, at the higher drug concentration, 10 µg/mL, there is a slight decrease of approximately 22% in cell viability associated with T-DM1 which is considered to be a result of unspecific effect derived from high drug concentration, in accordance with the observed effect in HCC1806 2D cultures reported above (87% reduction at the highest concentration). Having this in mind, one can conclude that hDFs are not sensitive to the effect of T-ADCs, so that, when co-cultured with HCC1954 spheroids, any cytotoxicity would only derive from the effect of T-ADCs towards cancer cells, which could be potentially modulated or not by the presence of hDFs, due to paracrine interactions and crosstalks established between both cell types.

Finally, a preliminary experiment consisting of HCC1954 mono- and co-culture with hDFs was performed to assess cell viability of the mono- versus the co-culture (Figure 3.20). It was observed a homogeneous distribution of fibroblasts and tumor spheroids within alginate spheroids, and that co-culture in shake flasks could be maintained at least 2 weeks without loss of cell viability. In addition, upon visual analysis, it was observed how, over time, spheroids have increased in size, suggesting tumor cell growth in both cultures.

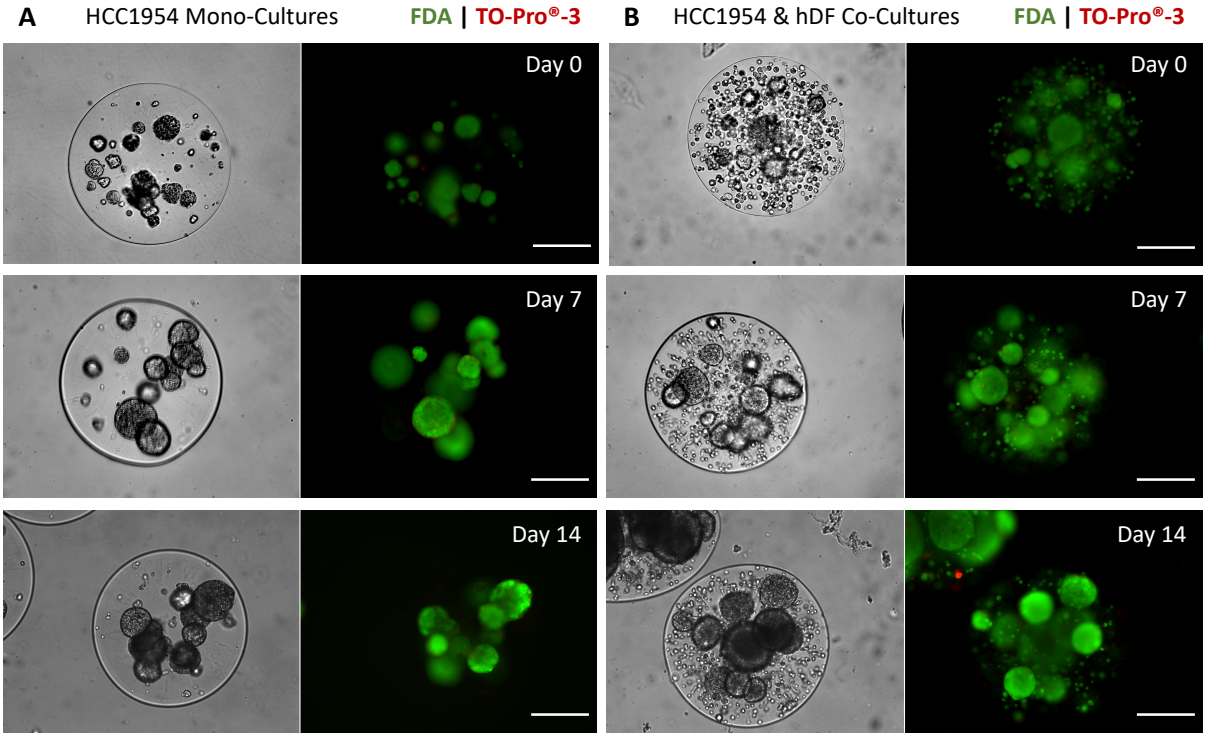

Figure 3.20. Characterization of cell viability of HCC1954 mono-culture and HCC1954 & hDF co-culture in encapsulated 3D spheroids (over 14 days) assessed by fluorescence microscopy. (A) HCC1954 mono-culture. (B) HCC1954 & hDF co-culture (ratio 1:1). Staining with FDA (green) shows live cells and staining with TO-Pro®-3 (red) shows dead cells. Scale bars represent 200 µm. Representative images from one experiment.

As such, in future experiments, we intend to perform drug challenge of these long-term mono- and co-culture models with all T-ADCs and mAb at the selected concentration from Figure 3.17 and Table 3.14 analysis. This would allow a thorough characterization of ADCs effect in an *in vitro* TME composed by different cell types and assess if acquired resistance mechanisms could be observed. To fulfil this purpose, some possibilities would rely on assessment whether reduced HER2 expression in HCC1954 cells co-cultured with hDFs could be determined [136] or if accumulation of ECM could be measured. Indeed, this last aspect was previously reported by the host Lab using lung cancer cells.[82] Stroma-targeting ADCs, in particular, have been described to elicit potent anti-cancer activity through an unexpected killing mechanism termed DAaRTS (drug activation and release through stroma), where tumor microenvironment localizes active drug at the tumor site and, following capture of ADC, stromal cells release MMAE free drug, killing nearby proliferating tumor cells in a target-independent manner.[137] Unfortunately, due to time limitations, these experiments were not pursued within the scope of this MSc thesis but remain an interesting point to develop.

Interestingly, a previously mentioned work from the host Lab by *Cartaxo et al., 2020* [119] provides a useful computational diffusion model to study Ab transport within the employed *in vitro* encapsulated tumor spheroids BC model, assessing Ab penetration in alginate, diffusion to tumor spheroids and even effect of

other cellular components, such as fibroblasts on these precise mechanisms. This platform could be further developed and combined with the described experimental model to assess the therapeutic antibody distribution within a recreated TME, not only to decipher how non-tumorous elements (as fibroblasts and collagen) interact with the tumor cells or TME in general and how they can influence drug transport, but also to work as a predictive tool. This would help reducing experimental burden and costs by identifying specific conditions of interest for experimental testing.

In summary, T-ADCs effect was shown to be specific for $HER2^+$ HCC1954 cell line, and that 3D cultures require longer drug challenge periods and higher drug concentrations to observe an equivalent effect of T-ADCs to the one observed in 2D cultures. Moreover, both HCC1806 TNBC cell line and hDF cells were shown not to be specifically targeted by T-ADCs, although HCC1806 was sensitive at the highest concentration.

This system has then proven to be suitable to analyze the potential effect of T-ADCs and has shown their increased effect on both reduction of cell viability and metabolic activity or increase in apoptosis induction and cytotoxicity in comparison to the mAbs alone. This effect was quantified in long-term 3D cultures resulting in determination of the EC50. Moreover, preliminary experiments regarding HCC1954 and hDFs co-cultures were carried out, demonstrating successful encapsulations which were homogeneous and maintained high cell viability over 2 weeks.

As such, addressing the relevance of 3D co-cultures of tumor cells with hDFs remains an interesting future point to pursue, since it represents trastuzumab-induced apoptosis better than 2D mono-cultures [139] and considering that stroma has been particularly described to be related to T cell resistance.[138] Nevertheless, to the best of our knowledge, none of the studies reporting the use of 3D spheroid cultures have assessed the effect of tumor cell co-cultures in response to T-DM1 or BC ADCs in general. Other co-culture models of tumor cells with NK cells, for instance, have been described for assessment of the effect of T-DM1 on overcoming trastuzumab resistance [140] but their use was limited to 2D cultures. In contrast, models based on tumor organoids, that have recently drawn major interest, face a major limitation due to absence of stroma, blood vessels and immune cells,[94] which could be accomplished in our 3D model by incorporation of fibroblasts, endothelial cells and/or monocytes, for example.

3.2. Assessment of the potential of endocrine therapies using an *ex-vivo* ER$^+$ BC PDE model

In the context of the second objective comprised by this thesis, patient-derived explants were kindly provided by Dr. Saudade André from IPOLFG, thanks to the fruitful collaboration established with iBET. Following the protocol implemented by the Lab, processed and encapsulated BC microtissues show maintenance of high viability, tissue heterogeneity, active ER expression and signaling and active metabolism.[91] At the same time, this strategy allows maintenance of original ECM components, preserving the desired tumor-stroma crosstalk and cell-cell contact by keeping the original tumor architecture. In the scope of this objective, we wanted to assess the amenability to use this BC *ex vivo* model to evaluate the antiestrogenic activity of targeted drugs. For this, we challenged the model with standard-of-care anti endocrine drugs, tamoxifen and fulvestrant, and analyzed *ER* downstream signaling by RT-qPCR. The general strategy used within this model is represented in Figure 3.21.

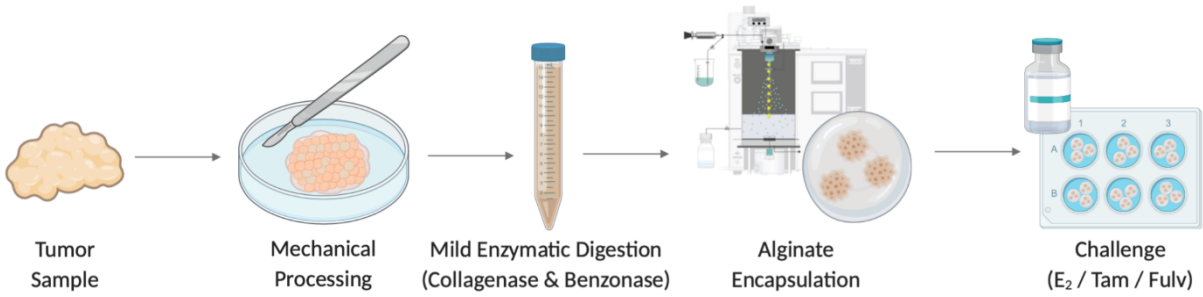

Figure 3.21. Schematic representation of the experimental design used for the *ex vivo* patient-derived explants culture and for the drug challenge. Tumor samples were mechanically processed, mildly digested and encapsulated in alginate to generate the *ex vivo* patient-derived explants model, which was subjected to challenge. Image created with BioRender ©.

Due to primary material limitation during the MSc thesis, we have only received four BC samples, of which one stands of particular relevance for being a male breast cancer (MBC) sample. This MBC sample, B104, had yet the particularity of being of mucinous type (or colloid), which comprise only 1% of the MBC cases.[32]

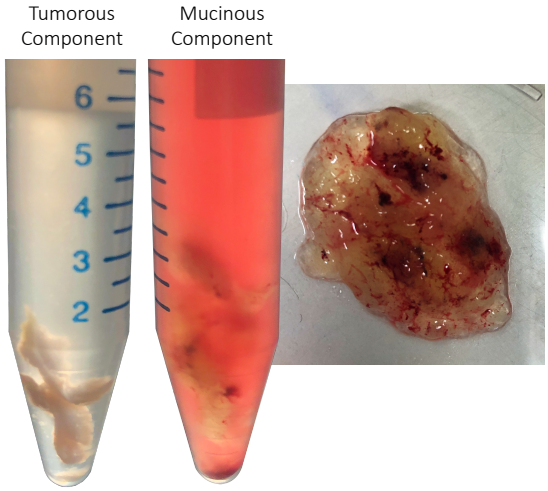

Figure 3.22. Sample B104: Mucinous (M) and Tumorous (T) component of a male breast cancer patient-derived explant (PDE). B104 sample information described in Table S.15.

Mucinous BC is characterized by clusters of generally small and uniform cells floating in large amounts of extra-cellular mucin.[16] Mucin is a heavily glycosylated protein produced by epithelial cells to form a mucous protective barrier.[16] Classic mucinous carcinoma is composed of more than 90% mucin (pure), although most common are mixtures with invasive carcinoma (IC) of no special type (NST).[16] B104 sample (Figure 3.22) was a mixed tumor and indeed possessed both an invasive mucinous carcinoma (IMC) component (B104 M) and an IC NST component (B104 T), reason why they were cultured as two independent samples.

For the drug challenge, tamoxifen and fulvestrant, both ER antagonists used in clinic as first line of treatment for ER^+ BC, were applied as a proof of concept to validate the model for further use in novel endocrine drugs development. Previous drug challenge experiences have been performed in the host Lab, only with fulvestrant (not tamoxifen). That data has shown that *PGR* and *TFF1* gene expression could not be properly assessed upon fulvestrant challenge, since that in the majority of the samples high Ct values were close to the detection limit and reliability of the PCR equipment. On the contrary, *AREG* resulted in being the highest expressed ER target gene and we could observe significant *AREG* gene expression reduction upon fulvestrant challenge.[91] Bearing that in mind, we optimized the method for qPCR-based readout, including a 24 h stimulus with 17β-estradiol (E_2) to activate ER signaling and allow both for 1) assessment of ER maintenance upon *ex vivo* culture and 2) facilitate qPCR-based analysis upon endocrine drug challenge, due to lower starting Ct numbers. A schematic of the estrogen stimulus and drug challenge experimental design used is represented in Figure 3.23. During 18 days drug challenge, two HMEC medium variants were used, a completed and a depleted one, as following described.

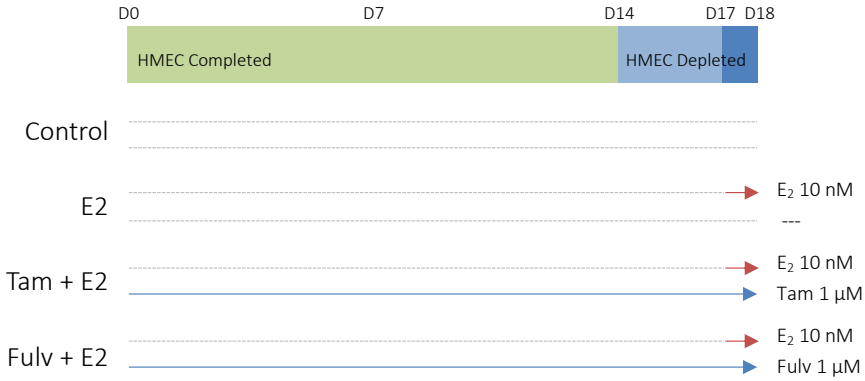

Figure 3.23. Schematic of the estrogen stimulus and endocrine drug challenge applied to the *ex-vivo* patient-derived explant (PDE) culture. Drug challenge with tamoxifen or fulvestrant (1 µM) was conducted for 18 days and estrogen stimulus (10 nM) applied for the last 24 h. PDE were cultured in HMEC completed medium and 3 days prior to estrogen stimulus replaced with HMEC depleted medium.

Culture in complete medium is specific for the needs of mammary epithelial cells and should promote epithelial tumor cell growth. The need for replacement of this medium with one depleted of EGF, insulin and hydrocortisone prior to estrogen addition is dictated by the fact that these factors participate in ER signaling cascade and promote activation of downstream gene expression, independently from E_2 presence. EGF and insulin, which stimulates IGF-I, both stimulate ER's transcriptional activity in an estrogen-independent manner through MAPK signaling pathway, for instance,[141] while glucocorticoids, such as hydrocortisone, inhibits estrogen-regulated ER^+ BC cell proliferation.[142] E_2 stimulation was applied in both challenged conditions and in an unchallenged condition (control), so that from one side we would have an indirect control of ER presence (activation of ER transcriptional activation) and, at the other side, a better evaluation of the effect of standard-of-care endocrine drugs.

3.2.1. Gene and protein expression profile of *ER* and associated genes in *ex vivo* PDE cultures.

In BC patients, about two-thirds of tumors are ER$^+$ and 50% of these are estrogen-dependent and respond to endocrine therapy. [143] Additionally, BC occurring in post-menopausal women are often ER$^+$ and many of these tumors significantly express more ER than the normal mammary epithelium.[143] With this in mind, maintenance of *ER* signaling is crucial for the correct recapitulation of *in vivo* ER$^+$ tumors. However, since the loss of ER expression in 2D cultures is a well-known phenomenon,[91] we started by evaluating the maintenance of ER signaling in an *ex vivo* 3D model of PDE, described to be amenable for this effect.[90,91]

For this purpose, gene expression of *ER* and downstream regulated genes *PGR*, *TFF1* and *AREG* was analyzed as depicted in Figure 3.24. *PGR* is the gene encoding progesterone receptor (PR) and a directly induced target gene of ER, involved in cell proliferation and with an estrogen response element (ERE) half site.[2,144] *TFF1* gene encodes trefoil factor 1, a secreted protein, with possible cell tumorigenesis functions in mammary cells,[28] which is a classic example of an estrogen-direct induced gene, since its promoter displays an estrogen response element (ERE) at 400 bp before TFF1 transcriptional starting site.[145] Lastly, *AREG* encodes amphiregulin, a protein member of EGF family regulated by ER and that binds to EGF promoting mammary gland development and it has been involved in BC tumorigenesis.[27]

Although E_2 is expected to stimulate expression of *ER* associated genes, *ER* itself appeared downregulated (Figure 3.24) as previously described by *Borrás et al., 1994* [146] and *Liu & Shi, 2015* [147] as a negative feedback mechanism. As to *PGR*, *TFF1* and *AREG*, it is observable an overall increase in gene expression upon E_2 stimulation, although with significant differences in magnitudes among them (up to 6-fold increase in *PGR*, 18-fold in *TFF1* and 11-fold in *AREG*). Even though, one can notice that some samples do not exhibit such a prominent overexpression of these genes when compared to other samples, which is attributable to the heterogeneity of PDE response from different donors, the general effect is in accordance with the expected findings. Interestingly, some samples (B95, B96 and B97) even showed down expression of *PGR* (Figure 3.24), but assessment of all genes showed no contradictory result simultaneously in all of them, supporting the different compensatory mechanism observed *in vivo* that can influence and mediate alternative responses.

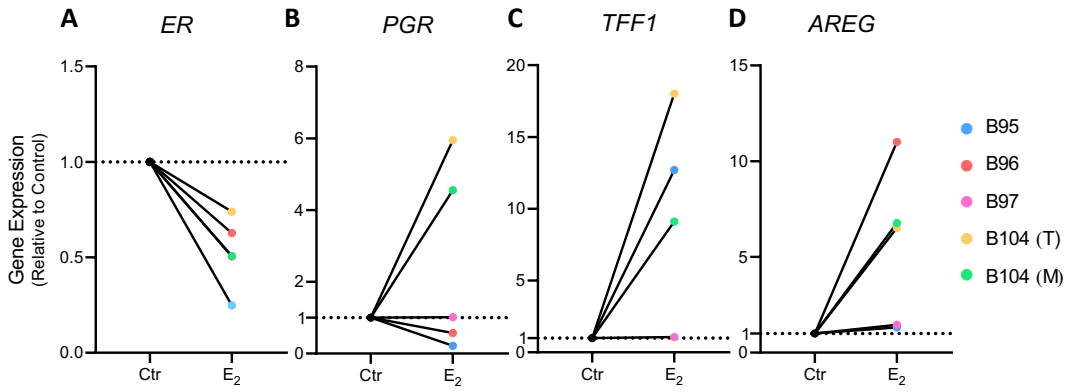

Figure 3.24. Effect of estrogen (E_2) stimulus on the relative gene expression profile of *ER* and its target genes (*PGR*, *TFF1* and *AREG*) in 18-days *ex vivo* patient-derived explant (PDE) culture, assessed by RT-qPCR. Fold change in relative gene expression of (A) *Estrogen Receptor (ER)*, (B) *Progesterone Receptor (PGR)*, (C) *Trefoil Factor 1 (TFF1)* and (D) *Amphiregulin (AREG)* upon 24 h estrogen stimulus (10 nM). Values were normalized to the expression of housekeeping genes *36B4* and *RPL22* and are represented as fold change relative to vehicle control (dashed line at y=1). Data shown as mean of technical triplicates determined by $2^{-\Delta\Delta Ct}$ method.

In line with these observations, and since B104 starting material allowed, additional cultures with E_2 stimulus were kept for protein extraction to assess both ER and PR detection by western blot (Figure 3.25). A control of MCF-7 protein extract was also loaded as a control. MCF-7 is a luminal ER^+/PR^+ cell line that acts as a control of basal detection levels of the assessed proteins.

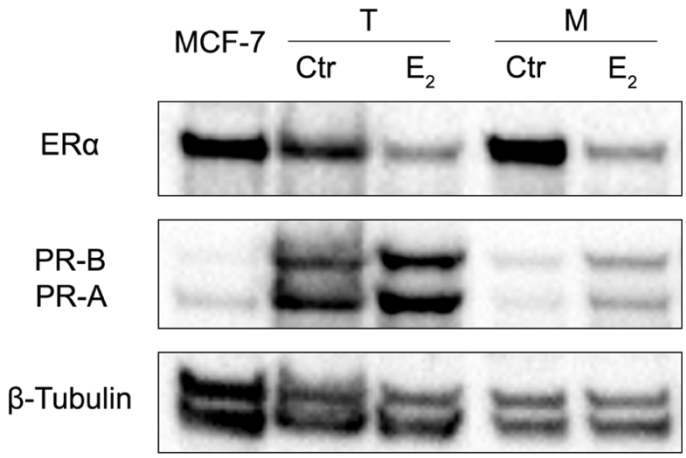

Figure 3.25. Effect of estrogen (E_2) stimulus on the ER and PR protein detection levels in 18-day *ex vivo* B104 (T) and (M) patient-derived explant culture, assessed by western blot. Observed effect upon 24 h E_2 stimulus (10 nM) and compared relative to vehicle control. MCF-7 [ER^+ / PR^+] cell line was used as a positive control; β-tubulin was used as a loading control. Uncropped scans of western blots are shown in Figures S.29 to S.31.

Analyzing the results from protein detection (Figure 3.25) it is possible to observe how ER protein level decreased upon E_2 stimulus in both B104 (T) and B104 (M) samples, which is in agreement with previous studies [147] and relative gene expression levels as here reported (Figure 3.24). As to PR, two isoforms, PR-A and PR-B,[148] were identified, and their detection levels were clearly induced by E_2 in these samples. Same trend was observed at RNA level (Figure 3.24), indicating that E_2 stimulus induced *de novo PGR* gene transcription and PR protein synthesis.

Interestingly, the previous ER and PR protein detection levels (Figure 3.25) of B104 (T) *versus* B104 (M) sample is in accordance with the observed result from gene expression analysis (Figure 3.24) in which, upon E_2 stimulus B104 (T), shows a less marked reduction in detection of ER but higher detection of PR, once again asserting the good correlation observed on the results obtained by these two complementary techniques.

Finally, β-tubulin, which was used as a loading control, depicts two bands where only one was expected. This result might be explained by partial protein degradation which become appreciable for highly expressed proteins such as β-tubulin. Future assays could include addition of an extra protease inhibitor cocktail to preserve samples from protease degradation. At the time the western blot was performed, this was not considered an issue since samples were used within one month of protein extraction and stored at -80 °C for a more stable conservation. Furthermore, extraction was performed with Laemmli lysis buffer, a denaturing buffer containing SDS, and whose protocol includes a boiling step, which is assumed to inactivate cellular enzymes like proteases.[149]

Taken together, these results suggest that *ER* signaling in these samples and under these culture conditions was maintained, since we could observe ER preservation at RNA and protein level, as well as downregulation of *ER* signaling upon challenging, similar to what had previously been reported for the model.[90,91] As aforementioned, maintenance of ER signaling was crucial for the relevance of the *ex vivo* PDE

model.[150,151] With this evaluated, we would next challenge the model with anti-estrogenic therapies since ER regulates the expression of a variety of genes including some growth factors, hormones and oncogenes with important role in the pathogenesis and maintenance of breast cancer.[143]

3.2.2. Assessment of the effect of endocrine therapy challenge in gene expression profile of *ER* and associated genes in *ex vivo* PDE cultures.

After assessment of *ER* signaling and maintenance, we addressed the amenability of the model to evaluate endocrine therapies potential. After 18 days of tamoxifen or fulvestrant challenge, gene expression profile of ER and downstream regulated genes *PR*, *TFF1* and *AREG* was assessed. In Figure 3.26 it is observable the relative gene expression of *ER* and associated genes upon estrogen stimulus and tamoxifen or fulvestrant challenge.

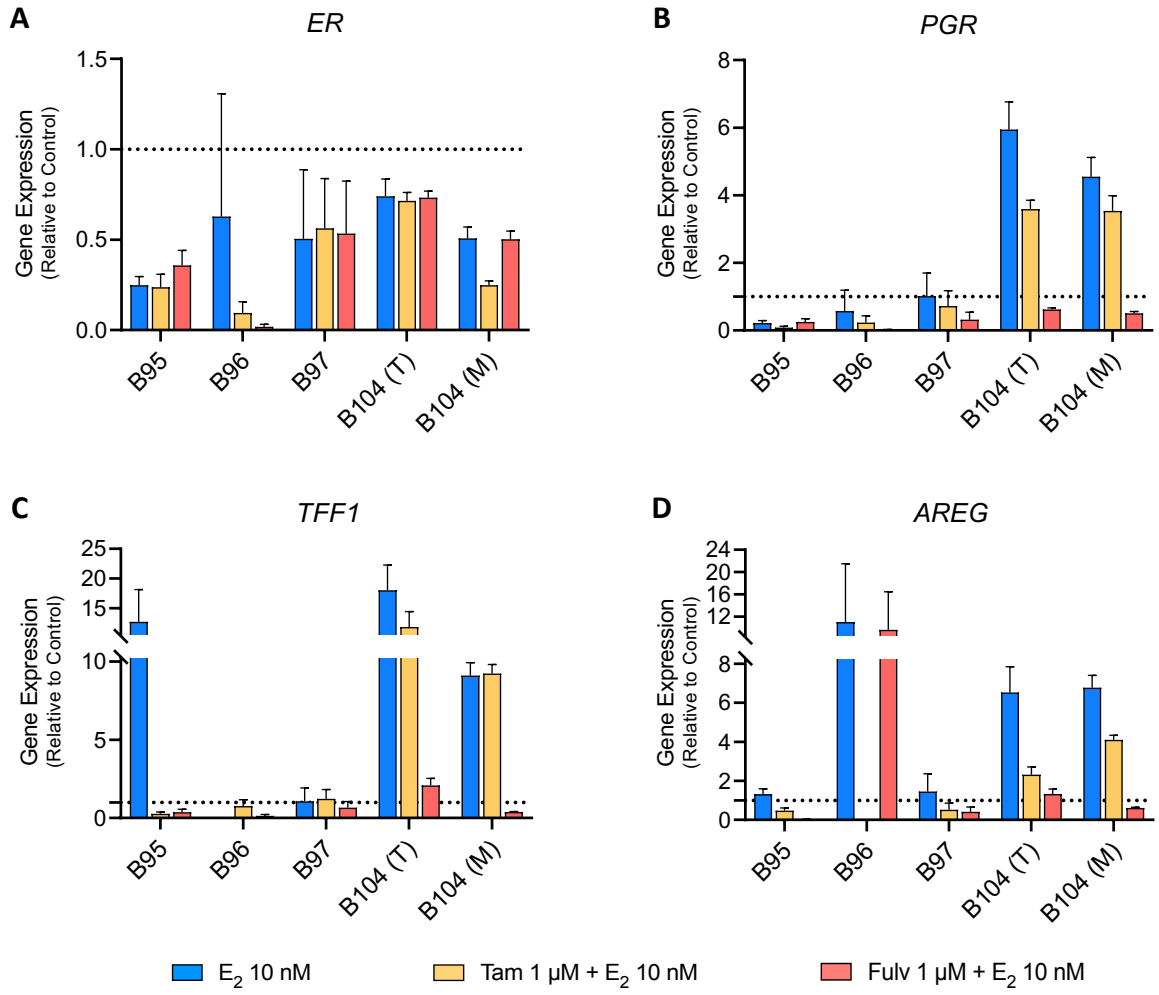

Figure 3.26. Effect of estrogen (E_2) stimulus and endocrine drug challenge on the relative gene expression of *ER* and its target genes (*PGR*, *TFF1* and *AREG*) in 18-days *ex vivo* patient-derived explant (PDE) culture, assessed by RT-qPCR. Fold change in relative gene expression of (A) *Estrogen Receptor (ER)*, (B) *Progesterone Receptor (PGR)*, (C) *Trefoil Factor 1 (TFF1)* and (D) *Amphiregulin (AREG)* upon 18-days tamoxifen or fulvestrant challenge (1 µM) and 24 h estrogen stimulus (10 nM). Values were normalized to the expression of housekeeping genes *36B4* and *RPL22* and are represented as fold change relative to vehicle control (dashed line at y=1). Data shown as mean ± SD of technical triplicates determined by $2^{-\Delta\Delta Ct}$ method. Error propagation of the standard deviation was calculated as described in Formula 1 from section 2.2.6.

The aforementioned effect of ER downregulation upon E_2 stimulus (Figure 3.24) is once again observed, compared to unchallenged condition, in PDE exposure to E_2 plus endocrine drug challenge (Figure 3.26), and, as such, all other conditions appear downregulated as well. In relation to *PR*, *TFF1* or *AREG*, an increase in E_2 stimulated condition is overall observed in all PDE samples, as previously described. Nevertheless, in presence of treatment (and E_2 stimulus), either with tamoxifen or fulvestrant, all the assessed genes were downregulated in comparison to the E_2 stimulus alone, following the predicted response. The combined analysis of *ER* and these three associated genes allowed evaluation of ER signaling response. As such, we could assess whether at least one of these gene expressions would be impaired upon drug challenge, since PDE tissue heterogeneity can translate in differential drug or stimulus response [96] which, in fact, it could.

A closer analysis of Figure 3.26 also shows how fulvestrant results in an increased down expression of the assessed genes in the majority of PDE samples, compared to tamoxifen. One explanation to this observation might be provided by the distinct mechanism of action of these compounds. While fulvestrant, a SERD, binds irreversibly to ER and leads to its destabilization and consequent degradation, tamoxifen, a SERM, acts as an antiestrogen that competes for ER binding.[45] As such, over time, and upon drug challenge, it is expected that cells from fulvestrant-challenged condition no longer present ER, while in tamoxifen-challenged PDEs, ER is present. Under this scenario, cells in tamoxifen challenged conditions have functional ER, where an antagonism effect between estrogen and tamoxifen occurs, which may explain the higher residual estrogen receptor activation in tamoxifen exposure when compared to fulvestrant.

The previous results of relative gene expression were also analyzed by normalization to the E_2 stimulated condition to quantify the downregulation observed (Figure 3.27), and relative gene expression transformed by Log_2 so that values below one appear as negative values.

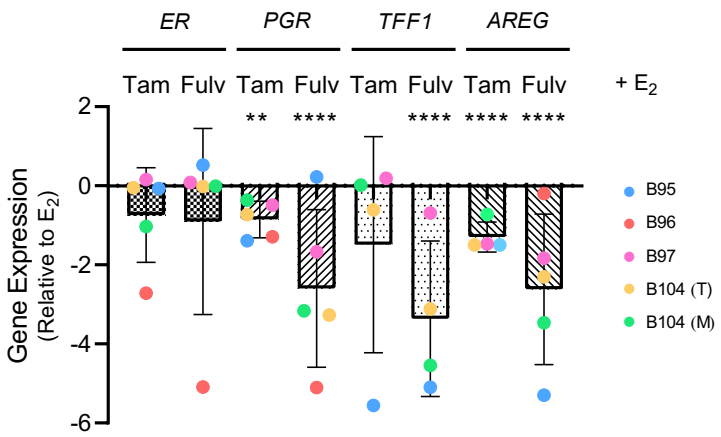

Figure 3.27. Effect of endocrine drug challenge on relative gene expression profile of *ER* and its target genes (*PGR*, *TFF1* and *AREG*) in 18-days *ex vivo* patient-derived explant (PDE) culture stimulated with estrogen (E_2), assessed by RT-qPCR. Log_2 of relative gene expression of conditions challenged for 18 days with endocrine therapies tamoxifen or fulvestrant (1 µM) and upon 24 h estrogen stimulus (10 nM). Values were normalized to the expression of housekeeping genes *36B4* and *RPL22* and are represented as fold change relative to E_2 stimulated condition. Data shown as mean ± SD of 5 independent biological sample experiments determined by $2^{-\Delta\Delta Ct}$ method. Error propagation of the standard deviation was calculated as described in Formula 2 form section 2.2.6. Nonparametric Mann-Whitney U Test was performed. Significances are depicted as: n.s.: not significant, *p < 0.05, **p < 0.01, ***p < 0.001, ****p < 0.0001.

In this representation (Figure 3.27) there was no significant *ER* repression after endocrine challenge, which is not surprising since the E_2 stimulus itself promoted already downregulation of *ER* through the aforementioned negative feedback mechanism. As *Borrás et al., 1994* [146] described, among the most

intensively studied negative modulators of ER levels are the estrogens themselves, through a phenomenon of homologous downregulation also called "processing".

For the majority of the remaining genes (*PGR*, *TFF1* and *AREG*) the effect of standard-of-care drug challenge resulted in their down expression, and fulvestrant in particular appears to have a stronger effect than tamoxifen in terms of suppression of *ER* signaling. This can be potentially explained by the differential mechanism of action of the two drugs mentioned above, although no significant difference was found between treatments, in line to what was previously described in randomized comparison trials.[152,153] Even though, considering the general response, all of assessed genes have shown to be downregulated upon endocrine challenge as we expected.

Pre-clinical models that are currently used as drug-testing platforms fall into three broad categories: *in vitro*, *in vivo* and *ex vivo*, and, as previously described, *in vitro* and in *vivo models* are often not recapitulative of the original human tumors.[96] For ER^+ BC in particular, while seminal ER signaling studies like the described E_2-induced downregulation of ER [146] were performed in *in vitro* 2D cultures of established cell lines (MCF-7 in that case), those models are simplifications of the *in situ* TME that have proven to lack cues which impact drug sensitivity. Although reconstruction approaches with combinations of non-tumor cell types have contributed to evaluation of drug responses and resistance, such *in vitro* models most often lead to loss of ER expression.[91,143]

To tackle these challenges, alternatives rely on more complex existing models, such as patient-derived organoids (*ex vivo*) and patient-derived xenografts (*in vivo*), which have many advantages as already stated, but even these models suffer from intrinsic limitations. While organoids major drawback is their lack of stroma, blood vessels and immune cells,[94] PDXs lack from not contextually preserving human tumor architecture and often relying on immunocompromised mice.[72,96] Moreover, although PDXs are described to preserve histological and phenotypical characteristics of the primary tumor with an acceptable 60 to 80% graft success rate,[72,99] it is established that original human TME is gradually replaced by murine cells, namely the stroma.[154] As such, ER^+ BC remains particularly challenging which results in low success rates of tested drugs in these models (4% to 7%), precisely due to the difficulty in recapitulating the *in situ* pathophysiology and TME characteristics.[128] Nevertheless, to date, *in vivo* models, such as PDXs, remain the most used and trusted alternative to *in vitro* cell line-derived models.[72,150,151]

By contrast, *ex vivo* PDE models facilitate drug testing of intact human tumors, and have proved to be particularly relevant in preservation of human TME,[96,97,125] namely with maintenance of BC architecture and ER signaling, as recently described in the work of *Cartaxo et al.*[91] from the host Lab. However, *Muraro et al.*[90] had also previously reported a similar *ex-vivo* model for assessment of drug response on BC primary tissue, precisely using fulvestrant (0.1 μM) although neither ER target genes were assessed. In this study, authors accomplished high cell viability, TME preservation and maintenance of ER up to 14 days culture of BC microstructures, when combining a collagen scaffold with a medium perfusion system. Despite of the many similarities, a striking difference to the model we employ is that BC tissue maintenance in the previous work is supported by taking advantage of collagen scaffolds. As aforementioned, these scaffolds are biologically active animal-derived biomaterials which bring variability, as well as environmental and ethical concerns, by opposition to the alginate scaffolds our model takes use of, which is a non-animal derived inert matrix. We can also argue that culture of the model we use is more feasible as it does not require perfusion-based bioreactor and, even more, that this model has previously been interrogated for 1 month of culture, without decline in cell viability of tissue microstructure, leaving us to hypothesize that the lifespan of encapsulated tissue microstructures could be extended for even longer periods, allowing for multiple drug challenge cycles, beyond 14 days.[90,91]

In the established PDE *ex vivo* model we used, maintenance of ER signaling was indeed confirmed and we successfully performed anti-estrogenic challenge of primary BC microstructures. The results presented have thus shown that this 3D PDE model is amenable to be challenged with endocrine therapies and can provide a potential pre-clinical model for the assessment of the effect of similar targeted compounds. This provides an interesting and useful tool to address the increased resistance of current therapies, while it widens the perspective for implementation of personalized medicine in a nearby future.[96]

In summary, while it is our view that no preclinical model can fully recapitulate the complexity of tumors or the physiological parameters determining intrinsic and acquired drug resistance, we consider that the best approach is to use a combination of models. With each model taking relevance in its rightful place, BC research can gain the most insightful information on drug responses, metabolism, pharmacodynamic biomarkers, etc. prior to clinical translation. PDEs in specific, have not been extensively incorporated into the cancer drug development pipeline so far, despite strong evidence of their clinical predictivity although they should be considered a powerful pre-clinical platform for generating proof-of-concept information.[96] As such, with this work we have extended the reported findings on the effect of endocrine therapies in ER^+ PDEs, and thus contributed to promote the model as a predictive tool for therapy response that could be established and incorporated in preclinical evaluation of anti-cancer drug development.

Chapter 4. Conclusion

In this work, *in vitro* and *ex vivo* 3D BC models previously developed by the host Lab have been established as an amenable platform to evaluate the potential of novel targeted compounds in pre-clinical drug development stages through the assessment of the effect of targeted therapies, namely anti-estrogenic and anti-HER2 therapies.

Following established methodologies, cell spheroids from trastuzumab-resistant $HER2^+$ cell line (and TNBC cell line as a control) were generated and encapsulated in a hydrogel scaffold. Using a TME reconstruction approach, challenge of an *in vitro* model with mAb trastuzumab and T-ADCs was successfully performed. The efficacy and specificity of T-ADCs was confirmed using metabolic activity, cell viability, assessment of apoptosis and cytotoxicity assays in 2D and 3D cultures. HCC1954 cells showed reduction in metabolic activity and cell viability in 2D upon drug challenge but required longer drug challenge periods and higher concentrations for observation an equivalent effect in 3D. Both the HCC1806 TNBC cell line and hDFs were shown not to be specifically targeted by the T-ADCs, although possible unspecific off-target effect might be observed at high ADC concentrations. In long-term 3D cultures, T-ADCs induced a higher reduction in cell viability and metabolism, associated with an increase in apoptosis induction and cytotoxicity in comparison to the mAb alone. The EC50 was determined and will be useful to design future drug challenges on mono- and co-cultures of $HER2^+$ tumor cells with hDFs, to assess the effect in stromal-induced resistance.

In parallel, it was performed *ex vivo* culture of ER^+ encapsulated microstructures of patient-derived explants, pursuing a TME maintenance approach. The model was stimulated with E_2 confirming the maintenance of ER signaling both at protein and gene expression level through upregulation of ER target genes and downregulation of ER itself, in agreement with the previously reported negative feedback mechanism. Challenge with the standard-of-care endocrine drugs, tamoxifen and fulvestrant, upon E2 stimulus was shown to promote downregulation of *ER* target genes *PGR*, *TFF1* and *AREG*, as predicted for ER antagonists. Fulvestrant showed increase effect in relation to tamoxifen, which has been postulated to derive from irreversible ER degradation by opposition to binding competition.

In summary, this thesis has accomplished the proposed aim of assessing the amenability of previously established 3D BC models recapitulative of the tumor microenvironment for pre-clinical evaluation of the potential of novel targeted therapies. In future experiments, long-term drug challenge could be pursued using the *in vitro* models with all the T-ADCs, at the determined EC50 range. Comparison of mono- and co-cultures of tumor cells with other TME components, such as stromal fibroblast would help characterize possible induced resistance mechanisms. In relation to the *ex vivo* BC PDE model, increase the number of biological samples of the PDE *ex vivo* model would help consolidate the observed results.

Ultimately, this work has contributed for the development of a drug testing platform to study the increased resistance of current therapies while complying with the crescent policies for replacement and reduction of animal experimentation.

5. References

1. Wild C, Weiderpass E, Stewart B. *World Cancer Report: Cancer Research for Cancer Prevention – IARC*.; 2020. Accessed May 26, 2020. https://www.iarc.fr/featured-news/new-world-cancer-report/
2. Harbeck N, Penault-Llorca F, Cortes J, et al. Breast cancer. *Nat Rev Dis Prim*. 2019;5(1):1-31. doi:10.1038/s41572-019-0111-2
3. Harbeck N, Gnant M. Breast cancer. *Lancet*. 2017;389(10074):1134-1150. doi:10.1016/S0140-6736(16)31891-8
4. Waks AG, Winer EP. Breast Cancer Treatment. *JAMA - J Am Med Assoc*. 2019;321(3):316. doi:10.1001/jama.2018.20751
5. Bray F, Ferlay J, Soerjomataram I, Siegel RL, Torre LA, Jemal A. Global cancer statistics 2018: GLOBOCAN estimates of incidence and mortality worldwide for 36 cancers in 185 countries. *CA Cancer J Clin*. 2018;68(6):394-424. doi:10.3322/caac.21492
6. Collaborative Group on Hormonal Factors in Breast Cancer. Breast cancer and hormonal contraceptives: Collaborative reanalysis of individual data on 53 297 women with breast cancer and 100 239 women without breast cancer from 54 epidemiological studies. *Lancet*. 1996;347(9017):1713-1727. doi:10.1016/S0140-6736(96)90806-5
7. Collaborative Group on Hormonal Factors in Breast Cancer. Breast cancer and hormone replacement therapy: Collaborative reanalysis of data from 51 epidemiological studies of 52,705 women with breast cancer and 108,411 women without breast cancer. *Lancet*. 1997;350(9089):1484. doi:10.1016/S0140-6736(05)64257-2
8. Brinton LA, Gaudet MM, Gierach GL. Breast Cancer. In: Thun M, Linet M, Cerhan J, Haiman C, Schottenfeld D, eds. *Cancer Epidemiology and Prevention*. 4th Editio. Oxford University Press; 2018:861-888. Accessed May 26, 2020. https://global.oup.com/academic/product/cancer-epidemiology-and-prevention-9780190238667?cc=pt&lang=en&
9. Ziegler R, Hoover R, Pike M, et al. Migration Patterns and Breast Cancer Risk in Asian-American Women | JNCI: Journal of the National Cancer Institute | Oxford Academic. *J Natl Cancer Inst*. 1993;85(22):1819-1827. Accessed May 26, 2020. https://academic.oup.com/jnci/article-abstract/85/22/1819/962711?redirectedFrom=PDF
10. Huen MSY, Sy SMH, Chen J. BRCA1 and its toolbox for the maintenance of genome integrity. *Nat Rev Mol Cell Biol*. 2010;11(2):138-148. doi:10.1038/nrm2831
11. Pasche B. Recent advances in breast cancer genetics. *Cancer Treat Res*. 2008;141:1-10. doi:10.1007/978-0-387-73161-2_1
12. Cobain EF, Milliron KJ, Merajver SD. Updates on breast cancer genetics: Clinical implications of detecting syndromes of inherited increased susceptibility to breast cancer. *Semin Oncol*. 2016;43(5):528-535. doi:10.1053/j.seminoncol.2016.10.001
13. Crawford B, Adams SB, Sittler T, et al. Multi-gene panel testing for hereditary cancer predisposition in unsolved high-risk breast and ovarian cancer patients. *Breast Cancer Res Treat*. 2017;163(2):383-390. doi:10.1007/s10549-017-4181-0
14. Tamimi RM, Spiegelman D, Smith-Warner SA, et al. Population Attributable Risk of Modifiable and Nonmodifiable Breast Cancer Risk Factors in Postmenopausal Breast Cancer. *Pract Epidemiol* . 2016;184(12). doi:10.1093/aje/kww145
15. Srigley JR, Mcgowan T, Maclean A, et al. Standardized synoptic cancer pathology reporting: A population-based approach. *J Surg Oncol*. 2009;99(8):517-524. doi:10.1002/jso.21282
16. World Health Organization. *WHO Classification of Tumours of the Breast*. 5th ed. (Sunil R. Lakhani, Ian O. Ellis, Stuart J. Schnitt, Puay Hoon Tan, Marc J. van de Vijver, eds.). International Agency for Research on Cancer; 2019.
17. Bloom HJ, Richardson WW. Histological grading and prognosis in breast cancer a study of 1409 cases of which 359 have been followed for 15 years. *Br J Cancer*. 1957;11(3):359-377. doi:10.1038/bjc.1957.43
18. Singletary SE, Allred C, Ashley P, et al. Staging system for breast cancer: Revisions for the 6th edition of the AJCC Cancer Staging Manual. *Surg Clin North Am*. 2003;83(4):803-819. doi:10.1016/S0039-6109(03)00034-3
19. Sørlie T, Tibshirani R, Parker J, et al. Repeated observation of breast tumor subtypes in independent gene expression data sets. *Proc Natl Acad Sci U S A*. 2003;100(14):8418-8423.

doi:10.1073/pnas.0932692100
20. Sørlie T, Perou CM, Tibshirani R, et al. Gene expression patterns of breast carcinomas distinguish tumor subclasses with clinical implications. *Proc Natl Acad Sci U S A*. 2001;98(19):10869-10874. doi:10.1073/pnas.191367098
21. Tibshirani R, Hastie T, Narasimhan B, Chu G. Diagnosis of multiple cancer types by shrunken centroids of gene expression. *Proc Natl Acad Sci U S A*. 2002;99(10):6567-6572. doi:10.1073/pnas.082099299
22. Bernard PS, Parker JS, Mullins M, et al. Supervised risk predictor of breast cancer based on intrinsic subtypes. *J Clin Oncol*. 2009;27(8):1160-1167. doi:10.1200/JCO.2008.18.1370
23. Dai X, Li T, Bai Z, et al. Breast cancer intrinsic subtype classification, clinical use and future trends. *undefined*. Published online 2015.
24. Atashgaran V, Wrin J, Barry SC, Dasari P, Ingman W V. Dissecting the biology of menstrual cycle-associated breast cancer risk. *Front Oncol*. 2016;6(DEC). doi:10.3389/fonc.2016.00267
25. Mallepell S, Krust A, Chambon P, Brisken C. Paracrine signaling through the epithelial estrogen receptor α is required for proliferation and morphogenesis in the mammary gland. *Proc Natl Acad Sci U S A*. 2006;103(7):2196-2201. doi:10.1073/pnas.0510974103
26. Zhu Y, Sullivan LL, Nair SS, et al. Coregulation of estrogen receptor by ERBB4/HER4 establishes a growth-promoting autocrine signal in breast tumor cells. *Cancer Res*. 2006;66(16):7991-7998. doi:10.1158/0008-5472.CAN-05-4397
27. Peterson EA, Jenkins EC, Lofgren KA, et al. Amphiregulin is a critical downstream effector of estrogen signaling in ERα-positive breast cancer. *Cancer Res*. 2015;75(22):4830-4838. doi:10.1158/0008-5472.CAN-15-0709
28. Amiry N, Kong X, Muniraj N, et al. Trefoil factor-1 (TFF1) enhances oncogenicity of mammary carcinoma cells. *Endocrinology*. 2009;150(10):4473-4483. doi:10.1210/en.2009-0066
29. Louie MC, Sevigny MB. Steroid hormone receptors as prognostic markers in breast cancer. *Am J Cancer Res*. 2017;7(8):1617-1636. Accessed September 2, 2020. www.ajcr.us/
30. Pernas S, Tolaney SM. HER2-positive breast cancer: new therapeutic frontiers and overcoming resistance. *Ther Adv Med Oncol*. 2019;11. doi:10.1177/1758835919833519
31. Brenton JD, Carey LA, Ahmed A, Caldas C. Molecular classification and molecular forecasting of breast cancer: Ready for clinical application? *J Clin Oncol*. 2005;23(29):7350-7360. doi:10.1200/JCO.2005.03.3845
32. Fentiman IS, Fourquet A, Hortobagyi GN. Male breast cancer. *Lancet*. 2006;367(9510):595-604. doi:10.1016/S0140-6736(06)68226-3
33. Radice D, Redaelli A. Breast cancer management: Quality-of-life and cost considerations. *Pharmacoeconomics*. 2003;21(6):383-396. doi:10.2165/00019053-200321060-00003
34. Karen LM, Mark AL, Peters SH. Treatment of Breast Cancer - American Family Physician. *Am Fam Physician*. 2010;11(81):1339-1346. Accessed May 26, 2020. https://www.aafp.org/afp/2010/0601/p1339.html
35. Freres P, Jerusalem G, Moonen M. Categories of Anticancer Treatments. In: Lancellotti P, Zamorano J, Galderis M, eds. *Anticancer Treatments and Cardiotoxicity: Mechanisms, Diagnostic and Therapeutic Interventions*. 1st Edition. Elsevier Inc.; 2017:7-11. doi:10.1016/B978-0-12-802509-3.00002-9
36. Marinello J, Delcuratolo M, Capranico G. Anthracyclines as Topoisomerase II Poisons: From Early Studies to New Perspectives. *Int J Mol Sci*. 2018;19(11):3480. doi:10.3390/ijms19113480
37. Siddik ZH. Mechanisms of Action of Cancer Chemotherapeutic Agents: DNA-Interactive Alkylating Agents and Antitumour Platinum-Based Drugs. In: *The Cancer Handbook*. John Wiley & Sons, Ltd; 2005. doi:10.1002/0470025077.chap84b
38. Lind MJ. Principles of cytotoxic chemotherapy. *Medicine (Baltimore)*. 2008;36(1):19-23. doi:10.1016/j.mpmed.2007.10.003
39. Parker WB. Enzymology of purine and pyrimidine antimetabolites used in the treatment of cancer. *Chem Rev*. 2009;109(7):2880-2893. doi:10.1021/cr900028p
40. Nelson DL, Cox MM. *Lehninger Principles of Biochemistry*. 5th ed. W. H. Freeman and Company; 2008.
41. Rowinsky EK, Donehower RC. The clinical pharmacology and use of antimicrotubule agents in cancer chemotherapeutics. *Pharmacol Ther*. 1991;52(1):35-84. doi:10.1016/0163-7258(91)90086-2
42. Lodish H, Berk A, Zipursky SL, Matsudaira P, Baltimore D, Darnell J. The Role of Topoisomerases in DNA Replication. Published online 2000.
43. Goodsell DS. The Molecular Perspective: DNA Topoisomerases. *Stem Cells*. 2002;20(5):470-471. doi:10.1634/stemcells.20-5-470
44. Lumachi F, Luisetto G, M.M. Basso S, Basso U, Brunello A, Camozzi V. Endocrine Therapy of Breast

Cancer. *Curr Med Chem*. 2011;4(18):513-522. doi:10.2174/092986711794480177
45. Patel HK, Bihani T. Selective estrogen receptor modulators (SERMs) and selective estrogen receptor degraders (SERDs) in cancer treatment. *Pharmacol Ther*. 2018;186:1-24. doi:10.1016/j.pharmthera.2017.12.012
46. DeVita VT, Hellman S, Rosenberg SA. Cancer: Principles & Practice of Oncology . Lippincott Williams & Wilkins. Published 2005. Accessed September 6, 2020. https://books.google.to/books?id=6htWwgEACAAJ&source=gbs_book_other_versions_r&cad=2
47. Tremont A, Lu J, Cole JT. Endocrine Therapy for Early Breast Cancer: Updated Review. *Ochsner J*. 2017;17(4):411.
48. Huerta-Reyes M, Maya-Núñez G, Pérez-Solis MA, et al. Treatment of Breast Cancer With Gonadotropin-Releasing Hormone Analogs. *Front Oncol*. 2019;9:943-943. doi:10.3389/fonc.2019.00943
49. Robertson JFR, Blamey RW. The use of gonadotrophin-releasing hormone (GnRH) agonists in early and advanced breast cancer in pre- and perimenopausal women. *Eur J Cancer*. 2003;39(7):861-869. doi:10.1016/S0959-8049(02)00810-9
50. Buss NAPS, Henderson SJ, McFarlane M, Shenton JM, de Haan L. Monoclonal antibody therapeutics: history and future. *Curr Opin Pharmacol*. 2012;12(5):615-622. doi:10.1016/j.coph.2012.08.001
51. Nielsen DL, Andersson M, Kamby C. HER2-targeted therapy in breast cancer. Monoclonal antibodies and tyrosine kinase inhibitors. *Cancer Treat Rev*. 2009;35(2):121-136. doi:10.1016/j.ctrv.2008.09.003
52. Stern M, Herrmann R. Overview of monoclonal antibodies in cancer therapy: Present and promise. *Crit Rev Oncol Hematol*. 2005;54(1):11-29. doi:10.1016/j.critrevonc.2004.10.011
53. Antibody Society. Antibody therapeutics approved or in regulatory review in the EU or US - The Antibody Society. Accessed January 12, 2021. https://www.antibodysociety.org/resources/approved-antibodies/
54. Leitzel BK, Teramoto Y, Konrad K, et al. Elevated Serum c-erbB-2 Antigen Levels and Decreased Response to Hormone Therapy of Breast Cancer. 1995;13(5):1129-1135.
55. Peters C, Brown S. Antibody-drug conjugates as novel anti-cancer chemotherapeutics. *Biosci Rep*. 2015;35(4). doi:10.1042/BSR20150089
56. Teicher BA, Chari RVJ. Antibody conjugate therapeutics: Challenges and potential. *Clin Cancer Res*. 2011;17(20):6389-6397. doi:10.1158/1078-0432.CCR-11-1417
57. Tsuchikama K, An Z. Antibody-drug conjugates: recent advances in conjugation and linker chemistries. *Protein Cell*. 2018;9(1):33-46. doi:10.1007/s13238-016-0323-0
58. Cruz E, Kayser V. Monoclonal antibody therapy of solid tumors: clinical limitations and novel strategies to enhance treatment efficacy. *Biol Targets Ther*. 2019;Volume 13:33-51. doi:10.2147/BTT.S166310
59. Huryn DM, Wipf P. *Natural Product Chemistry and Cancer Drug Discovery*. Second Edi. Elsevier; 2013. doi:10.1016/B978-0-12-396521-9.00003-6
60. Kirschning A, Harmrolfs K, Knobloch T. The chemistry and biology of the maytansinoid antitumor agents. *Comptes Rendus Chim*. 2008;11(11-12):1523-1543. doi:10.1016/j.crci.2008.02.006
61. EMA - European Medicines Agency. Kadcyla. Accessed January 31, 2021. https://www.ema.europa.eu/en/medicines/human/EPAR/kadcyla#product-information-section
62. EMA - European Medicines Agency. Enhertu. Accessed January 31, 2021. https://www.ema.europa.eu/en/medicines/human/summaries-opinion/enhertu
63. Hoffmann RM, Coumbe BGT, Josephs DH, et al. Antibody structure and engineering considerations for the design and function of Antibody Drug Conjugates (ADCs). *Oncoimmunology*. 2018;7(3). doi:10.1080/2162402X.2017.1395127
64. Arora A, Scholar EM. Role of tyrosine kinase inhibitors in cancer therapy. *J Pharmacol Exp Ther*. 2005;315(3):971-979. doi:10.1124/jpet.105.084145
65. Metibemu DS, Akinloye OA, Akamo AJ, Ojo DA, Okeowo OT, Omotuyi IO. Exploring receptor tyrosine kinases-inhibitors in Cancer treatments. *Egypt J Med Hum Genet*. 2019;20(1):1-16. doi:10.1186/s43042-019-0035-0
66. Mcmillin DW, Negri JM, Mitsiades CS. The role of tumour-stromal interactions in modifying drug response: Challenges and opportunities. *Nat Rev Drug Discov*. 2013;12(3):217-228. doi:10.1038/nrd3870
67. Pietras K, Östman A. Hallmarks of cancer: Interactions with the tumor stroma. *Exp Cell Res*. 2010;316(8):1324-1331. doi:10.1016/j.yexcr.2010.02.045
68. Tlsty TD, Coussens LM. Tumor stroma and regulation of cancer development. *Annu Rev Pathol*. 2006;1:119-150. doi:10.1146/annurev.pathol.1.110304.100224
69. Hoarau-Véchot J, Rafii A, Touboul C, Pasquier J. Halfway between 2D and animal models: Are 3D cultures the ideal tool to study cancer-microenvironment interactions? *Int J Mol Sci*. 2018;19(1). doi:10.3390/ijms19010181

70. Junttila MR, De Sauvage FJ. Influence of tumour micro-environment heterogeneity on therapeutic response. *Nature*. 2013;501(7467):346-354. doi:10.1038/nature12626
71. Senthebane DA, Rowe A, Thomford NE, et al. The role of tumor microenvironment in chemoresistance: To survive, keep your enemies closer. *Int J Mol Sci*. 2017;18(7). doi:10.3390/ijms18071586
72. Holen I, Speirs V, Morrissey B, Blyth K. In vivo models in breast cancer research: Progress, challenges and future directions. *DMM Dis Model Mech*. 2017;10(4):359-371. doi:10.1242/dmm.028274
73. Hickman JA, Graeser R, de Hoogt R, et al. Three-dimensional models of cancer for pharmacology and cancer cell biology: Capturing tumor complexity in vitro/ex vivo. *Biotechnol J*. 2014;9(9):1115-1128. doi:10.1002/biot.201300492
74. Katt ME, Placone AL, Wong AD, Xu ZS, Searson PC. In vitro tumor models: Advantages, disadvantages, variables, and selecting the right platform. *Front Bioeng Biotechnol*. 2016;4(FEB):12. doi:10.3389/fbioe.2016.00012
75. Meijer TG, Naipal KA, Jager A, van Gent DC. Ex vivo tumor culture systems for functional drug testing and therapy response prediction. *Futur Sci OA*. 2017;3(2):FSO190. doi:10.4155/fsoa-2017-0003
76. Mirabelli P, Coppola L, Salvatore M. Cancer cell lines are useful model systems for medical research. *Cancers (Basel)*. 2019;11(8). doi:10.3390/cancers11081098
77. Ben-David U, Beroukhim R, Golub TR. Genomic evolution of cancer models: perils and opportunities. *Nat Rev Cancer*. 2019;19(2):97-109. doi:10.1038/s41568-018-0095-3
78. Friedl P, Sahai E, Weiss S, Yamada KM. New dimensions in cell migration. *Nat Rev Mol Cell Biol*. 2012;13(11):743-747. doi:10.1038/nrm3459
79. Stock K, Estrada MF, Vidic S, et al. Capturing tumor complexity in vitro: Comparative analysis of 2D and 3D tumor models for drug discovery. *Sci Reports 2016 6*. 2016;6:28951. doi:10.1038/srep28951
80. Singh M, Mukundan S, Jaramillo M, Oesterreich S, Sant S. Three-dimensional breast cancer models mimic hallmarks of size-induced tumor progression. *Cancer Res*. 2016;76(13):3702-3710. doi:10.1158/0008-5472.CAN-15-2304
81. Rebelo SP, Pinto C, Martins TR, et al. 3D-3-culture: A tool to unveil macrophage plasticity in the tumour microenvironment. *Biomaterials*. 2018;163:185-197. doi:10.1016/J.BIOMATERIALS.2018.02.030
82. Estrada MF, Rebelo SP, Davies EJ, et al. Modelling the tumour microenvironment in long-term microencapsulated 3D co-cultures recapitulates phenotypic features of disease progression. *Biomaterials*. 2016;78:50-61. doi:10.1016/J.BIOMATERIALS.2015.11.030
83. Laranga R, Duchi S, Ibrahim T, Guerrieri AN, Donati DM, Lucarelli E. Trends in bone metastasis modeling. *Cancers (Basel)*. 2020;12(8):1-26. doi:10.3390/cancers12082315
84. Rodrigues J, Heinrich MA, Teixeira LM, Prakash J. 3D In Vitro Model (R)evolution: Unveiling Tumor–Stroma Interactions. *Trends in Cancer*. 2021;7(3):249-264. doi:10.1016/j.trecan.2020.10.009
85. Tibbitt MW, Anseth KS. Hydrogels as extracellular matrix mimics for 3D cell culture. *Biotechnol Bioeng*. 2009;103(4):655-663. doi:10.1002/bit.22361
86. Caliari SR, Burdick JA. A practical guide to hydrogels for cell culture. *Nat Methods*. 2016;13(5):405-414. doi:10.1038/nmeth.3839
87. Augst AD, Kong HJ, Mooney DJ. Alginate hydrogels as biomaterials. *Macromol Biosci*. 2006;6(8):623-633. doi:10.1002/mabi.200600069
88. Cavo M, Fato M, Peñuela L, Beltrame F, Raiteri R, Scaglione S. Microenvironment complexity and matrix stiffness regulate breast cancer cell activity in a 3D in vitro model. *Sci Rep*. 2016;6. doi:10.1038/srep35367
89. Thakuri PS, Liu C, Luker GD, Tavana H. Biomaterials-Based Approaches to Tumor Spheroid and Organoid Modeling. *Adv Healthc Mater*. 2018;7(6):1-21. doi:10.1002/adhm.201700980
90. Muraro MG, Muenst S, Mele V, et al. Ex-vivo assessment of drug response on breast cancer primary tissue with preserved microenvironments. *Oncoimmunology*. 2017;6(7):1-12. doi:10.1080/2162402X.2017.1331798
91. Cartaxo AL, Estrada MF, Domenici G, et al. A novel culture method that sustains ERα signaling in human breast cancer tissue microstructures. *J Exp Clin Cancer Res*. 2020;39(1):1-14. doi:10.1186/s13046-020-01653-4
92. Nagle PW, Plukker JTM, Muijs CT, van Luijk P, Coppes RP. Patient-derived tumor organoids for prediction of cancer treatment response. *Semin Cancer Biol*. 2018;53:258-264. doi:10.1016/j.semcancer.2018.06.005
93. Tuveson D, Clevers H. Cancer modeling meets human organoid technology. *Science (80-)*. 2019;364(6444):952-955. doi:10.1126/science.aaw6985
94. Drost J, Clevers H. Organoids in cancer research. *Nat Rev Cancer*. 2018;18(7):407-418.

doi:10.1038/s41568-018-0007-6
95. Fan H, Demirci U, Chen P. Emerging organoid models: Leaping forward in cancer research. *J Hematol Oncol*. 2019;12(1):142. doi:10.1186/s13045-019-0832-4
96. Powley IR, Patel M, Miles G, et al. Patient-derived explants (PDEs) as a powerful preclinical platform for anti-cancer drug and biomarker discovery. *Br J Cancer*. 2020;122(6):735-744. doi:10.1038/s41416-019-0672-6
97. Collins A, Miles GJ, Wood J, MacFarlane M, Pritchard C, Moss E. Patient-derived explants, xenografts and organoids: 3-dimensional patient-relevant pre-clinical models in endometrial cancer. *Gynecol Oncol*. 2020;156(1):251-259. doi:10.1016/j.ygyno.2019.11.020
98. Mendes N, Carvalho PD, Martins F, et al. *Animal Models to Study Cancer and Its Microenvironment*. Vol 1219. (Serpa J, ed.). Springer Nature; 2020. doi:10.1007/978-3-030-34025-4_11
99. Whittle JR, Lewis MT, Lindeman GJ, Visvader JE. Patient-derived xenograft models of breast cancer and their predictive power. Published online 2015. doi:10.1186/s13058-015-0523-1
100. Jaganathan H, Gage J, Leonard F, et al. Three-dimensional in vitro co-culture model of breast tumor using magnetic levitation. *Sci Rep*. 2014;4. doi:10.1038/srep06468
101. Chung M, Ahn J, Son K, Kim S, Jeon NL. Biomimetic Model of Tumor Microenvironment on Microfluidic Platform. *Adv Healthc Mater*. 2017;6(15). doi:10.1002/adhm.201700196
102. Hirt C, Papadimitropoulos A, Muraro MG, et al. Bioreactor-engineered cancer tissue-like structures mimic phenotypes, gene expression profiles and drug resistance patterns observed "in vivo." *Biomaterials*. 2015;62:138-146. doi:10.1016/j.biomaterials.2015.05.037
103. Marshall LE, Goliwas KF, Miller LM, Penman AD, Frost AR, Berry JL. Flow–perfusion bioreactor system for engineered breast cancer surrogates to be used in preclinical testing. *J Tissue Eng Regen Med*. Published online 2015. doi:10.1002/term
104. Guller AE, Grebenyuk PN, Shekhter AB, Zvyagin A V., Deyev SM. Bioreactor-based tumor tissue engineering. *Acta Naturae*. 2016;8(3):44-58. doi:10.32607/20758251-2016-8-3-44-58
105. Sokol ES, Miller DH, Breggia A, Spencer KC, Arendt LM, Gupta PB. Growth of human breast tissues from patient cells in 3D hydrogel scaffolds. *Breast Cancer Res*. 2016;18(1):19. doi:10.1186/s13058-016-0677-5
106. Jensen C, Teng Y. Is It Time to Start Transitioning From 2D to 3D Cell Culture? *Front Mol Biosci*. 2020;7(March):1-15. doi:10.3389/fmolb.2020.00033
107. Zhang B, Korolj A, Lai BFL, Radisic M. Advances in organ-on-a-chip engineering. *Nat Rev Mater*. 2018;3(8):257-278. doi:10.1038/s41578-018-0034-7
108. Ahmad A. *Breast Cancer Metastasis and Drug Resistance: Challenges and Progress*. Vol 1152. Springer New York LLC; 2019. doi:10.1007/978-3-030-20301-6_1
109. Fenwick N, Griffin G, Gauthier C. Animal Welfare. *Can Vet J*. 2009;50(11):1166-1168.
110. Livak KJ, Schmittgen TD. Analysis of relative gene expression data using real-time quantitative PCR and the 2-ΔΔCT method. *Methods*. 2001;25(4):402-408. doi:10.1006/meth.2001.1262
111. Sigma-Aldrich. PCR/qPCR Data Analysis: A Technical Guide to PCR Technologies. Accessed February 11, 2021. https://www.sigmaaldrich.com/technical-documents/articles/biology/data-analysis.html
112. Chakrabarty A, Bhola NE, Sutton C, et al. Trastuzumab-resistant cells rely on a HER2-PI3K-FoxO-survivin axis and are sensitive to PI3K inhibitors. *Cancer Res*. 2013;73(3):1190-1200. doi:10.1158/0008-5472.CAN-12-2440
113. Minard JM. Development of antibody-based antitumor therapies based on Trastuzumab: antibody-drug conjugates, immunocytokines and fragment conjugates. Published online 2019.
114. Lewis Phillips GD, Li G, Dugger DL, et al. Targeting HER2-positive breast cancer with trastuzumab-DM1, an antibody-cytotoxic drug conjugate. *Cancer Res*. 2008;68(22):9280-9290. doi:10.1158/0008-5472.CAN-08-1776
115. Saatci Ö, Borgoni S, Akbulut Ö, et al. Targeting PLK1 overcomes T-DM1 resistance via CDK1-dependent phosphorylation and inactivation of Bcl-2/xL in HER2-positive breast cancer. *Oncogene*. 2018;37(17):2251-2269. doi:10.1038/s41388-017-0108-9
116. Abdollahpour-Alitappeh M, Lotfinia M, Bagheri N, et al. Trastuzumab-monomethyl auristatin E conjugate exhibits potent cytotoxic activity in vitro against HER2-positive human breast cancer. *J Cell Physiol*. 2019;234(3):2693-2704. doi:10.1002/jcp.27085
117. Jang IS, Neto EC, Guinney J, Friend SH, Margolin AA. Systematic assessment of analytical methods for drug sensitivity prediction from cancer cell line data. *Pacific Symp Biocomput*. Published online 2014:63-74. doi:10.1142/9789814583220_0007
118. Huang S, Pang L. Comparing statistical methods for quantifying drug sensitivity based on in vitro dose-response assays. *Assay Drug Dev Technol*. 2012;10(1):88-96. doi:10.1089/adt.2011.0388

119. Cartaxo AL, Almeida J, Gualda EJ, et al. A computational diffusion model to study antibody transport within reconstructed tumor microenvironments. *BMC Bioinformatics*. 2020;21(1):1-19. doi:10.1186/s12859-020-03854-2
120. Dalziel M, Beers SA, Cragg MS, Crispin M. Through the barricades: Overcoming the barriers to effective antibody-based cancer therapeutics. *Glycobiology*. 2018;28(9):697-712. doi:10.1093/glycob/cwy043
121. Baker JHE, Kyle AH, Reinsberg SA, et al. Heterogeneous distribution of trastuzumab in HER2-positive xenografts and metastases: role of the tumor microenvironment. *Clin Exp Metastasis*. 2018;35(7):691-705. doi:10.1007/s10585-018-9929-3
122. Bartelink IH, Jones EF, Shahidi-Latham SK, et al. Tumor Drug Penetration Measurements Could Be the Neglected Piece of the Personalized Cancer Treatment Puzzle. *Clin Pharmacol Ther*. 2019;106(1):148-163. doi:10.1002/cpt.1211
123. Gordon J, Brown M, Reynolds M. Cell-Based Methods for Determination of Efficacy for Candidate Therapeutics in the Clinical Management of Cancer. *Diseases*. 2018;6(4):85. doi:10.3390/diseases6040085
124. Fotakis G, Timbrell JA. In vitro cytotoxicity assays: Comparison of LDH, neutral red, MTT and protein assay in hepatoma cell lines following exposure to cadmium chloride. *Toxicol Lett*. 2006;160(2):171-177. doi:10.1016/j.toxlet.2005.07.001
125. Abreu S, Silva F, Mendes R, et al. Patient-derived ovarian cancer explants: preserved viability and histopathological features in long-term agitation-based cultures. *Sci Rep*. 2020;10(1):1-13. doi:10.1038/s41598-020-76291-z
126. Santo VE, Rebelo SP, Estrada MF, Alves PM, Boghaert E, Brito C. Drug screening in 3D in vitro tumor models: overcoming current pitfalls of efficacy read-outs. *Biotechnol J*. 2017;12(1):1600505. doi:10.1002/biot.201600505
127. Mehta G, Hsiao AY, Ingram M, Luker GD, Takayama S. Opportunities and challenges for use of tumor spheroids as models to test drug delivery and efficacy. *J Control Release*. 2012;164(2):192-204. doi:10.1016/j.jconrel.2012.04.045
128. Weeber F, Ooft SN, Dijkstra KK, Voest EE. Tumor Organoids as a Pre-clinical Cancer Model for Drug Discovery. *Cell Chem Biol*. 2017;24(9):1092-1100. doi:10.1016/j.chembiol.2017.06.012
129. Sachs N, de Ligt J, Kopper O, et al. A Living Biobank of Breast Cancer Organoids Captures Disease Heterogeneity. *Cell*. 2018;172(1-2):373-386.e10. doi:10.1016/j.cell.2017.11.010
130. Cardillo TM, Govindan S V., Zalath MB, et al. IMMU-140, a novel SN-38 antibody-drug conjugate targeting HLA-DR, mediates dual cytotoxic effects in hematologic cancers and malignant melanoma. *Mol Cancer Ther*. 2018;17(1):150-160. doi:10.1158/1535-7163.MCT-17-0354
131. Arhoma A, Chantry AD, Haywood-Small SL, Cross NA. SAHA-induced TRAIL-sensitisation of Multiple Myeloma cells is enhanced in 3D cell culture. *Exp Cell Res*. 2017;360(2):226-235. doi:10.1016/j.yexcr.2017.09.012
132. Durbin KR, Nottoli MS, Jenkins GJ. Effects of microtubule-inhibiting small molecule and antibody-drug conjugate treatment on differentially-sized A431 squamous carcinoma spheroids. *Sci Rep*. 2020;10(1):1-11. doi:10.1038/s41598-020-57789-y
133. Rybinska I, Sandri M, Bianchi F, et al. Extracellular Matrix Features Discriminate Aggressive HER2-Positive Breast Cancer Patients Who Benefit from Trastuzumab Treatment. *Cells*. 2020;9(2):434. doi:10.3390/cells9020434
134. Sonnenblick A, Salmon-Divon M, Salgado R, et al. Reactive stroma and trastuzumab resistance in HER2-positive early breast cancer. *Int J Cancer*. 2020;147(1):266-276. doi:10.1002/ijc.32859
135. Fiszman GL, Jasnis MA. Molecular Mechanisms of Trastuzumab Resistance in HER2 Overexpressing Breast Cancer. *Int J Breast Cancer*. 2011;2011:1-11. doi:10.4061/2011/352182
136. Rexer BN, Arteaga CL. Intrinsic and acquired resistance to HER2-targeted therapies in HER2 gene-amplified breast cancer: mechanisms and clinical implications. *Crit Rev Oncog*. 2012;17(1):1-16. doi:10.1615/CritRevOncog.v17.i1.20
137. Szot C, Dimitrov DS, Croix BS, et al. Tumor stroma – targeted antibody-drug conjugate triggers localized anticancer drug release Graphical abstract Find the latest version : Tumor stroma – targeted antibody-drug conjugate triggers localized anticancer drug release. 2018;128(7):2927-2943.
138. Dittmer J, Leyh B. The impact of tumor stroma on drug response in breast cancer. *Semin Cancer Biol*. 2015;31:3-15. doi:10.1016/j.semcancer.2014.05.006
139. Tatara T, Mukohara T, Tanaka R, et al. 3D Culture Represents Apoptosis Induced by Trastuzumab Better than 2D Monolayer Culture. *Anticancer Res*. 2018;38(5):2831-2839. doi:10.21873/anticanres.12528
140. Diessner J, Bruttel V, Stein RG, et al. Targeting of preexisting and induced breast cancer stem cells with

trastuzumab and trastuzumab emtansine (T-DM1). *Cell Death Dis*. 2014;5(3):1-13. doi:10.1038/cddis.2014.115
141. Smith CL. Cross-talk between peptide growth factor and estrogen receptor signaling pathways. *Biol Reprod*. 1998;58(3):627-632. doi:10.1095/biolreprod58.3.627
142. Karmakar S, Jin Y, Nagaich AK. Interaction of glucocorticoid receptor (GR) with estrogen receptor (ER) α and activator protein 1 (AP1) in dexamethasone-mediated interference of ERα activity. *J Biol Chem*. 2013;288(33):24020-24034. doi:10.1074/jbc.M113.473819
143. Kang KS, Morita I, Cruz A, Jeon YJ, Trosko JE, Chang CC. Expression of estrogen receptors in a normal human breast epithelial cell type with luminal and stem cell characteristics and its neoplastically transformed cell lines. *Carcinogenesis*. 1997;18(2):251-257. doi:10.1093/carcin/18.2.251
144. Petz LN, Ziegler YS, Schultz JR, Kim H, Kemper JK, Nardulli AM. Differential regulation of the human progesterone receptor gene through an estrogen response element half site and Sp1 sites. *J Steroid Biochem Mol Biol*. 2004;88(2):113-122. doi:10.1016/j.jsbmb.2003.11.008
145. Sun JM, Spencer VA, Li L, Yu Chen H, Yu J, Davie JR. Estrogen regulation of trefoil factor 1 expression by estrogen receptor α and Sp proteins. *Exp Cell Res*. 2005;302(1):96-107. doi:10.1016/j.yexcr.2004.08.015
146. Borrás M, Hardy L, Lempereur F, et al. Estradiol-induced Down-regulation of estrogen receptor. Effect of various modulators of protein synthesis and expression. *J Steroid Biochem Mol Biol*. 1994;48(4):325-336. doi:10.1016/0960-0760(94)90072-8
147. Liu X, Shi H. Regulation of Estrogen Receptor Expression in the Hypothalamus by Sex Steroids: Implication in the Regulation of Energy Homeostasis. *Int J Endocrinol*. 2015;2015. doi:10.1155/2015/949085
148. Chen C, Opazo JC, Erez O, et al. The human progesterone receptor shows evidence of adaptive evolution associated with its ability to act as a transcription factor. *Mol Phylogenet Evol*. 2008;47(2):637-649. doi:10.1016/j.ympev.2007.12.026
149. Janes KA. An analysis of critical factors for quantitative immunoblotting. *Sci Signal*. 2015;8(371):1-12. doi:10.1126/scisignal.2005966
150. Özdemir BC, Sflomos G, Brisken C. The challenges of modeling hormone receptor-positive breast cancer in mice. *Endocr Relat Cancer*. 2018;25(5):R319-R330. doi:10.1530/ERC-18-0063
151. Sflomos G, Dormoy V, Metsalu T, et al. A Preclinical Model for ERα-Positive Breast Cancer Points to the Epithelial Microenvironment as Determinant of Luminal Phenotype and Hormone Response. *Cancer Cell*. 2016;29(3):407-422. doi:10.1016/j.ccell.2016.02.002
152. Raina V. Is fulvestrant more effective than tamoxifen for treating ER-positive breast cancer in postmenopausal women? *Nat Clin Pract Oncol*. 2004;1(1):20-21. doi:10.1038/ncponc0010
153. Howell A, Robertson JFR, Abram P, et al. Comparison of fulvestrant versus tamoxifen for the treatment of advanced breast cancer in postmenopausal women previously untreated with endocrine therapy: A multinational, double-blind, randomized trial. *J Clin Oncol*. 2004;22(9):1605-1613. doi:10.1200/JCO.2004.02.112
154. Cho S-Y. Patient-derived xenografts as compatible models for precision oncology. *Lab Anim Res*. 2020;36(1):1-11. doi:10.1186/s42826-020-00045-1

Supplementary Information

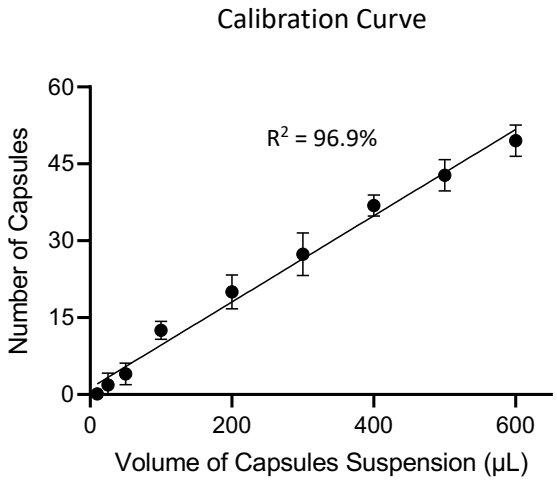

Figure S.28. Calibration curve of the number of capsules contained in a range of volumes of capsules suspension plated. Data shown as mean ± SD of eight technical replicates. Linear regression, with an R^2 of 96.9%.

Table S.15. Information of patient-derived explant samples. Histological classification and grade, TNM classification and immunohistochemistry status determined according to "World Health Organization Classification of Tumors of the Breast, 5th ed. (2019)" and provided by the cytopathology Lab - anatomic pathology unit of Instituto Português de Oncologia de Lisboa Francisco Gentil (IPOLFG). For histological classification purposes the following nomenclature was used: invasive lobular carcinoma (ILC), invasive carcinoma of no special type (IC NST), invasive mucinous carcinoma (IMC). For HER2 immunohistochemistry status: negative (N).

Sample	Gender	Age	Histological Classification[16]	Histological Grade[16]	TNM Classification[16]	Immunohistochemistry Status			
						ER	PR	HER2	Ki67
B95	Female	51	ILC	G2	pT2 pN1a	100%	80%	N	25%
B96	Female	69	IC NST	G2	pT1c pN0	100%	95%	N	20%
B97	Female	65	ILC	G2	pT1c pN0	100%	95%	N	15%
B104	Male	65	IC NST 40% & IMC 60%	G2	pT3 pN0	100%	100%	N	35%

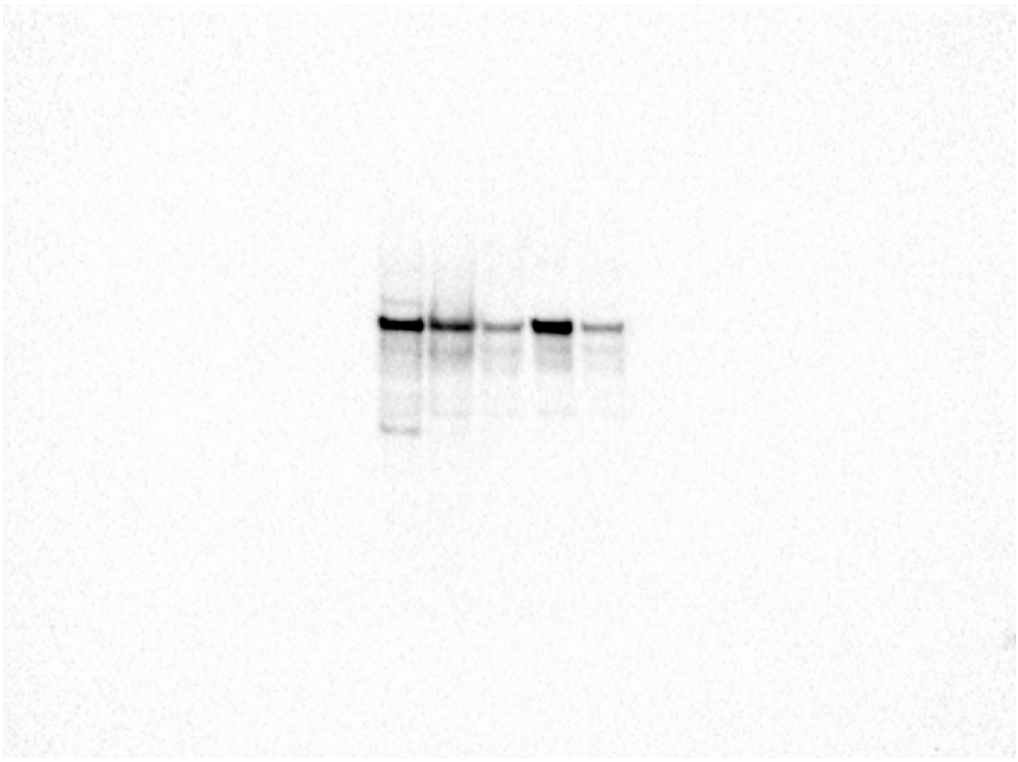

Figure S.29. Uncropped scan of ER western blot. Primary antibody: anti-estrogen receptor α (1D5) from Invitrogen (#MA5-13191), IgG from rabbit (monoclonal), was used at 1 : 500 dilution. Secondary antibody: ECL anti-rabbit HRP-Linked from GE Healthcare (#NA934), IgG from donkey (monoclonal) was used at 1 : 20 000 dilution. Detection with Amersham ECL Select western blotting detection reagent from GE Healthcare (#RPN2235), was performed in a ChemiDoc XRS+ Imaging System (Bio-Rad), using Chemi Hi Sensitivity protocol for Blots.

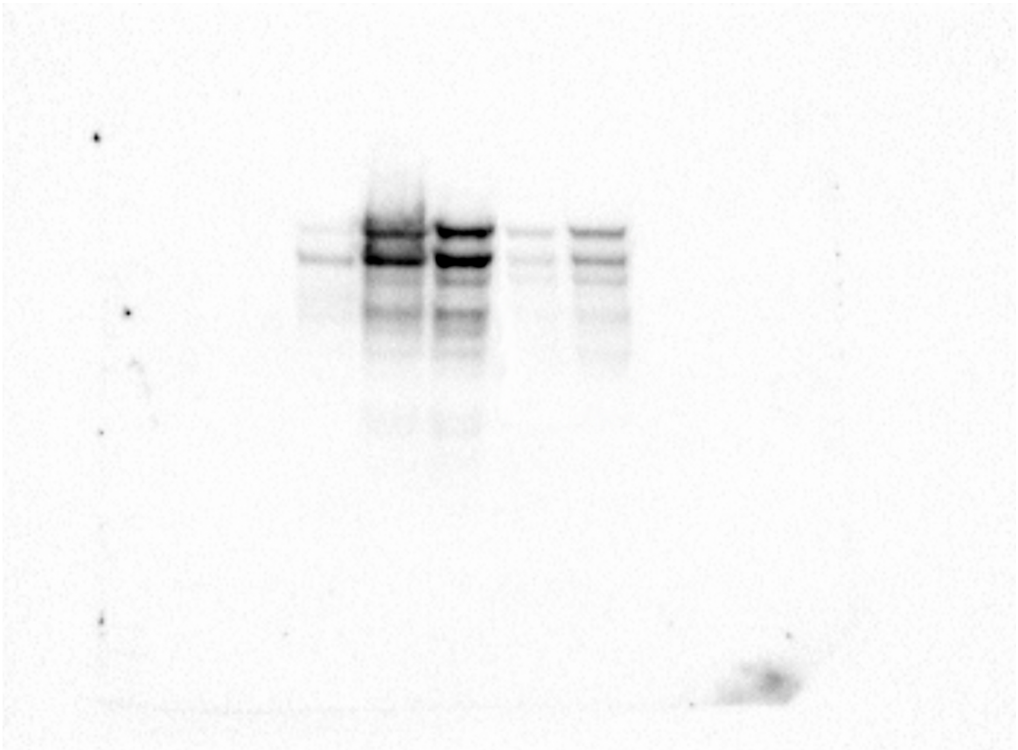

Figure S.30. Uncropped scan of PR western blot. Primary antibody: anti-progesterone receptor (1E2) from Ventana (#790-2223), IgG from mouse (monoclonal), was used at 1 : 100 dilution. Secondary antibody: ECL anti-mouse HRP-Linked from GE Healthcare (#NA931), IgG from sheep (monoclonal) was used at 1 : 20 000 dilution. Detection with Amersham ECL Select western blotting detection reagent from GE Healthcare (#RPN2235), was performed in a ChemiDoc XRS+ Imaging System (Bio-Rad), using Chemi Hi Sensitivity protocol for Blots.

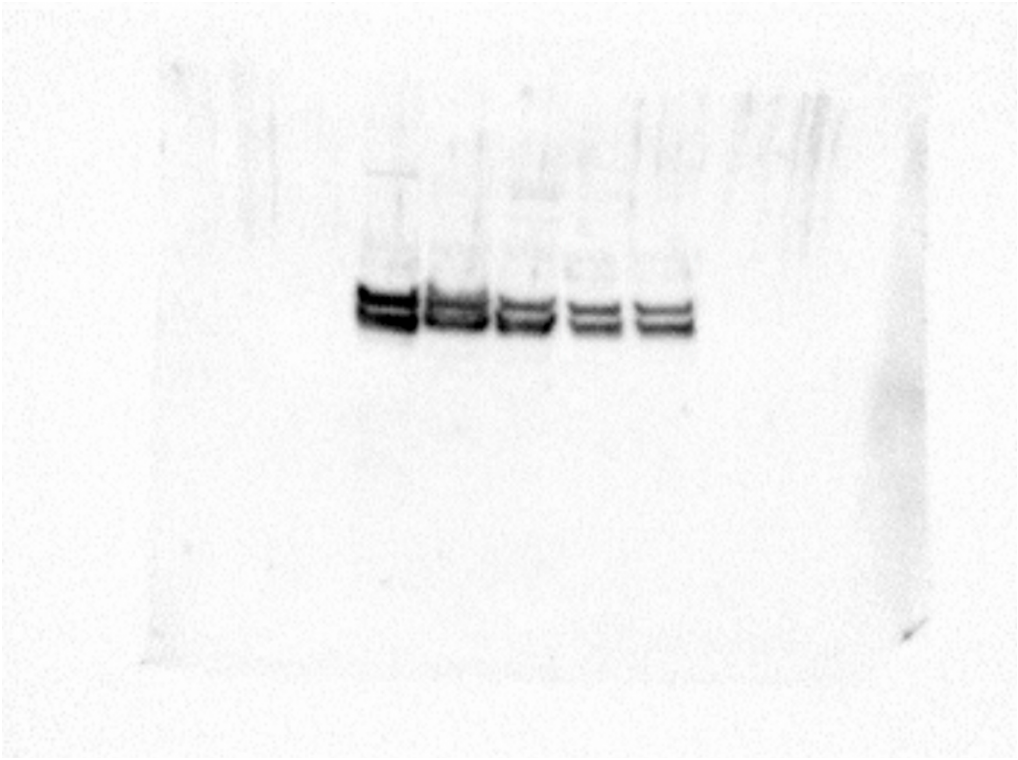

Figure S.31. Uncropped scan of β-Tubulin western blot. Primary antibody: anti-β Tubulin (H-235) from Santa Cruz Biotechnology (#SC-9104), IgG from mouse (polyclonal), was used at 1 : 1 000 dilution. Secondary antibody: ECL anti-mouse HRP-Linked from GE Healthcare (#NA931), IgG from sheep (clonal) was used at 1 : 20 000 dilution. Detection with Amersham ECL Select western blotting detection reagent from GE Healthcare (#RPN2235), was performed in a ChemiDoc XRS+ Imaging System (Bio-Rad), using Chemi Hi Sensitivity protocol for Blots.